Estimating patterns and rates of coastal cliff retreat around Tauranga Harbour

A thesis submitted in partial fulfilment

of the requirements for the degree

of

Masters of Science (Research)

in Earth Sciences

at

The University of Waikato

by

Camillia Pauline Garae

The University of Waikato
2015

THE UNIVERSITY OF
WAIKATO
Te Whare Wānanga o Waikato

Abstract

Cliffs are common around the shores of Tauranga Harbour, including in the urban areas. The existence of cliffs indicates a potential hazard to people living close to the cliff edge, as they imply both a tendency for the upper surfaces to erode, and for the debris to fall onto lower areas. To identify the relative risk around the harbour shoreline, it is useful to determine the rates and patterns of shoreline erosion.

This study initially determined the shoreline changes between 1943, 1982 and 2011 using a combination of aerial photograph analysis using Digital Shoreline Analysis System (DSAS), airborne LiDAR data and Laser scan data. Long term rate of retreat was determined for the study area with the use of digitised aerial photographs and DSAS applications. Cliff locations are often difficult to determine from aerial photographs due to shadows and vegetation obscuring the ground surface. Hence, LiDAR data were used to initially identify the cliff edge positions in 2011. These results were compared to the 2011 aerial photograph to assess how easily the cliff edge can be identified with the photographs. The inferred cliff edge from the 2011 aerial photograph was digitised in GIS, and the corresponding cliff edge for 1943 was also determined and digitised using stereopairs to aid cliff edge identification. The 1982 aerial photograph was scanned, georeferenced and shoreline digitised. Using the DSAS software, the rates were computed. However, this was also compared to other methods using the intersection points generated from DSAS. Laser scan surveys were conducted to determine surface volume changes to acquire short term rate of retreat at the cliff face. This analysis involved surveys carried out within a period from May 2014, July 2014 – November 2014. The data collected was compared to earlier laser scan data from September 2012 – July 2013 and LiDAR data from September 2011.

Several approaches were used to determine the best estimate of rate of retreat from the DSAS analyses. It was identified that the buffer end-point rate produced the best rate cliff retreat in the study area. The range of rate of retreat using this method was -0.2 ± 0.16 to 0.07 ± 0.16 $m.y^{-1}$. It was also identified that the Matua Subgroup had the highest rate of erosion within the study area located at South west Matakana Island. The rate was lowest at East Pahoia Peninsula. Although laser scans were conducted only over a short period of time, comparing the dataset to earlier laser scan data a range of rates were obtained -0.01 to 0.02 $m.y^{-1}$. Although rates were determined for both methods the errors were large and need to be considered.

Acknowledgements

Firstly, I would like to thank Ministry of Foreign Affairs and Trade (MFAT) for awarding me with a scholarship to undertake, masterate research. Special thanks to the Western Bay of Plenty District Council and to the Broad Memorial Trust for financial support. The financial assistance provided has enabled me to carry out this research.

Secondly, I would like to acknowledge the great support and guidance from my supervisors Dr Willem de Lange and Dr Vicki Moon. Thank you for suggesting a topic for me to undertake at Tauranga related to the coastal erosion issues faced in Vanuatu. I have enjoyed carrying out this research and hope to take the skills and knowledge gained and apply them to Vanuatu. A big thank you to you both for putting up with my constant queries with this research. It was a great challenge and I have enjoyed it to the end.

I would also like to extend a word of thanks to all Waikato University staff who have encouraged me throughout the duration of my research with encouragement, expertise in editing and in providing information that has assisted me with my research namely Professor David Lowe, Dr Roger Briggs, Glen Stitchbury and Geua Boe-Gibson.

I am grateful to my fellow office mates, Amy Christophers and Melissa Kleyburg. Sharing an office with you both was probably the highlight of this research, and I enjoyed your company. The late nights, the laughter and the constant questions have made this research reach another level. In the end I can say that I have not only acquired the skills and knowledge needed from this research but also that I have made friendships that will last.

To Dad and Mum - thank you for encouraging me throughout my research. Your constant persuasion for me to return back to uni has motivated me to get this far.

Finally, to my husband, Jeff, and my son Caleb, in the end I can say we all did it! Thank you for your support in the field, (especially Caleb for being my 1 - metre scale) and for all those late nights in the lab. You both encouraged me to keep going right to the very end of this research.

Table of Contents

List of Figures

List of Tables

Chapter 1
INTRODUCTION

1.1 Background

Tauranga Harbour is a large estuary surrounded by soft coastal cliffs located in the Bay of Plenty (Figure 1.1). The catchment has an area of 1300 km^2 and a population of more than 100,000 people (Lawrie, 2006). An issue affecting the harbour over the last 7000 years is the high rate of sediment infill. Previous studies have attempted to estimate the rate of sediment discharge from catchment, with discharge into the harbour being approximately 188,026 tonnes per year (Hall, 2013) of suspended sediment. However, there has been limited study focused on the contribution of sediment from erosion of the shoreline. The shoreline erosion around the harbour is associated with landslip failure which has led to the loss of coastal properties over the past few decades.

1.2 Thesis Objectives

The principal aim of this study is to evaluate the patterns and rates of coastal erosion, particularly of shoreline cliffs, within the central portion of Tauranga Harbour in order to develop an approach for defining the coastal hazard zone associated with cliff retreat. This aim will be achieved through the following objectives:

- to determine the long term rate of retreat;
- to determine the short term rate of retreat and
- to generate a map of the distribution of erosion rates.

1.3 Area of Study

The area of study is located in the central part of Tauranga Harbour (Figure 1.1), an area which had previously experienced landslip failures. This area is in the inner part of the harbour between Waitui Reserve and Matahui point on the mainland, and from Opureroa Marae to northern coastal part of Matakana Island, opposite from Aongatete. The increased concern for the rapid retreat of coastal

cliffs in the study area by the residents had forced the Western Bay District council to find the probable causes promoting cliff instability as well as determine the rate of cliff retreat.

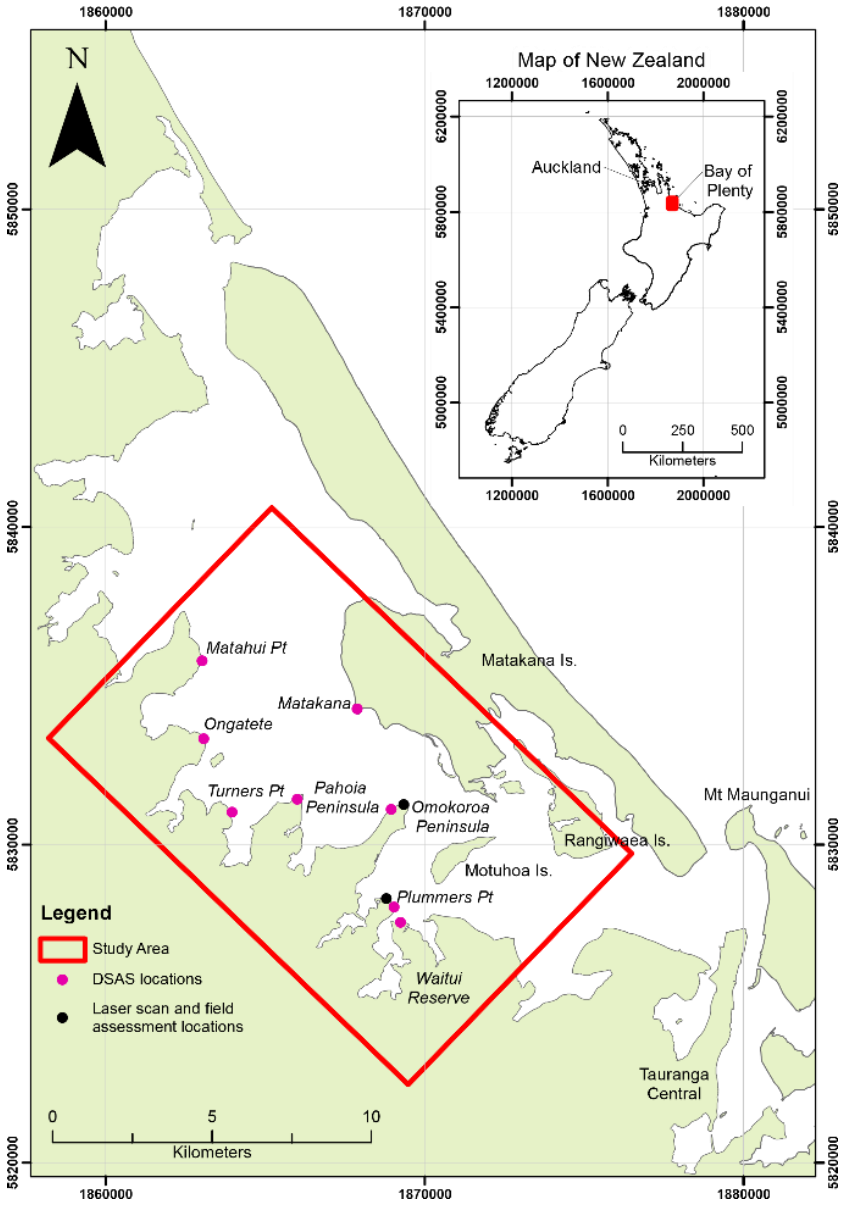

Figure 1.1: Location of study area

1.4 **Regional Setting**

Tauranga Harbour is a shallow mesotidal estuarine lagoon (Healy & Kirk, 1982). It is also known to be one of the largest estuaries in New Zealand occupying an area of 210 km^2 (Lawrie, 2006). The harbour is about 35 km in length and 5 km in width positioned in a northwest to southeast direction along the Bay of Plenty coastline (Briggs *et al.*, 1996). Furthermore, the harbour is defined by tombolos of

Mt Maunganui and Bowentown which are located at the entrances into the harbour, plus the 25 km long barrier island, Matakana (Briggs *et al.*, 1996). The harbour is located within the Tauranga Basin which is covering an area of 570 km^2 bounded by the Kaimai Range, Whakamarama Plateau to the west, Mamaku Plateau to the south and the Papamoa Range to the south (Harmsworth, 1983; Whitbread-Edwards, 1994; Briggs *et al.*, 1996) (Figure 1.2).

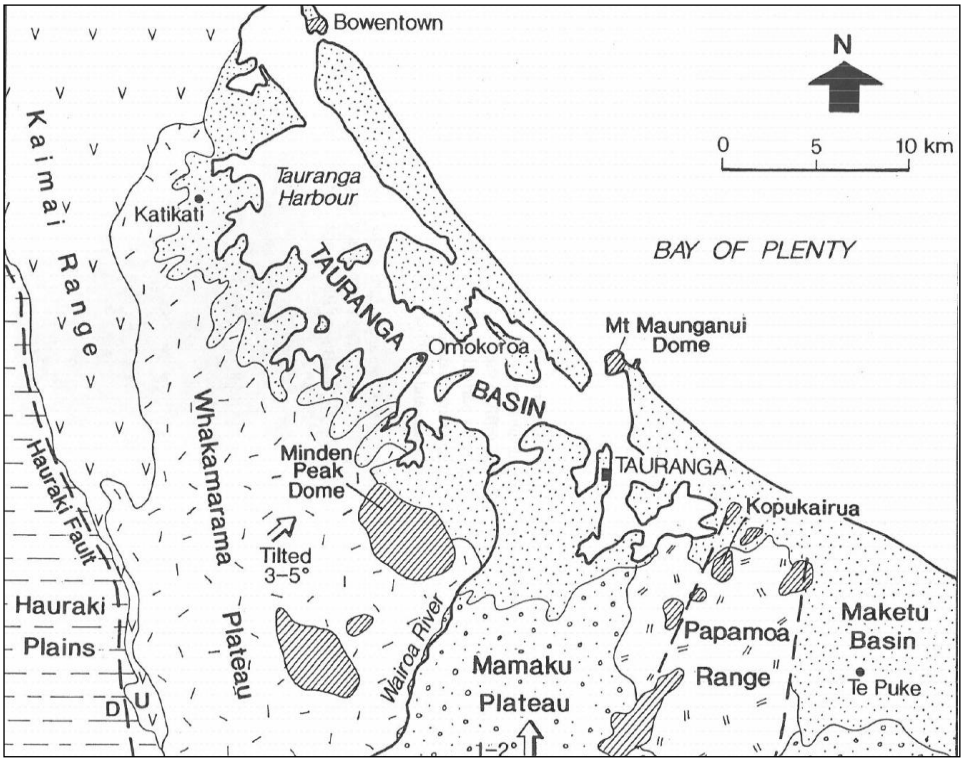

Figure 1.2: Map of physiographic features of Tauranga area (Briggs *et al.*, 1996)

The Tauranga Basin also has glacio-eustatic terraces that occur along the coastal areas of northern and southern Tauranga Basin. Four terraces were identified by Kear and Waterhouse, (1961) at Waihi beach. These terraces measured 6 ft (1.8 m), 6 -10 ft (1.8-3 m), 10 ft-15 ft (3- 4.6 m) and 25- 35 ft (7.6 -10.7 m). Harmsworth (1983) stated that the terraces originated by:

1) volcanic constructional surfaces such as the degradation of the top lobes of pyroclastic flow deposits;
2) volcanic and/ or fluvial degradation surfaces modified by airfall tephra as evident at Plummers Point;
3) fluvial terraces formed by either aggradation or lateral erosion, and variably degraded; or

4) terraces formed by marine aggradation as a result of higher than present sea level.

1.5 **Geological Setting**

The Tauranga Basin is a fluvial- estuarine basin that was infilled after the eruption of the Waitеariki Ignimbrite (2.18 – 2.13 Ma) (Briggs *et al.*, 1996). The sediments that infilled the basin are predominantly primary and secondary volcanogenic in origin deposited in late Pliocene to Pleistocene (Briggs *et al.*, 1996). The primary volcanics were sourced from the southern Coromandel Volcanic Zone (CVZ) and the Taupo Volcanic Zone (TVZ) of which the oldest units are derived from the Coromandel Volcanic Zone whilst most recent deposits originate from the Taupo Volcanic Zone (Briggs *et al.*, 1996). The location of the Tauranga Basin in the transitional zone between Coromandel Volcanic Zone and Taupo Volcanic Zone has resulted in the diversity of rock types from both volcanic zones (Whitbread-Edwards, 1994) deposition by estuarine and fluvial processes (Briggs *et al.*, 1996); Briggs *et al.*, (2005). The secondary volcanic deposits have been reworked prior to Deposition by estuarine and fluvial processes (Briggs *et al.*, 2005).

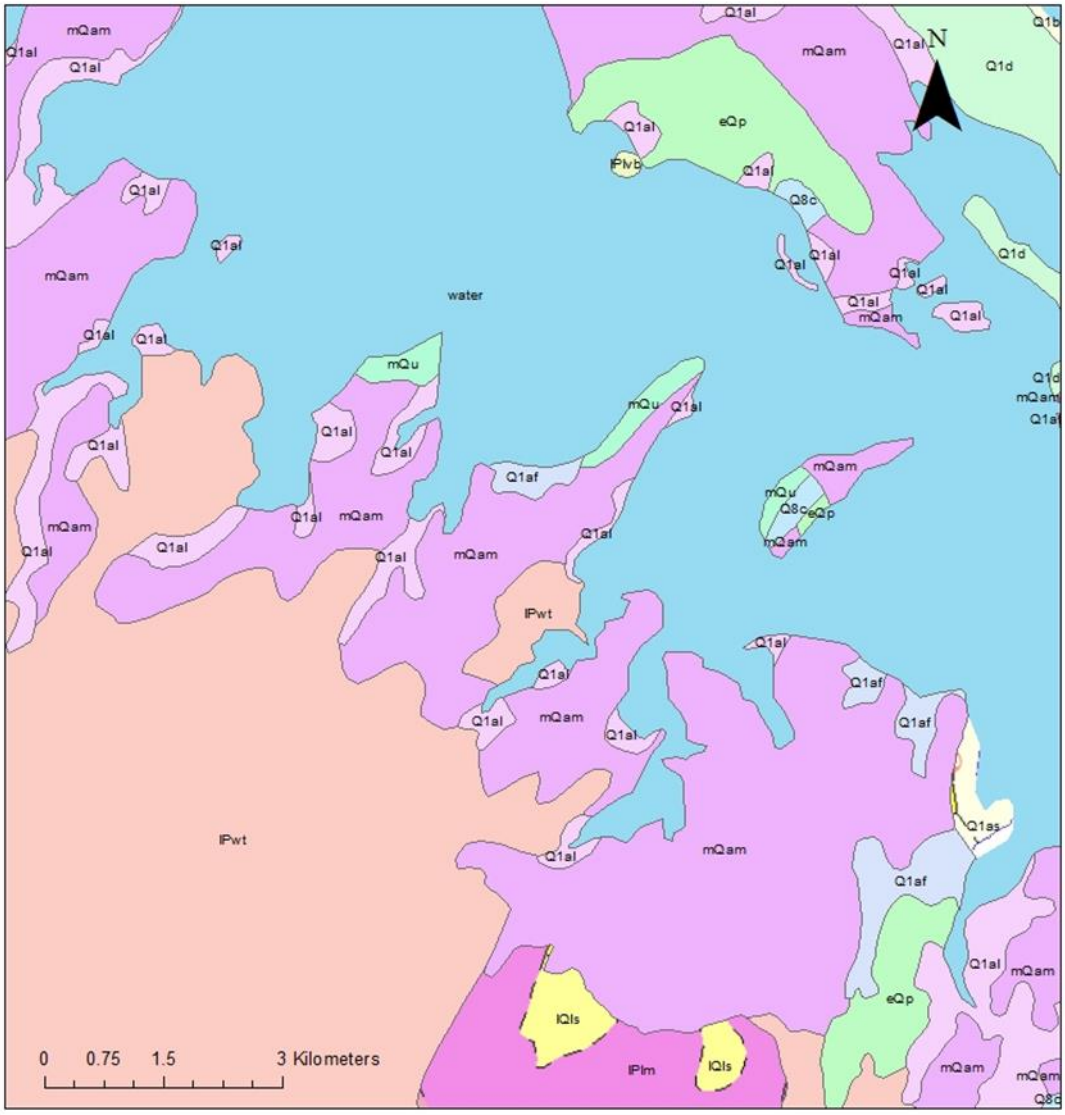

Legend

- Water
- Te Puna Ignimbrite, mQu
- Pakaumanu Group, (undifferentiated), eQp
- Alluvial gravel, sand, silt of modern rivers, Q1af
- Alluvial gravel, sand, silt and clays of modern rivers,Q1al
- Undifferentiated dunes and facies, Q1d
- Matua Subgroup, mQam
- Waitetariki Ignimbrite, lPwt
- Matakana basalt, lPlvb
- Te Ranga Ignimbrite, Q8c

Figure 1.3: Geology Map of Tauranga showing the distribution of lithologies within the area of study in the map view (Briggs et al., 1996; Leonard et al., 2010).

1.6 **Thesis Layout**

Chapter 2 reviews previous literature on prediction models that have been used for determining rates of soft cliffs internationally and specifically in New Zealand. The review then narrows down to the methods used by previous research on determining rate of cliff retreat in Tauranga as well as reviewing previous work on the causes of cliff retreat in Tauranga. Chapter 3 describes the methods used including GIS analysis, field investigations, laser scan surveys and laboratory analysis. Chapter 4 presents the results from the Digital Shoreline Analysis Systems, applied to determine long term rates of cliff retreat. Chapter 5 covers field assessments and laboratory results which correspond to this field investigations. Chapter 6 presents the laser scan results determining short term rates of retreat. Chapter 7 provides a discussion of the findings and Chapter 8 draws in conclusions to the research and suggests a way forward.

Chapter 2
LITERATURE REVIEW

2.1 Introduction

Cliff recession is common for soft coastal cliffs. It can be defined as the landward movement of a cliff face, with recession from the foot to the top of the profile (Lee & Clark, 2002). This recession can occur as a result of shoreline processes such as marine action acting on the cliff face or by slope processes occurring within the cliff structure (Lee & Clark, 2002). Cliff recession is a four stage process which involves (i) the detachment of particles or blocks of material, (ii) the transport of the material, (iii) the deposition on the foreshore, and (iv) the removal of the debris by marine action (Lee & Clark, 2002). Evaluating cliff recession rates is important because such rates provide a means of determining coastal management procedures to minimise or mitigate the phenomena (Carpenter *et al.*, 2012). Cliff recession rates have been calculated by various methods over the past years. This literature review will investigate coastal recession methods that have been utilised to determine cliff recession rates, firstly looking at international examples followed by national and then focusing on the Tauranga area.

2.2 International cliff retreat models

Cliff recession of soft rocks is quite common in many countries in the Northern Hemisphere. In the Northern Hemisphere, coastal cliff retreat measurements were directed toward sandstone, clay, shale and mudstone coastal cliffs of Japan (Young *et al.*, 2009), United States of America (Hapke & Plant, 2010), the United Kingdom (Castedo *et al.*, 2012), the Mediterranean (Katz & Mushkin, 2013) and France (Pierre, 2006). These studies have used particular models and techniques for identifying rates of coastal cliff retreat. The models will be described according to their relevance to this thesis research. Firstly, a review of the Bayesian model will be covered, focusing on parameters which interact with the cliff structure. Secondly, this section will outline the method of airborne LiDAR

followed by terrestrial laser scanning. Lastly, the method of GIS analysis will be covered.

2.2.1 **Model parameters**

Coastal recession models are developed to enhance the understanding of the mechanisms contributing to cliff retreat, as well as to provide methods for predicting cliff retreat. Models consist of a number of parameters that interact together under certain conditions in an environment. Previous models for predicting cliff recession have applied the Bruun rule (Bray & Hooke, 1997). However, more recently probabilistic models have been developed. Lee *et al.* (2001) argued that cliff retreat events do not occur as an independent event but occur in response to previous historic events (Hapke & Plant, 2010). Probabilistic models are useful as they demonstrate how variables are used in predicting coastal cliff recession. Hall *et al.* (2002) used probabilistic models to determine cliff failure based on historic cliff retreat data and developed a Bayesian model. A Bayesian model is a probabilistic model used to predict cliff recession using historic information and correlating the numerous variables influencing this process (Hapke & Plant, 2010). According to Hapke & Plant (2010), the model uses parameters such as cliff height, cliff slope, geology and historical cliff retreat rates, which, when combined, interact to produce cliff erosion. This is an advantage of the Bayesian model since it has the capacity to combine multiple variables and make a statistical forecast (Hapke & Plant, 2010).

A more recent model was developed by Castedo *et al*. (2012) which differs from the Bayesian model since it places less emphasis on historical records of the magnitude and frequency of events but is largely based on geotechnical parameters such as cohesion, friction angle and uniaxial compressive strength of a rock or soil of the cliff structure. As a result, the model avoids misinterpretation of results that correspond entirely with historical records. Lee & Clark (2002) supported the idea that previous approaches relying on historical recession rates are misleading and have many constraints because of unpredicted weather conditions and uncertainty in recession events in. Although neither of the models were used for this thesis research, the models have informed the researcher's

understanding of the possible factors that could contribute to cliff failure of soft coastal cliffs.

2.2.2 **Airborne LiDAR**

Cliff recession has previously been estimated from the recession of the cliff top or cliff base with the use of data derived from aerial photographs, topographic maps or *in situ* surveys. This strategy has been utilised in a number of studies, for example, those of *(Budetta et al., 2000; Hapke & Richmond, 2002; Dornbusch et al., 2008)*. However, more recent technology has improved this method with the use of three-dimensional high resolution maps obtained from LiDAR, which provide an estimation of the entire cliff face retreat rate (Young *et al.*, 2009). An advantage of this application is that it enables the collection of data along coastal areas that have limited access (Young *et al.*, 2010). Furthermore, the technology is useful for capturing cliff top and crests which is useful for estimating cliff retreat. Another advantage is its ability to identify deep seated landslides that extend out from the cliff face (Young *et al.*, 2010).

Airborne LiDAR is a type of technology mentioned by Zhang *et al.* (2003), which involves an aircraft having a laser scanner beneath the flight path measuring the reflection of objects within its path (Figure 2.1). The measurements are obtained from the horizontal coordinates and their corresponding elevation is then used to develop digital terrain models (DTM). However, prior to producing the models, the scanned objects have to be distinguished between non-ground features such as buildings, vegetation canopy, or ground features (Zhang *et al.*, 2003). Once this is accomplished the non-ground features are removed and the DTM generated (Zhang *et al.*, 2003).

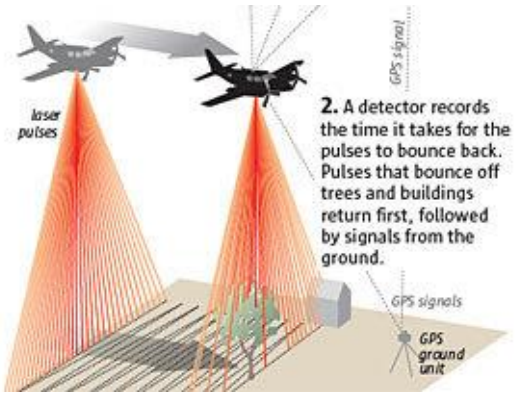

Src: http://seattletimes.com/html/localnews/2023244512_mudslidelidarxml.html
Figure 2.1: How LiDAR data are collected

Based on Young *et al.* (2009), cliff morphology changes can be measured with the use of airborne LiDAR data. Their survey revealed changes in cliff morphology (cliff base, cliff top and cliff face) after each survey conducted. The data were collected over a time span from 2002 – 2006 and were compared after processing the data with regard to previous Digital Elevation Models (DEM). However, a limit for using airborne LiDAR data is that there can be inaccuracy in the results such as data showing accretion of material when in actual fact there is no accretion occurring since cliff tops erode but do not accrete. Young *et al*. (2010) addressed this issue and identified that the LiDAR surveys revealed negative and positive changes of the cliff, which represented erosion and accretion of the cliff profile. This error is most likely encountered due to beam divergence, cliff geometry, and position of the scanner relative to the cliff and vegetation cover.

Young *et al.* (2010) clearly revealed possible errors that may have contributed towards misleading results. They documented that by comparing the two methods, aerial and terrestrial LiDAR (Figure 2.2), that airborne LiDAR underestimated negative change (erosion). This is because the airborne LiDAR was unable to measure layers less than 0.38 m into the cliff face. Therefore, it takes readings of large scale landslides but cannot detect minute changes. However, in terms of measuring positive changes (deposition), both methods had similar results since the eroded debris had relocated to the base of the cliff allowing airborne LiDAR to detect the changes. Thus, there is greater precision and accuracy using terrestrial LiDAR compared to using airborne LiDAR for measuring small negative changes (erosion) on a cliff face.

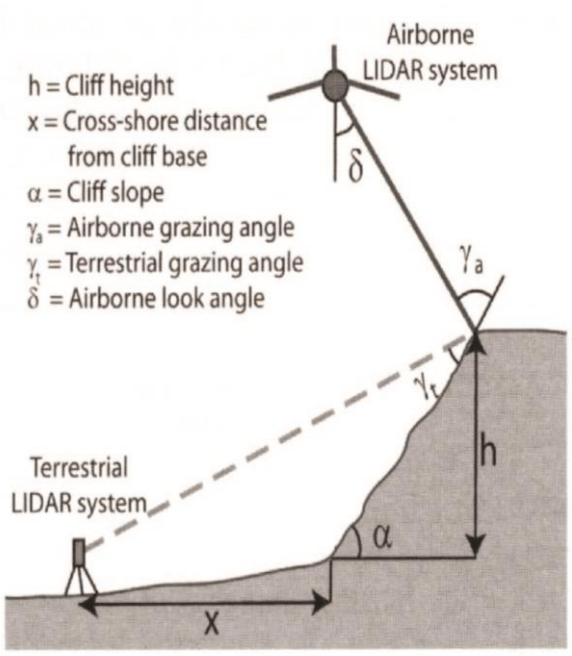

Figure 2.2: Schematic diagram comparing airborne LiDAR and terrestrial LiDAR systems (Young *et al.*, 2010)

2.2.3 Terrestrial laser scanning (ground-based LiDAR)

Another step beyond the analysis of historic aerial photographs, topographic maps and survey plans to estimate coastal cliff retreat, the LiDAR technology with its scanning range and accuracy has been widely used for estimating short-term cliff retreat. Terrestrial laser scanning, also referred to as ground-based LiDAR, appeared towards the end of the 1990s (Wang *et al.*, 2013). This method has been applied for estimating cliff retreat (Rosser *et al.*, 2005; Olsen, 2009; Young *et al.*, 2010). Advantages of using such technology is that it quantifies failures ranging from a few centimetres of block detachment to large rock falls or debris falls over 1000 m^3 in volume, and collection of data is carried out on site and is rapid (Rosser *et al.*, 2005). Furthermore, as noted already in the previous section, terrestrial LiDAR has the capacity to detect small cliff changes that may go undetected by airborne LiDAR (Young *et al.*, 2010).

Terrestrial laser scanning (TLS) is a ground-based LiDAR (light detection and ranging) technique that uses a "time-of-flight detection of a reflectorless laser beam for determining the distance between the instrument and a point on a reflective surface" (Kuhn & Prüfer, 2014, p. 156) (Figure 2.2). The scanner

captures the 3D position of the data point during surveys as x, y , and z coordinates, which are then used to generate digital elevation models (DEMs) mapped on map software applications (Oppikofer *et al.*, 2009; Katz & Mushkin, 2013; Kuhn & Prüfer, 2014) (Figure 2.3). The analysis of the data can be interpreted as 2D with a side view using the results obtained and also by 3D, which involves constructing 3D surface models and comparing these DEMs and calculating difference maps between them (Kuhn & Prüfer, 2014).

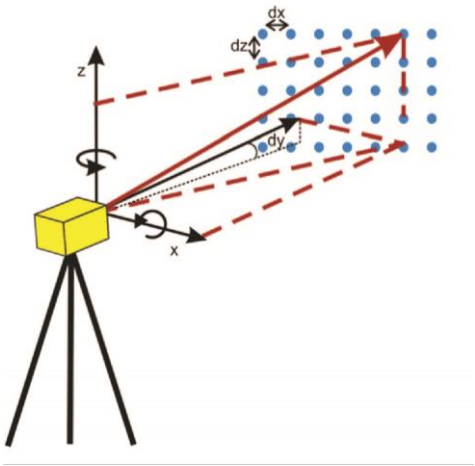

Figure 2.3 Terrestrial laser scanner capturing 3D position of data points (Kuhn & Prüfer, 2014, p. 157)

Cliff retreat data collected by terrestrial laser scanning do not determine the likely causes of retreat, such as erosion from storm events and escarpment retreat (Katz & Mushkin, 2013). Therefore, the method has its drawbacks but it is a suitable method to use as it quantifies volume and geometry changes of the cliff. Hence, the method was included in the thesis research to be discussed in the next chapter since it quantifies volume changes of the coastal cliffs with relative accuracy. Young *et al.* (2010) compared three LiDAR based estimates for cliff retreat obtained by observing the cliff top, cliff face and cliff base and found they all have their limitations. There are errors and also slope changes between the beach and cliff face and between the cliff face and cliff top are not clearly defined. For cliff face changes, the LiDAR captures the cliff top and cliff base and therefore it is an adequate method to use since it includes all these changes. The cliff-base method measures changes from basal erosion. However, changes in marine beach sediment near the base and talus deposition can complicate the results.

2.2.4 **Digital shoreline analysis system (DSAS)**

DSAS is a software application that is used within Environmental Systems Research Institute (ESRI) Geographic Information System (Arc GIS) software (Thieler et al., 2009). The application has the capability of calculating shoreline rate of change from shoreline data acquired from historical maps and aerial photographs (Thieler & Danforth, 2010). This application has been widely used by various studies. For example, Brooks and Spencer (2010) and Del Río and Gracia (2009) used DSAS to determine cliff recession rates.

Brooks and Spencer (2010) focused on determining cliff recession rates of soft cliffs and sediment input to nearby coastal systems in the Suffolk coast in the United Kingdom. Historic shorelines were digitised from aerial photographs and historic maps, followed by transects generated from DSAS to determine long term retreat rates from 1883-2008 (Brooks & Spencer, 2010). The shoreline was determined by considering the cliff base and cliff top from historic maps (Brooks & Spencer, 2010). To determine shoreline change using DSAS, the End Point Rate (EPR) was used from the result spreadsheet. EPR is the difference in the position between the oldest and most recent shoreline divided by the time between these surveys. Furthermore, in DSAS it is possible to calculate the Linear Regression Rate (LRR) of change by fitting a least square regression, using all the points where the shoreline intersects.

Del Río and Gracia (2009) used digital orthophotographs for digitising the cliff top, but used the cliff foot for sections that were heavily vegetated. The same method has been used in this thesis research. However, shoreline was not determined from historic maps but from aerial photographs using GIS application tools. Shoreline was also only determined from the cliff top.

Chand and Acharya (2010) undertook their research based in the Bhitarkanika Wild Life Sanctuary in central coast of Orissa in India. Their focus was to determine the shoreline change with one of the methods being the use of DSAS. The analytical techniques used included EPR and LRR. However, they stated that a drawback of EPR is that it suppresses the shoreline behaviour for long-term shoreline when there are more than two shorelines. This is because it only

considers the recent and oldest shoreline position, and therefore any changes in shoreline position within this time frame are not considered. Thus, this method is only appropriate for short-term changes. LRR on the other hand, considers all the intersection points for multiple shorelines. Therefore, LRR was used in the research since it considered all the intersection points for the multiple shorelines.

Castedo *et al.* (2015) used GIS data to determine the rate of change for the cliff top and estimate future trends between Bridlington and Hornsea in Holderness Coast (UK). They also used linear regression to acquire the rate of change since it was able to provide the evolution changes from the multiple shorelines used within the period of 1852-2011.

The Cadiz cliffed coasts in southwest Spain were also subject to cliff recession. Therefore a study was undertaken by Del Rio *et al.* (2009) to determine the rate of cliff retreat by analysing a set of photographs for varying time scales and using GIS tools to digitise the top and toe of the cliffs and applying the rate of change calculation by Thieler *et al.*(2003). The rates recorded varied with location as well as the cause of recession, being triggered by rock or debris falls, slides, or topples. The maximum recession rate was 1.6 $m.y^{-1}$ caused by a combination of marine action and water erosion at the top part of the cliff Del Rio *et al.* (2009)

2.3 **New Zealand cliff retreat models**

"In New Zealand about 3% of the exposed coastline has retreated from rapid rates of erosion" (Gibb, 1979). The different models proposed by several authors in New Zealand will be discussed chronologically. This section will discuss the method of surveying bench marks and observing changes in the shoreline as well as using GIS analysis to determine rate of cliff recession.

Gibb (1979) determined rates of erosion and accretion along New Zealand coastal areas. Gibb (1978) stated that cliff recession in New Zealand occurs at a rate between 0.25 – 1.0 $m.y^{-1}$. Gibb (1979) identified that sea cliffs were eroding at an average net rate of between 0.3 $m.y^{-1}$ and 1.5 $m.y^{-1}$ with maxima of 2.3 $m.y^{-1}$ for mudstone at Cape Turnagain, whereas conglomerate material retreated at a rate of

2.0 m.y $^{-1}$ (determined for South Waitaki fan), and 0.4 m.y $^{-1}$ was the erosion rate for sandstone measured at Te Kaukau Point.

The rates were determined by the changes in the position of the shoreline, between a fixed point on land and the shoreline at various intervals. (Gibb, 1978) recorded that the methodology for calculating rates was achieved from aerial photographs and field measurements. Rates were calculated by dividing the amount of horizontal displacement by the time interval between each successive survey. However, the research conducted was limited by the frequency of surveys. Therefore, Bird (1981) stated that surveying of the base of a cliff should be done every 3-5 years to provide rates of basal erosion. Another limitation with the (Gibb, 1978) survey conducted was that it was only focused on cliffed coasts dominated by mudstone and conglomerate lithology.

A rate of cliff retreat was also determined for coastal sections near Gisborne. Gibb (1999) created a coastal sensitivity index which classifies lithological material into variables depicting the erosional sensitivity of the cliff face to shoreline retreat. Therefore, the lithology of the cliff structure can indicate how susceptible the cliff will be to cliff retreat. Gibb (1999) stated that retreating rates of -0.3 m.y $^{-1}$ at Makorori Beach and -0.18 m.y $^{-1}$ were determined for Tatapouri Point with lithological units consisting of sandstone - siltstone rocks. The coastal sensitivity index for both areas was classified as medium to high.

The research of Gibb (1978) provided rates of cliff retreat in New Zealand for other substrate material other than soft volcanic cliffs. Following his work, there still lies a gap in research for determining rate of cliff retreat for soft volcanic materials in New Zealand. From this, it is evident that further research has to be undertaken to determine the rate of cliff retreat for volcanic rocks.

2.4 **Tauranga**

Previous research has focused on the mechanisms triggering landslide events along the steep coastal cliffs of Tauranga. This is summarised in this section with the first part looking at previous landslip events. The second part addresses the

contribution of rainfall to landslip and the last part focuses on previous studies revealing the contributions of soil sensitivity to cliff failure.

2.4.1 **Landslip failures**

Steep cliffs are present along the coastal margins of Tauranga Harbour. Most cliffs have been subject to landslide events and investigated over the years. This section clearly shows that although previous work has attempted to determine the mechanism promoting cliff failure, there is still limited research focused on determining the rate and pattern of cliff retreat for the entire harbour area. Gulliver & Houghton (1980) examined the Bramley Drive landslip failure of 1979, which formed a tongue-like sheet of debris extending out 150 m from the cliff generated from the removal of 60 m width of cliff segment of material at 16 m depth. They characterised the failure as a translational slide and flow slide since it consisted of a large volume of material mobilised and spread over a vast area. The failure was triggered by a number of factors which included the nature of soil conditions, the frequency of rainfall, marine erosion, subdivisional development and drainage and waste disposal systems (Gulliver & Houghton, 1980).

Grocott (1989) stated from his investigations that the coastal margin of Tauranga was eroding due to undercutting occurrences at the base of the cliff that took place at a slow rate whilst landsliding accelerated at the top of the cliffs. Oliver (1997) identified four types of failures triggering landslides on Maungatapu peninsula:

- Large scale block failure occurred as the result of downcutting of cliff edges by streams during glaciation periods (late Pleistocene to Otiran).
- Piping-triggered block failure resulted from high rainfall permeating through soil layers via fractures, rootlets, buried channels and exfoliation defects increasing pore water pressure in aquifers. The increased pore water pressure forces water to exit through points of weakness (exfoliation defect or defects) laterally within the structure, producing pipe structured failure generating a circular failure. Within the geological structure, internal defects have the capacity to break up blocks of material within the aquifer

generating a debris flow. Hungr *et al.* (2013) defines debris flow as a very rapid to extremely rapid surging flow of saturated debris in a steep channel.

- Wave-erosion triggered block failure occurs as a result of intense wave energy impacting the cliff face at high mean water level when heavy rainfall occurs during storm periods. Failure initially is caused by cavities created by colluvium/topsoil layers located at the base of the cliff, which are eroded by wave action and rainfall. These cavities are the point of weakness that creates block failure above the shear plane.
- Shallow regolith failure occurs as a result of undercutting by wave action that removes support to the overlying layers. This has resulted in sliding of overlying vegetation and soil mass. Failure type depends on the saturation of the material. A rapid slide will occur if mass is not too saturated.

Bird (1981) conducted similar research at Maungatapu Peninsula. This was carried out after the 1979 landslips and he identified three types of cliffs. Type 1 and 2 represent those exposed to westerly fetch and in proximity to tidal channels. The type 3 cliffs represent cliffs that retreat as a result of rill erosion, wind attrition, toppling and may generate translational landslides (Bird, 1981).

Bell *et al.* (2001) stated that Bird (1981) analysis only considered water pressure from a phreatic surface and no consideration was taken into account for water pressures that may have been present in the tension cracks. Bell *et al.* (2001) focused on comparing the research on slope failures at Maungatapu undertaken by Oliver (1997) with failure records at 1979 Bramley Drive failure at Omokoroa Peninsula. Bell *et al.* (2001) stated that slope failure was different at each locations. Omokoroa had lower slope angle compared to Maungatapu which had slopes exceeding 60°. This was because within the Tauranga Harbour the Omokoroa peninsula is more sheltered from strong wave action than Maungatapu (Bell *et al.*, 2001). Hughes (1998) reported 21 landslip failures along the western Omokoroa Peninsula, most of which occur within the same area as reported by Gulliver & Houghton (1980), and include Hamurana Drive, Kowhai Grove,

walkway from Bramley to Ruamoana Place, Walnut Grove, north of Gerald Place and Gerald Crapp Historic Reserve. These sites were assumed to be affected by similar causes triggering failure such as that of the Bramley Drive 1979 event related mainly to heavy rainfall events.

Keam (2011) stated that the reactivation of the Bramley Drive landslip, which occurred in May 2011, resulted in regression of the cliff face and deposition of debris creating a bench below the head scarp which covered a sensitive ash layer.

Keam (2008) conducted a thorough investigation of Omokoroa Peninsula and attempted to analyse the geological properties of the deposits in the study area and the failures that occur within the sites. He used LiDAR data for geomorphological analysis, which was used to discover slides initiated by the presence of basal silt layers that acted on the surface of the failure plane. He mentioned that the Bramley Drive failure, according to the classification of Cruden and Varnes (1996), is complex because it transitioned from a compound earth slide to a flow as a result of gravitational forces and the addition of water. The Bramley Drive slides ranged from <10 m wide and 20 m in length to 60 m width and 130 m in length, displacing over 36,000 m^3 of material. The Bramley Drive failure resulted from sensitive silts (sand silt layer) within the rupture surfaces (Keam 2008). Apart from the sensitive silts, other causes for the compound slides along the western Omokoroa Peninsula include (Keam 2008):

- A variety of permeabilities in the groundwater system;
- Ground water flow within paleotopographic channels increasing pore water pressure and creating eroded channels;
- High rainfall;
- Marine erosion of the toe of the slope; and
- Subdivisional development with improper drainage systems.

Cunningham (2012) focused his research on analysing the sensitivity of soils which has been a main contributor to soil failures in Tauranga region. His study area consisted of three sites with sensitive soils: Omokoroa, Pahoia Peninsula and Te Puna. The methods included triaxial tests, X-ray diffraction analysis and scanning electron microscopy (SEM) for determining mineralogical properties.

Wyatt (2009) focused his research on sensitive weathered material, particularly silica-rich tephra-fall derived pyroclastic material of mid-Pleistocene age in the Tauranga region. His field work was undertaken in Tauriko and Otumoetai. The geomechanical investigation of sensitive soil materials showed that they had a high moisture content (>60%), low dry bulk density (<966 kg m-3), and high porosity (>60%). As a result, the poorly drained soil with its small pores (and highly siliceous character) provides suitable conditions for halloysite formation (rather than allophane or kaolinite) (Churchman & Lowe, 2012). Upon disturbance, the soil will flow since it exceeds its liquid limit with water also released from the small pores.

Arthur (2010) carried out field investigations and identified that the soils are syn-eruptively reworked pyroclastic deposits. The soils he studied were from basal shear plane of landslides in Auckland and Tauranga region. He undertook X-ray diffraction studies and found that clay minerals halloysite and kaolinite associated with quartz and plagioclase.

2.4.2 **Contribution of climate to cliff instability**

Cliff instability can also be triggered by poor weather conditions. Hay (1991) undertook a separate study on the storm and oceanographic database of part of the Western Bay of Plenty. His study area was from Mt Maunganui to the southern end of Papamoa township. The aim of his study was to compile a storm database (containing storm variables and associated wave parameters). It would identify the magnitude of historical storm events and associated wave parameters experienced in the area. The other database compiled was an oceanographic database (containing mean sea level, sea surface temperature and tidal parameters). It was used to compile information on wave refraction, and seasonal beach fluctuations. The last aim was to establish a relationship between the storm events and the southern oscillation in the study area. Hay (1991) discovered that the Bay of Plenty climate is influenced by El Nino Southern Oscillation phenomenon (ENSO). The ENSO affecting New Zealand is in the negative phase (El Nino) which is associated with westerly wind patterns. Therefore, by identifying the

type of ENSO affecting the Bay of Plenty a relationship can be determined between climatic oscillations and wave patterns. The positive phase (La Nina) is associated with a greater frequency of north easterly winds and warmer sea surface temperatures.

Several investigation studies have focused on landslide failure on Omokoroa Peninsula. Gulliver & Houghton (1980) issued an investigation report after the occurrence of the landslide in August 1979, which was triggered by heavy rainfall. Apparently, the rainfall record show that there was high rainfall in March 1979, which was the second highest rainfall recorded since 1898 with 504 mm rainfall. However, the landslip occurred in August of that year indicating that occurrences of landslips are influenced by rainfall from a prolonged period (6-12 months) and triggered by a short rainfall event. The exposed cliff face was about 34 m in height and 60 m in length. The report also included other past landslide occurrences on in 1962 at Omokoroa: 30 and 31 Hamurana Road, 17 Kaharoa Avenue and 36 Harbour View Road that occurred after heavy rainfall. At Hamurana, the landslip removed a section with a width of about 60 m and a depth of 20 m. This cliff section also slipped in November to December 1962 following heavy rainfall that occurred that occurred in December 1961–May 1962 with rainfall of 1000 mm and from July to December 1962. These records show that landslips may be caused by heavy rainfall 6-12 months prior to the catastrophic event but triggered by small rainfall events (Gulliver & Houghton, 1980). Thus, it is suggested that soil failure at Omokoroa usually occurs after torrential rainfall.

Tonkin & Taylor (1981) used aerial photographs and identified areas of erosion which were associated with gullies that had been infilled, or sites of previous landslides events, suggesting that water had accumulated in these areas and water pressure was triggering landslip failure. Shrimpton and Lipinski (1998) also found that the 1998 landslip failures at Omokoroa Peninsula at various locations resulted from increased ground water levels in older pyroclastic (volcanic ash) layers after torrential rainfall. Opus (2000) identified water seepage at three locations along the coastal cliff sections as occurring between the interface of older ash and underlying Tauranga Group deposits. Two boreholes were drilled and piezometers placed in them. Monitoring of the middle piezometer positioned within the failure

plane revealed that the ground water is perched above the water level of the lower piezometer (positioned in the Tauranga Group) (OPUS, 2000). Therefore, this perching suggests that there is a permeable layer within the failure plane that allows water to flow and weaken the sensitive soil structure, thereby initiating landslip failure (OPUS, 2000). Tonkin & Taylor (2011, 2014) noted that the landslide at Bramley Drive reactivated in May 2011 as a result of heavy rainfall and caused a section of the headscarp to regress 6 m. There was further headscarp regression at this location in April and August 2012 by 1.5 m, and more recent slope failure in the northern portion as observed in June 2014 (Tonkin & Taylor Ltd, 2014).

Tonkin & Taylor, (2011) commented that landslip failure was caused by heavy rainfall as well as the presence of sensitive soils.

2.4.3 **Contribution of soil sensitivity to cliff failure**

The combinations of climatic conditions, saturation from heavy rainfall, as well as the presence of sensitive soils in Tauranga have triggered landslides that occurred in the 1960s and 1970s. Sensitive soils are materials that lose their strength upon remoulding (Cunningham, 2012). Several research projects have been undertaken to show that soil sensitivity contributes to cliff failure. Gulliver & Houghton (1980) stated that the high permeability of the pumiceous lapilli and ash rich Rotoehu Ash on Omokoroa Peninsula enhances the infiltration of the surface layer of the younger ash as opposed to the deeper and more weathered, clay-rich older ash which are less permeable due to the abundance of clay. Thus, they further added, the infiltration of rainfall into these layers with water from the nearby residents artificial soak pits could have triggered the landslip of 1979. Bird (1981) also found that the soil failure resulted from high pressure of phreatic waters within units above the sensitive clays. Wesley (2007) suggested that the landslips which occurred at Otumoetai in a storm event during May 2005 resulted from excess water supply that softened the soil creating a lubricated surface for failure. Failure was suggested to have occurred with increasing pore water pressure in the sensitive soil (Wesley, 2007). Keam (2008) also stated that during his investigations at Omokoroa a sensitive silt layer was identified. It was located at

the base of the slope and was probably responsible for triggering the initiation of the failure. Furthermore, he suggested that negative pore water pressures provide stability to undisturbed sensitive soils. However, upon saturation the pressure increases resulting in the soil losing its strength. Keam (2008) also stated that the main factors contributing to the initiation and occurrence of slope movement are: (1) large trees such as pohutukawa that initiate shallow seated failures by creating tension cracks, (2) sea level rise, which causes marine erosion and over steepening, and (3) anthropogenic surcharges from leaking septic tanks and runoff from the houses. The weight of infrastructures (houses) also contributes to pressure on the underlying silt layers.

Arthurs (2010) studied the sensitivity of soils in Tauranga. He suggested several factors contributed to the development of sensitive soils. These include the soil having a low density pyroclastic structure and it being highly weathered to produce clay minerals such as halloysite and kaolinite (Gibb, 1979; Wyatt, 2009; Arthurs, 2010). In addition, the soil has a microstructure formed by weathering of the pyroclastic material which has high water content (Jacquet, 1987; Arthurs, 2010).

Tonkin and Taylor (2011) suggested that landslip failure at Omokoroa was partly caused by the saturation of sensitive soils that created a perched water table, hence generating a slip plane for the failure.

Cunningham's (2012) field investigations of sensitive soils in Tauranga revealed that sensitive soils were associated with Te Puna Tephra. Moon *et al*. (2013) have suggested that Tauranga sensitive soil failure occurs after heavy rainfall events and the failures were associated with the so-called Pahoia Tuffs (or tephras), a widely variable group of multiple units including a range of lithologies of primary reworked pyroclastic materials as well as buried soils (Briggs et al, 1996). Moon *et al.* (2013) also indicated that the soils predominantly consist of the clay mineral halloysite of multiple morphologies that are loosely packed, having high porosity (51- 77 %) and low permeability due to the micro pores within the soil structure. These features result in the constant wet texture of the material after rainfall events (near-constant wetness is probably essential for the formation of halloysite

rather than kaolinite: Churchman *et al*. 2010; Churchman & Lowe, 2012). Therefore, it is apparent that pore water pressure raised to this level creates an aquifer which triggers landslip failure as a result of saturated pore space within the Pahoia tephra sequence.

Wendt (2013) tried to better understand the mechanism of failure. He conducted a detailed study stratigraphic column of the Bramley Drive landslip. Furthermore, he sampled each layer and conducted geotechnical tests in the laboratory to determine the geomechanical properties. Thus, the geological units in Tauranga are important to thoroughly study as their properties may provide indicate some relationship to cliff failure.

2.5 **Geology of Tauranga**

Briggs *et al.* (1996) stated that the underlying geology of the Tauranga region comprised of late Pliocene to Pleistocene volcanic rocks and volcanogenic sediments. The Tauranga Basin is a Pleistocene, fluvial/estuarine basin infilled as a result of rapid subsidence following the Waiteariki Ignimbrite eruption from 2.18-2.13 Ma (Briggs *et al.,* 1996). The stratigraphy of the Tauranga region consists mainly of primary and secondary volcanic or pyroclastic material (both fall deposits and those from pyroclastic flows) as well as other materials such as marine and aeolian sediments and buried soils. The primary volcanics and pyroclastics were sourced from the Southern Coromandel Volcanic Zone (CVZ) and the Taupo Volcanic Zone (TVZ). They consist of basaltic to rhyolitic lavas, dacitic to rhyolitic ignimbrites (mainly welded) and unconsolidated pyroclastic deposists (also called tephras) (Briggs *et al.*, 1996). The stratigraphy is arranged in chronological order from oldest deposit to the most recent deposit (Figure 2.4).

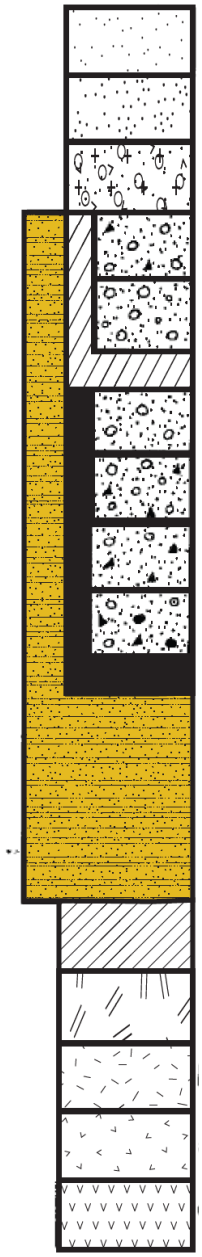

	Age
Holocene alluvium and dunes	≤11.5 ka
Holocene and late Pleistocene tephras	< 50 ka
Rotoehu Ash	c. 50 ka
Mamaku Ignimbrite	0.22 Ma
Waimakariri Ignimbrite	<0.27 Ma
Hamilton Ash	0.35 Ma – c. 0.1 Ma
Te Ranga Ignimbrite	0.27 Ma
Te Puna Ignimbrite	0.93 Ma
Ongatiti Ignimbrite	1.34 Ma
Papamoa Ignimbrite	2.40 Ma - 1.9 Ma
Pahoia tephras	2.18 Ma – 0.35 Ma
Matua Subgroup (fluviatile sands and gravels, lignites, estuarine sands, lacustrine silts)	c. 2 Ma – c. 50 ka
Waitieriki Ignimbrite	2.09 Ma
Kopukairua Dacite	2.20 Ma
Matakana Basalt	2.7 Ma
Minden Rhyolite	2.89 – 1.95 Ma
Otawa Volcanics	2.95 – 2.54 Ma

Figure 2.4: Stratigraphy of the Tauranga region after Briggs *et al.*, (1996); (2005) . ka, thousands of years ago; Ma, millions of years ago

According to Briggs *et al.* (2005) the oldest deposits are the underlying Otawa Volcanics (2.95 to 2.54 Ma). Overlying this deposit are a number of volcanic domes and flows (Minden Ryolite, Matakana Basalt and Kopukairua Dacite), which have an age range of 2.18 Ma to 2.36 Ma. These volcanics are overlain by the Waitieriki Ignimbrite 2.89–2.09 Ma. This is followed by another layer overlaying it known as the Matua Subgroup.

The Matua Subgroup (~ 50 ka to 2.09 Ma) represents terrestrial and estuarine sedimentary deposits deposited after the Waiteariki Ignimbrite eruption. These deposits infill the Tauranga Basin to a depth of approximately 150 m (Harmsworth, 1983). The sequence consists of fluvial, pumiceous and rhyolitic silts, sands and gravels, lacustrine (diatomaceous) and estuarine muds, lignites and peats (Harmsworth, 1983). The sequence of deposits are intercalated with tephra fall deposits and thin distal ignimbrites. Varieties of structures are present in this unit, such as cross bedding, planar stratified and water escape structures. Variation in structures is the result of sediments being reworked (Briggs *et al.*, 1996).

The Pahoia tephras (0.35–2.18 Ma) are weathered white and olive coloured tephras and buried soils with a thickness of 10-20 m (Whitbread-Edwards, 1994). They were observed at Maungatapu, Matua and Omokoroa (Briggs *et al.*, 1996). Furthermore, they include correlatives of the Kauroa Formation (> 0.78 Ma to 2.24 Ma) (Briggs *et al*. 1996; Lowe et al., 2001), which is a very weathered, clay-rich (70-90% clay) sequence up to 12 m in thickness (Lowe *et al.*, 2001).

The Papamoa Ignimbrite (2.40 Ma – 1.9 Ma) consists of multiple pyroclastic flow depositsand tephra-fall deposits. The Ongatiti Ignimbrite (1.34 Ma) is partially to densely welded (Briggs *et al.* 1996). The Te Puna Ignimbrite (0.93 Ma) is the most common ignimbrite sequence identified in coastal sections. Whitbread-Edwards (1994) stated that the Te Puna Ignimbrite was well exposed on coastal cliffs in Omokoroa and is a nonwelded to partially welded brown ignimbrite. Briggs *et al*. (2005) noted that the Te Puna Ignimbrite at Omokoroa overlays lignites and fluvial sands suggesting that it was deposited in a swampy or estuarine environment. Another ignimbrite overlying the Te Puna Ignimbrite is known as the Te Ranga Ignimbrite (0.27 Ma).

The Hamilton Ash sequence overlies the Te Ranga Ignimbrite and has an age range extending from 0.35 Ma to c. 0.1 Ma (the topmost beds have not been dated). It represents a sequence of strongly weathered, clay textured (about 60-85% clay) rhyolitic tephra beds and paleosols (Briggs *et al.*, 1996; Lowe *et al.*, 2001)

with units having a thickness of up to 6 m. This sequence consists of seven defined members (H1–H7) (McCraw, 2011). H1 is the lowest member and is now known widely as the Rangitawa Tephra (Lowe *et al*., 2001). Hamilton Ash may also contain some loess beds (Lowe *et al.*, 2001). Overlying the Hamilton Ash is the Waimakariri Ignimbrite which has no defined age, followed by the Mamaku Ignimbrite which overlies it with an age of 0.22 Ma.

The Rotoehu Ash is a bedded tephra fall unit ranging from 0.3 to 2.4 m in thickness in the Tauranga area (Briggs *et al.*, 1996). Gullivan and Houghton (1980) identified layers of Rotoehu Ash, and recent soils, at 2-4 m depth at Omokoroa. The Rotoehu Ash and associated Rotoiti Ignimbrite (together comprising Rotoiti Tephra) are aged c. 50 ka (Danišík *et al.*, 2012). The post-Rotoehu Ash layer is comprised of a number of tephras mainly from Okataina and Taupo volcanic centres (and Tuhua Volcanic Centre), which are partly blended and weathered in a modern soil-forming environment and hence are not differentiated (see Briggs et al., 2006). The Holocene sedimentary deposits (younger than 11,700 years old) consist of river, stream alluvium and peat deposits which are composed of silts, sands, clays, gravels and carbonaceous material, and estuarine sediments.

2.6 **GIS analysis**

Healy *et al*. (2010) attempted to determine the rate of shoreline erosion for a part of Tauranga Harbour, which includes East Te Puna, West Te Puna, North Motuhoa Island, West Motuhoa Island, and Southeast Motuhoa Island, and Rangiwea Island, as shown in Figure 2.5. This survey was conducted by aerial photography and GIS analysis along coastlines within the eastern area of Tauranga Harbour. This method consisted of using a series of aerial photographs that were scanned at high resolution (1943, 1982, 1996) or orthorectified (2002). The shorelines were digitised after photographs were georeferenced and certain locations were selected for the analysis.

Figure 2.5: Tauranga area showing locations used by Healy *et al.* (2010)

A table was constructed and the resulting analysis was based on the distance from the erosion analysis point selected to the shoreline. Rates obtained from the study varied across the study area with accretion and erosion rates obtained as a result of errors during the processing of the data. The maximum erosion rate was 1.73 m/y^{-1} from 1943–1982 located at Te Puna Beach.

Although the method used by Healy *et al.* (2010) provided rates of shoreline erosion, including for soft volcanic/pyroclastic cliffs, there were errors encountered as a result of not correctly orthorectifying the aerial photographs.

Georeferencing, as mentioned by Healy *et al.* (2010), was also an issue as the aerial photographs lacked control points (houses and roads) in the images.

2.7 Measures for mitigating cliff retreat

The occurrence of landslip failure events around Tauranga coastal cliff sections has caused various geotechnical personnel to develop mitigation measures. This section will address measures for mitigating cliff retreat by enhancing cliff stability, establishing proper drainage and revegetating the cliff slopes.

2.7.1 Cliff stability and construction of protective infrastructures

The construction of protective infrastructures have been utilised by different researches to attempt to stabilise erosive cliffs. Bird (1981) suggested that basal erosion of cliffs must be controlled by protective methods such as sea walls, groynes or beach nourishment to eliminate landslides in the long term.

Keam (2011) proposed remedial options such as earthworks to stabilise the landslip of Bramley Drive. Another method suggested was the construction of a palisade wall with dimensions of 600-750 mm diameter reinforced with concrete piles and erected by 25 to 30 m long anchors. Other options suggested by (Keam, 2011) included the construction of rockfill buttress by dumping 35,000 m^3 of quarry material benched into the slope and installing horizontal drains to remove any groundwater seeping below the buttress. Rather than attempt to mitigate landslip failure, Tonkin & Taylor (2011) suggested an option, particularly for the Bramley Drive cliff landslips, was to allow the cliff to recede until it reaches a stable angle that hinders recession. This will involve setting the fence line for the hazardous area further back and weekly monitoring of the cliff face. For Ruamoana, a recommendation is to restrict public access behind the landslip and set up a safety barrier some distance from the headscarp. This method will reduce the risk of injury or loss of life.

2.7.2 **Proper drainage**

Bird (1981) and Gulliver & Houghton (1980) proposed the monitoring of rising ground water tables within boreholes. Gulliver & Houghton (1980) suggested that monitoring of the water table will provide warnings of possible failure. Bird (1981) proposed lowering the water table after heavy rainfall will reduce risk of failure as well as ensure household drainage is piped to a proper sewage system. Installation of drainage, by placing two drains into the main scarp on the upper and lower surface of the sensitive soil, could also allow the reduction of pore water pressure and thereby reduce recession rates. Drained water has to be collected by perforated pipes and discharged well away from the base of the slope.

2.7.3 **Vegetation management**

Vegetation management is an option that has been used to protect the cliff face from further erosion. This option involved the removal of large trees prone to high winds located at the top of the scarp and the replanting of shrubs at the base of the slope. Shrubs with deep root systems planted on the slopes provide slope stability (Keam, 2008; Tonkin & Taylor, 2011). Keam (2011) stated that the uprooting of the big trees by wind has resulted in the removal of important soil materials, and may continue to cause small-scale shallow seated failures, and therefore such trees need to be removed and replaced with shrubs.

Nautilus (2011) also supported the planting of vegetation cover, particularly pohutukawa plants, since these plants have the ability to withstand steep coastal terrain and are well suited to barren ground which is a characteristic not common to other plants. Furthermore, these plants can tolerate wind and semi-saline conditions (Nautilus, 2011). Therefore, to ensure that these plants have a set spacing along the cliff profile, Nautilus (2011) suggested that these plants have a set spacing along the cliff profile.

2.8 **Summary**

Previous research undertaken has focused on measuring cliff recession rates using various models both internationally and nationally. The methods focused mainly

on measuring cliff recession rates for sandstone or mudstone cliffs. These methods used include model parameters to measure cliff retreat, Airborne LiDAR, Terrestrial laser scanning (Ground based LiDAR), Digital Shoreline Analysis System, Assessing rates using Aerial photographs to identify shoreline changes.

Cliff recession rates were also measured by Healy *et al.* (2010) to determine changes of the shoreline within Tauranga Harbour. However, this research only covered a small part of Tauranga Harbour and generally used the method of analysing aerial photographs. There has not been any further study that covers the entire Harbour area to determine the rate of cliff retreat.

Having reviewed the past literature, and the techniques used to determine the rate of cliff recession methods were identified to suit this research. For LiDAR analysis in this research, the methods that were used involves using the cloud points from Airborne LiDAR to generate DEMs. These DEMs were used to compare with differences in shape and volume changes of coastal cliffs. Another method used involved conducting laser scans and collecting the data from laser surveys to create DEMs to compare with Airborne LiDAR data

The techniques used were carried out on coastal sections within Tauranga Harbour. The underlying stratigraphy of these coastal sections are comprised of soft volcanics : Waitеariki Ignimbrite, Matua Subgroup, Pahoia Tephras, Te Puna Ignimbrite Te Ranga, Hamilton Ash and Rotoehu Ash.

Since coastal sections around Tauranga Harbour have been subject to landslip failures, this issue has raised concerns by residents living in proximity to risk areas to determine the rate of cliff retreat and the pattern of retreat. This is a gap in research and is one of the main objectives to be covered in this research.

Chapter 3
METHODOLOGY

3.1 Introduction

Determining the rate of cliff retreat around Tauranga Harbour was accomplished by two methods: GIS analysis using digital shoreline analysis system (DSAS), and by calculating rate of change from conducting laser scans. The patterns of cliff retreat could be determined by field analysis at various sites. This chapter will discuss the desktop study undertaken used in this research which include GIS analysis in terms of digitizing shorelines and determining the rates of cliff retreat using the DSAS software. It also covers field analysis of selected sites and laser scan surveys of the selected sites.

3.2 GIS Analysis

In order to digitize the coastal cliff edge around the margins of Tauranga Harbour, an aerial image had to be used as a base map. A set of digital orthorectified georeferenced aerial images of surveys conducted around Tauranga Harbour on 9 February 1943 was purchased from New Zealand Aerial Mapping Ltd (NZAM). The images were selected since they are the oldest set of aerial images withheld by NZAM survey collection. These images have fewer control points for digitising compared to photos from recent years as shown in the image of Omokoroa Peninsula in Figure 3.1. Comparing this aerial image to another set of aerial images for 22 July 1982 from NZAM there is a large difference shown by the development in Omokoroa Peninsula (Figure 3.2). A final set of orthorectified aerial georeferenced images from a 2011 survey was also used in the analysis (Figure 3.3). The 8 March 2011 aerial image was the most recent image from NZAM survey collection. By comparing these aerial images from the different years and LiDAR data obtained from NZAM by the Western Bay of Plenty District Council flown between 9 September 2011 and 17 April 2012 was also used for the analysis.

For this research, the cliff top was selected for analysis. This is because it is easier to identify the cliff top from aerial view than the cliff base. In addition, the cliff top is easily identified using LiDAR data. By viewing the aerial images, it was noticeable that the cliff edges could only be visualized in some areas. The cliff tops were obscured in some sections as a result of heavily vegetated cover, particularly trees located near the cliff edge. These particular areas that could not be identified were not included in digitising. The beach shoreline could not be used since it is a complex changing environment that periodically is impacted by wave action causing deposition or erosion of sediment.

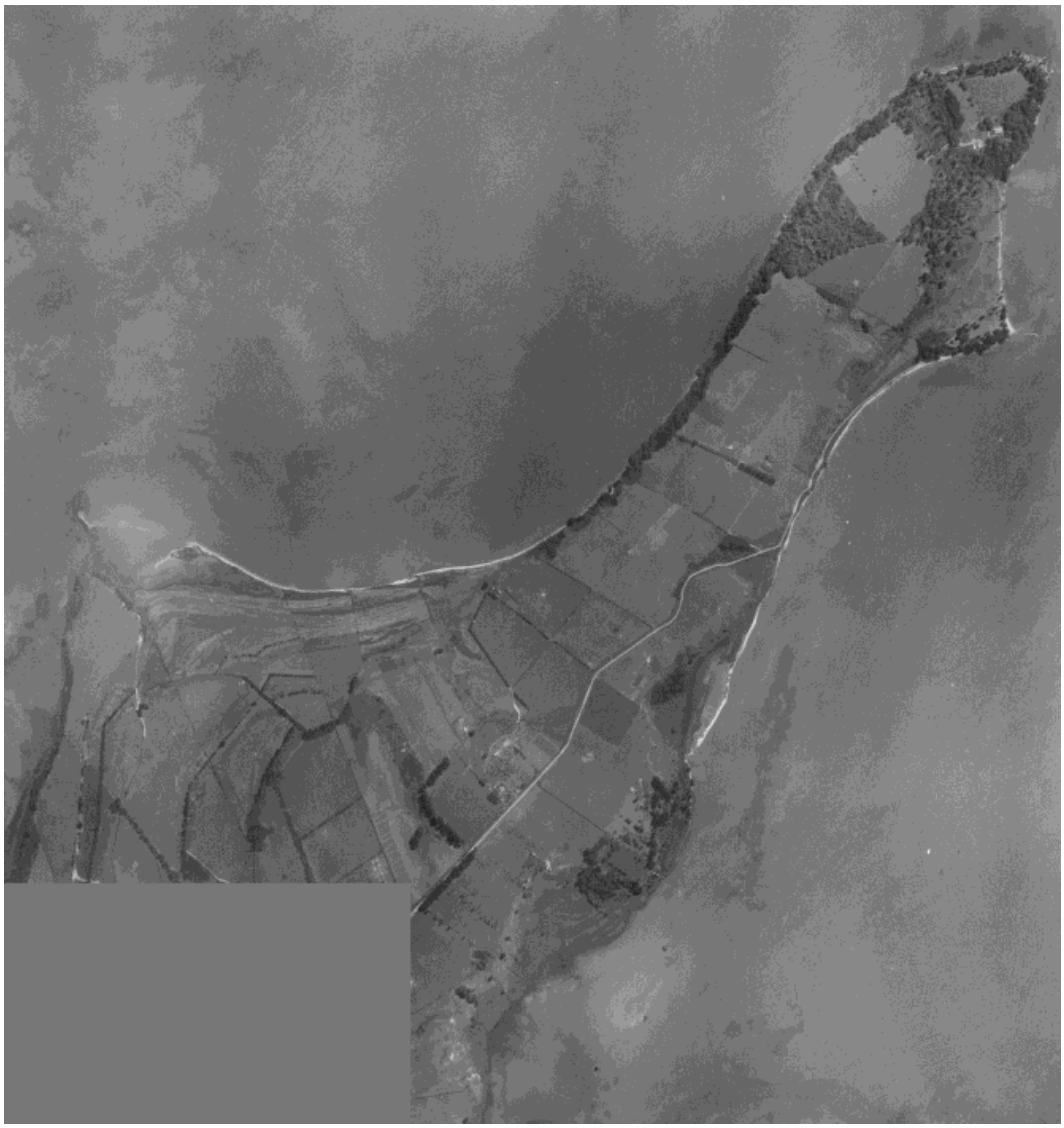

Figure 3.1: 1943 ortho rectified georeferenced photograph of Omokoroa Peninsula (New Zealand Aerial Mapping (NZAM), 2014)

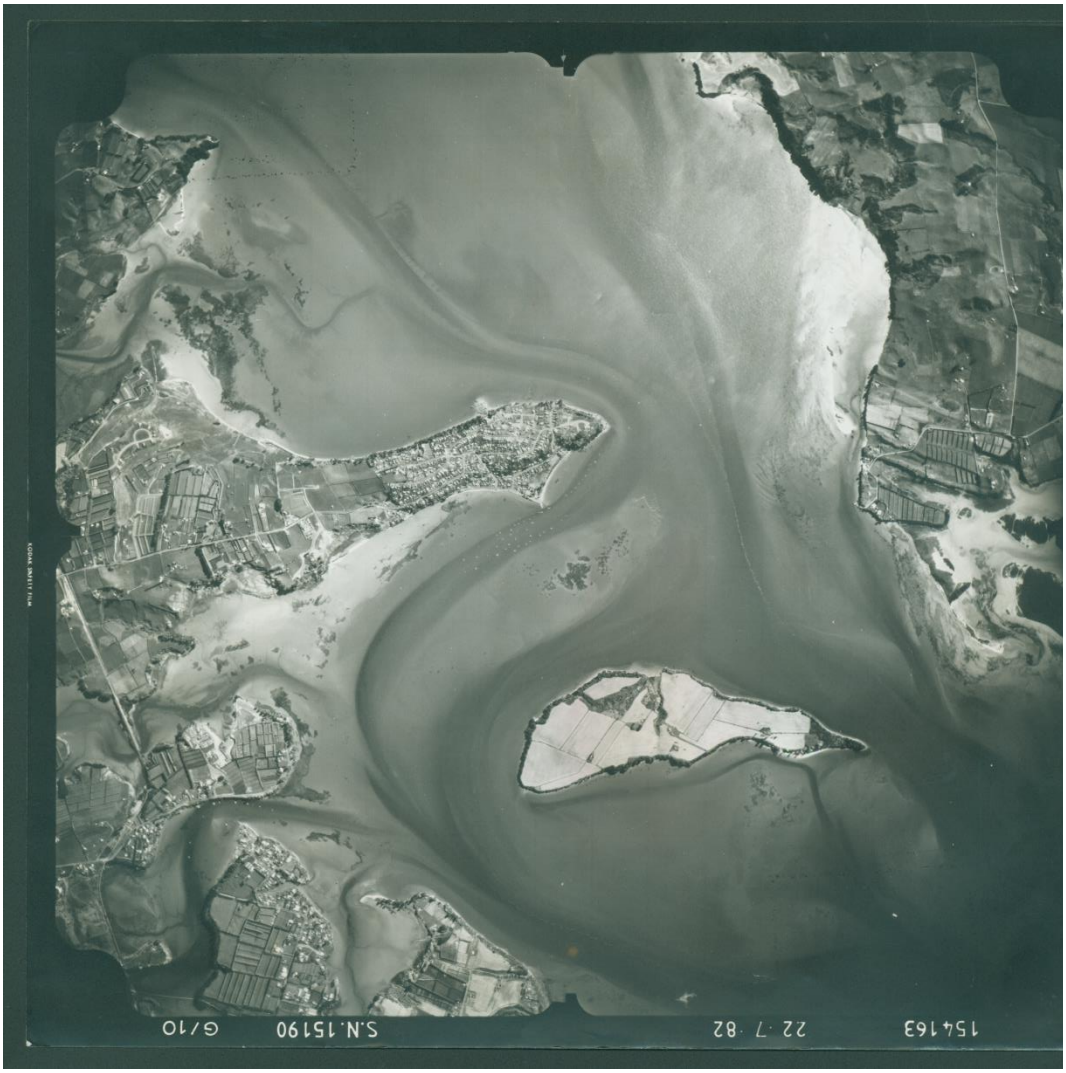

Figure 3.2: 1982 aerial photograph of Omokoroa
(New Zealand Aerial Mapping (NZAM), 2014)

Figure 3.3: 2011 Ortho rectified georeferenced photograph of portion of Tauranga Harbour including Omokoroa Peninsula (New Zealand Aerial Mapping (NZAM), 2014)

3.2.1 **Digital 1943 aerial image**

To help determine the top of the coastal cliff edge on the 1943 aerial image, aerial photo prints flown on the 9th February 1943 (SN 229) were used. When the 1943 aerial photograph was overlain over the 2011 aerial photography it was obvious that the images did not completely align. This is evident by the roads on the 1943 aerial image of Plummers Point, Pahoia and Matahui Points not aligning with the 2011 aerial image. To undertake georeferencing, houses were used as control points if they appeared on both aerial images. After re-georeferencing was completed, the stereopairs were viewed under a stereoscope. The stereoscope enhanced the visualization of the images to appear as a 3D image. This revealed the actual topography of the landscape and confirmed the location of the cliff edge near coastal areas on the 1943 digital aerial image. Although this was a manual task to conduct, it was the only way that the coastal cliff edge could be determined

for this time period. There remained areas identified where the slope break could not be clearly defined. This was because vegetation cover had obscured the cliff top, hence the section was not digitised.

3.2.2 **Digital 1982 aerial image**

For determining the top of the coastal cliff edge for the year 1982 aerial images (SN15190 H/8, H/9, G/8, and G10) were used. The obtained images were not orthorectified or georeferenced. These images were scanned in 300–900 dpi and georeferenced to the 2011 aerial image. The control points used for georeferencing included corners of roof tops, jetties and the centre of road intersections. However, at many coastal sections it was difficult to locate a control point for this aerial image compared to the other aerial sets (2011 and 1943). For this set of aerial images, the cliff top was recognised by just looking for sharp edges that protrude out near coastal section. It was rather difficult to identify the cliff edge in places since the quality of the image was not so good. Six aerial photographs covering the study area were used for digitising the 1982 coastal cliff edge.

3.2.3 **Digital 2011 aerial image**

The digital 2011 aerial image consisted of just 1 photograph sheet for the entire study area (SN50932D). To determine the coastal cliff edge for the 2011 aerial image, LiDAR point data were used to generate DEMs to identify the top of the cliff. The LiDAR data exposed the landscape terrain and clearly showed a distinction between flat terrain and steep slope terrain. This was revealed on the image as dull shades representing flat terrain whilst shiny surfaces portrayed steep slopes. Thus, the cliff itself was clearly visible with the top edge of the cliff being further inland while the base of the cliff being closest to the shoreline. The 2011 aerial image was compared to the LiDAR data for cliff edge determination.

A GIS 3D analyst tool (surface slope) was also used to generate DEMs to assist identifying the top cliff edge. This tool displayed a map with colours representing different slope angles. On the map, the dark green shades represented lower slope angles while the dark red shades represented steep slope angles (Figure 3.4). The

slope analyst image was then compared to the aerial image and LiDAR image using the map analyst tool which allowed the images to be alternated as you scrolled back and forth. By comparing all images, the top of the cliff edge was determined and digitising was completed.

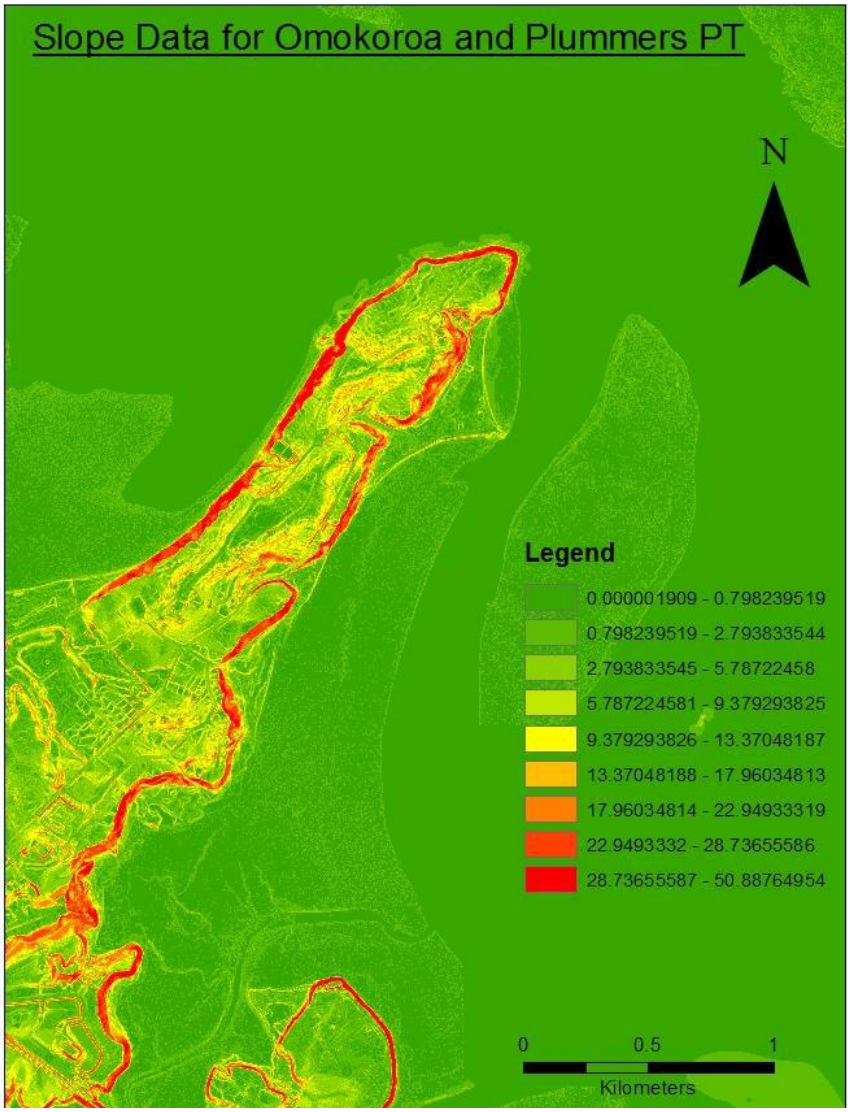

Figure 3.4: Slope image of Omokoroa Peninsula from slope 3D analyst tool

3.3 **Digitising**

The determination of the cliff edge was achieved for all the aerial images using the various methods previously discussed. This led on to the next step of actually digitising the cliff edge onto the aerial image. A shapefile was created on Arc GIS for each year and using the method used for determining the cliff edge the

shapefile was made editable and a polyline drawn over the aerial image representing the cliff edge.

The 1943 shapefile was named *1943 shoreline*, the 1982 shapefile named *1982 shoreline* and the 2011 shapefile was called *2011 shoreline.* The next step involved combining all three shoreline shapefiles as one shapefile to be presented in maps. This combined shapefile was achieved by creating a personal database and importing all shapefiles into the database. The 2011 shoreline was then copied and repasted into the database and renamed as *all shorelines* under the appending tool on Arc GIS. This new feature class named *all shorelines* comprised of 1943, 1982 and 2011 shoreline data combined into a single feature class. The shapefile property of the feature class was then edited so that the three shorelines would be distinguishable as different colour patterns for each shoreline and not appear as one colour pattern (which was what happened when the feature class was created). An example of this is shown in Figure 3.5.

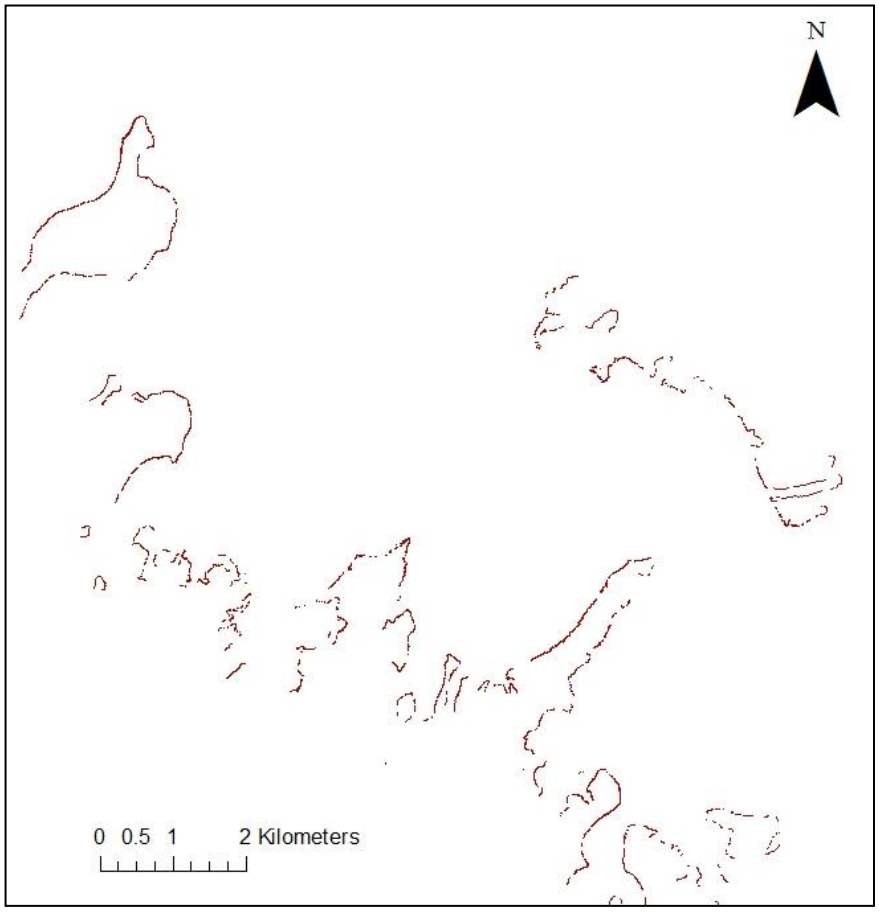

Figure 3.5: All shoreline shapefile

Digital shoreline

3.3.1 **Baseline construction**

After digitising was completed, the next step was to create a shapefile for the baseline. The baseline is used to measure perpendicular distances. It is drawn as a polyline perpendicular to the shorelines. Two methods were used for constructing baselines. They included creating a baseline from a buffer polygon shapefile and creating separate single baseline segments.

3.3.1.1 **Buffered baseline**

The buffered baseline was created from a polygon shapefile having a 10 m buffer around the three shorelines using the buffer tool on Arc GIS. A tracing tool was used on the offshore part of the buffer to create the baselines However, an issue with regard to tracing the buffered line was that the curves of the buffer had to be avoided in order to minimise transect lines being tilted away from the frontal shoreline when they were generated. Therefore, in order to avoid this, only the straight outer part of the buffer polygon was traced, the curved edges of the polygon were not traced (Figure 3.6). The advantage of drawing the baseline this way is that it avoids transects intersecting the shorelines at angles non-perpendicular.

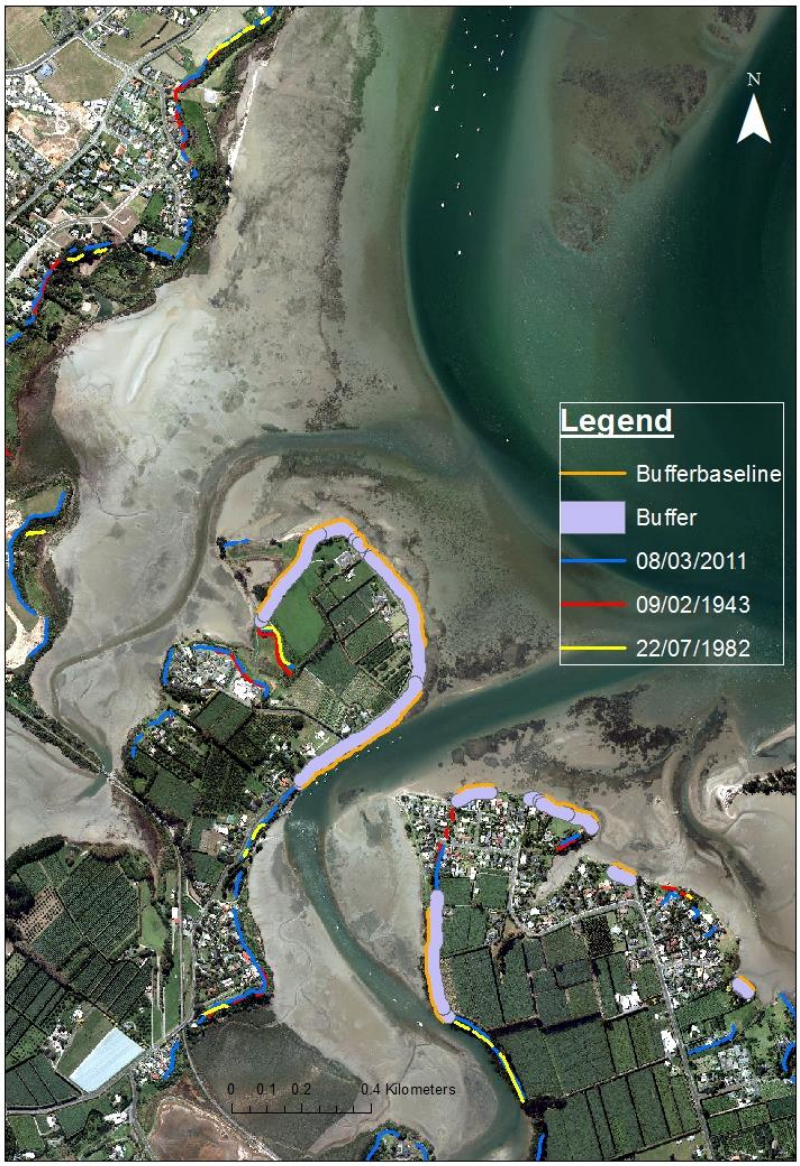

Figure 3.6: Generating buffered baseline using buffered polygon

3.3.1.2 **Straight baseline**

The straight baseline was created from a shapefile comprised of a polyline. It was only drawn where all three shorelines (1943, 1982 and 2011) appeared together alongside one another (Figure 3.7). Other areas without the three shorelines all together were avoided since it was impossible to calculate results using DSAS for fewer than three shorelines. However, in many places the 1982 aerial shoreline was not digitised due to the poor quality of the image; therefore there were fewer areas where three shorelines existed together.

Figure 3.7: Generating straight baseline using polyline shapefile

3.3.2 **Digital shoreline analysis system (DSAS)**

Digital shoreline analysis system is computer software that is used as a tool in Arc GIS. The tool is used for generating transect lines on the existing baselines (buffer or straight) and to calculate the EPR and LRR as well as producing a spreadsheet with the intersect points of all intersections. This spreadsheet shows the position of intersection of transect with the three shorelines.

3.3.2.1 **Generating transect lines**

In order to generate the transect lines, a baseline on the base map had to be selected. Then the length of the transect line had to be determined to ensure that the transect line intersects all cliff shorelines to enable rates of retreat to be calculated. These transects were set at 10 m spacing intervals. Subsequent to having all the properties adjusted for the proposed transect of a specified baseline, the transect was generated (Figure 3.8). Therefore, by selecting a baseline for a particular area, transects can be easily generated and automatically placed against a specified baseline.

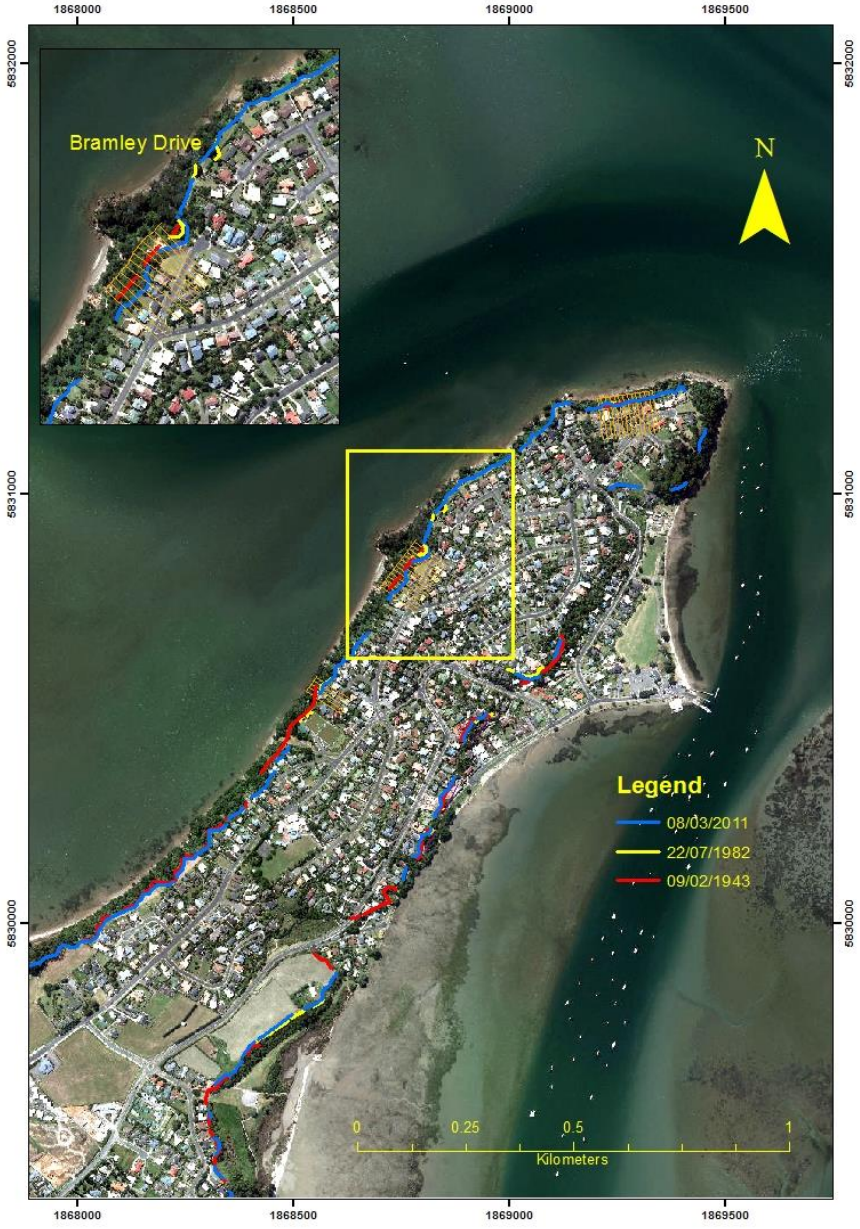

Figure 3.8: Transect generation for baseline on Omokoroa Peninsula

3.3.2.2 **Calculating rates of cliff retreat**

After having generated the transect lines that intersect all the shorelines the next step was to calculate the rates of cliff retreat. To calculate the rate of retreat, the calculate change statistics icon on the DSAS tab on Arc GIS was selected for the transect layer chosen and calculations were conducted. When the calculate icon on the menu was selected, two spreadsheets were produced: the rate spreadsheet consisted of the EPR and LRR while the intersection spreadsheet consisted of the intersection coordinates. The EPR was calculated by dividing the distance of shoreline movement by the time elapsed between the oldest and most recent shoreline (Thieler *et al.*, 2009). This EPR is automatically generated and only calculated where a transect intersects all three shorelines. The LRR on the other hand is determined by fitting a least squares regression line to all the shoreline points for a particular transect (Thieler *et al.*, 2009). This LRR method was not used since there were not enough intersection points for the 1982 data. Therefore, the EPR method was more suitable to use but, to acquire more intersection points, the intersection points were used and manually calculated since there were more intersection points compared to the DSAS-generated EPR. This method included taking the difference for the X and Y intersects and dividing by 68 years to obtain the rate of change per year in meters

3.4 **Laser Scanning**

A 3D laser scanner (Trimble ® VX ^{TM} Spatial Station) was used as another method to acquire the short term rate of cliff retreat. The scanner had a range of 1 to 250 m, measured 15 points per second and a spatial resolution of notionally 10 mm. Surveys were set up with the coordinate system projected at Mount Eden 2000 projection and later converted to New Zealand Transverse Mercator 2000.

Prior to setting up the scanner, three marker pegs were placed at each location: Bramley Drive landslip and at Plummers Point landslip. The pegs were arranged at each location with one or two pegs centered directly facing the landslip (survey sites) while the other pegs were positioned further away as backsights.

3.4.1 **Bramley Drive**

At Bramley Drive two pegs were placed close to the toe of the cliff face known as Bramly 2 (Brm2) and Bramly 1 (Brm1). The peg installed further back from the cliff face was referred to as the Bramly backsight (BrmB) as shown in Figure 3.9. These pegs were installed on the site with the projections presented in New Zealand Transverse Mercator 2000 (Table 3.1). The coordinates have also been presented as World Geodetic System 1984 (Table 3.2). The advantage of having three monitoring pegs is that if one of the pegs is removed or shifted accidently then it could be reinstalled using the other marker peg as a reference.

Figure 3.9: Location of Bramley Drive pegs

Table 3.1: Peg coordinate positions in New Zealand Transverse Mercator 2000

Peg name	Northing	Easting
Brm1	5830889	1868738
Brm2	5830864	1868785
BrmB	5830990	1868806

Table 3.2: Peg coordinate positions in World Geodetic System 1984

Peg name	Latitude	Longitude
Brm1	37 37 47.493 S	176 02 43.009 E
Brm2	37 37 48.260 S	176 02 44.957 E
BrmB	37 37 44.130 S	176 02 45.621 E

The installed pegs consisted of iron rods roughly 1 m in length that were hammered into the ground. A yellow cap with a centre point clearly marked was glued onto the iron rod for visibility. When the scanner was set up it was placed on a tripod that was placed over the centered peg and readings were taken. The scanner functioned by selecting an area to be scanned on the screen, time selected for the scan will determine the resolution of the scan. Therefore, longer scans produce better resolution and more scan points. The laser scanner returns a cloud of dated points with precisely located x,y,z (coordinates and elevation) values.

Scans were either conducted from Brm1 or Brm2. Brm1 is the centred peg shown in.Figure 3.10. The laser scans were conducted at this site repeatedly on 14/05/2014, 11/08/2014, 18/08/2014, 07/09/2014, 23/10/2014, 22/11/2014.

Figure 3.10: Centered peg at Bramley Drive landslip

3.4.2 **Plummers Point**

At Plummers Point, a cliff exposure was selected and three monitoring pegs installed in the proximity of the landslip (Figure 3.11). These pegs were GPS and the coordinates projections presented as New Zealand Transverse Mercator 2000 in Table 3.3. The peg coordinates are also presented in World Geodetic System 1984 in Table 3.4. For conducting laser scans of the cliff face the laser scanner was always placed at the centered peg (Plum 1) positioned adjacent to the cliff scarp (Figure 3.11). The two backsights are Plum B1 and Plum B2. When scans are conducted, Plum B1 is the backsight used for measurements while the other backsight Plum B2 is used as a reference peg. The advantage of the reference peg is to be used to locate the other two pegs if either peg is removed.

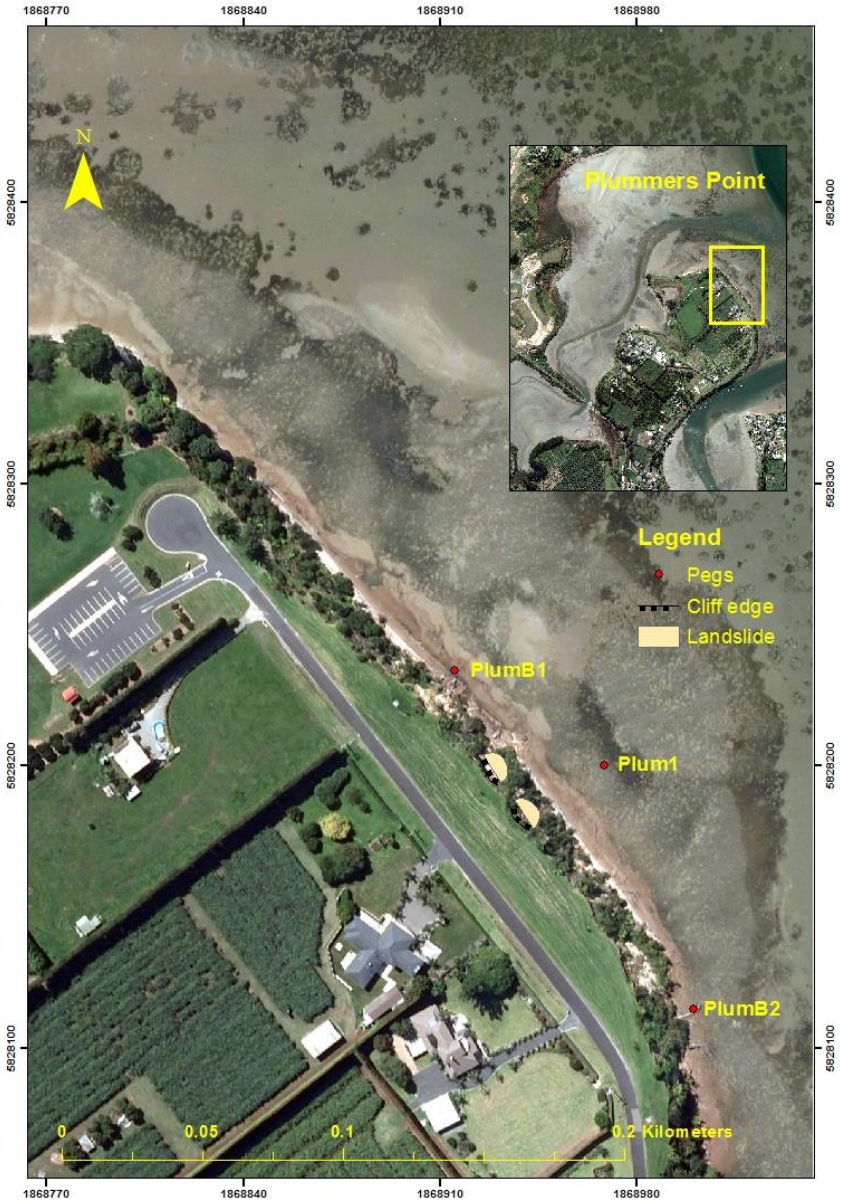

Figure 3.11: Location of Plummers Point pegs

Table 3.3: Peg coordinate positions in New Zealand Transverse Mercator 2000

Peg name	Northing coordinate	Easting coordinate
Plum1	5828200	1868968
PlumB1	5828234	1868915
PlumB2	5828114	1869000

Table 3.4: Peg coordinate positions in World Geodetic System 1984

Peg name	Latitude	Longitude
Plum1	37 39 14.374 S	176 02 55.947 E
PlumB1	37 39 13.328 S	176 02 53.742 E
PlumB2	37 39 17.140 S	176 02 57.362 E

The cliff face at Plummers Point was divided into three sections and scanned separately. The purpose of this practice is to ensure that each section is scanned in detail within a set time frame of about 1.5 hours and, if there is a change in weather conditions, the scan can be completed in one section and continued at another given time. Therefore, there is more accuracy in scanning a small section than scanning a large area and having to re-do the whole scan if certain conditions or technical issues arise. After completing a scan of the first section, the Trimble VX spatial station head is rotated to the next scan section and laser scan conducted. The laser scans were conducted on the following dates: 14/05/2014, 29/07/2014, 07/08/2014, 23/08/2014, 09/09/2014, 11/10/2014 and 08/11/2014.

Figure 3.12: Plummers Point centered peg

3.4.3 **GIS analysis**

After completing a survey, the scan points from each scan is downloaded as an ASCII file and saved as a TXT file. These points were then uploaded on Arc GIS and used to create triangulated irregular network (TIN); these were then converted to raster images (TIN to raster). Once the raster images were created, Arc Scene

was used to view them. This enabled effects such as hillshade to be added, as well as properties to be adjusted to allow the image to float on the surface. The image could then be in 3D, with different shading colours used to reveal the movement of the landslip on the cliff face.

To calculate volume change for a given surface this was carried out using the 3D analyst tool on Arc GIS known as surface volume (3D Analyst). It calculates the area and volume of a known raster data surface above or below a reference plane. The reference plane is the ground level, therefore the volume is either calculated above the ground level or below the ground level. For this research, the surface volume was calculated for above the reference plane.

3.4.4 **Airborne LiDAR data analysis**

LiDAR data was also used for the purpose of obtaining scan points that could be compared to changes post-dating the 2011 landslip failure and torrential rainfall. The LiDAR data (described in section 3.2) consisted of scattered points which were then clipped to reveal only the areas of interest at Bramley Drive and Plummers Point. These points were then used to DEMs and compared to other DEMs from other surveys to distinguish changes in the cliff face and determine a rate of cliff recession.

3.5 **Field description**

Profile description was undertaken at exposed cliff sections at Plummers Point, Ruamoana and South landslip following standard methods from (NZGS, 2005) . The following parameters were described:

- For identifying the soil colour of a layer, a small portion of material was sampled and moistened to reveal the actual colour. The Munsell soil colour chart book was then used to compare the soil colour and designate a colour code.

- The grain size was determined for each identified soil layer using a grain size comparator. Grain size particles are classified as either being organic,

fine or coarse size particles based on the particle size on the grain size comparator. The sample was saturated and was also pressed against the fingers to confirm if it was granular or fine. The saturated soil sample was then tested for quick behavior. Silt displays quick behavior (NZGS, 2005). It has the tendency to liquefy when shaken. Thus, the sample was molded in the palm of the hand as a round ball and shaken to observe if it would liquefy. If it did not reveal such a character then it would be classified as a clay (NZGS, 2005).

- For determining plasticity of a layer, a sample was rolled into a thin rope to observe the plasticity character. If the sample could be molded into a thin rope then it was classified as having high plasticity. However, if it crumbled between the fingers, then it was classified as having low plasticity.

- For shear vane measurements a calibrated hand shear vane apparatus. The shearing procedure used was followed from the NZGS (2011) and Arthurs (2010). The shear vane apparatus consisted of a 16 cm vane blade, 20 cm vane blade and a torque wrench and dial gauge. Depending on the texture of the soil tested determined the type of vane blade that would be used. The smaller vane blade was used for hard soil whilst the larger vane blade was used for weak soil. The small vane was pushed into the soil to a depth of 6 cm when used whilst the large vane was pushed to a depth of 9 cm when used. When the vane was pushed into the soil, the shear vane was turned until the inbuilt spring tightened then it was released and measurements recorded as undisturbed shear strength. The shear vane was then rotated 5 revolutions to remould the soil while it was still *in situ* from the initial measurement. However, there were instances, when the vane could not be pushed into the soil since it was too dry and hard. The undisturbed and remoulded shear strength values were both used to calculate the sensitivity of the soil. Selby (1993) defined sensitivity as

$$Sensitivity = \frac{Undisturbed\ undrained\ peak\ strength}{Remoulded\ undrained\ peak\ shear\ strength}$$
$$(at\ the\ same\ moisture\ content)$$

3.5.1 **Soil/geological classification**

Following the tests undertaken, the soil/geological layers were classified and description names given based on classifications from previous literature on the geology of Tauranga. The soil layers were also measured using a measurement tape to identify the thickness of the layers. Following that procedure, a photograph was then taken and a stratigraphic log was drawn of the investigated site.

3.6 **Laboratory analysis**

Soil piping structures found at Plummers Point were sampled from layers within the stratigraphy to identify dispersive soils. Dispersive soils are susceptible to erosion mostly, but sometimes can be purely physical dispersion (Umesh *et al.*, 2011). Upon saturation the soils erode and segregate causing instability of the earth. The dispersive character is a result of the soil's mineralogical and clay chemistry properties. The following dispersive clay tests were carried out: crumb test, pinhole test and laser sizing.

3.6.1 **Crumb test**

This procedure was carried out following the procedures outlined in Head & Epps (2011) and the standard ASTM D6572 (ASTM International, 2014). The test consisted of just a petri dish filled to near the top edge of the rim with distilled water. A crumb of the soil to be tested measuring 2 cm was dropped at the edge of the petri dish and time recorded for a period of 1 hour to observe any changes to the sample with regard to clay dispersion. The sample was then left over night to observe any further changes after 24 hours.

3.6.2 **Pinhole test**

This test followed the procedures outlined in the Standard ASTM D4647 outlined in ASTM International (2013). However, some steps were not used due to the apparatus used. Tap water was used instead of distilled water to ensure that there was a constant head of 50 mm. Tap water was piped into a container and an outlet valve connected to the pinhole apparatus was used (Figure 3.13).

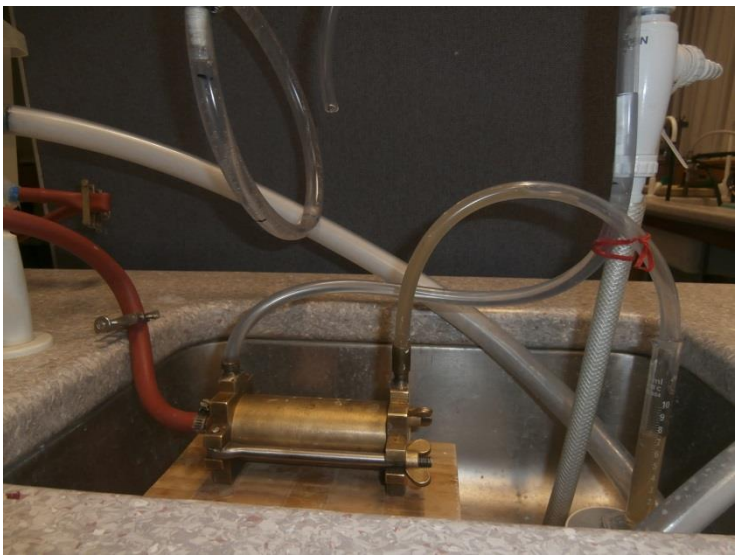

Figure 3.13: Pinhole test apparatus set up

The procedure for carrying out this experiment consisted of a sample of 3.8 cm weighed, sieved and compacted into the pinhole test cylinder which had 2 mm gravel placed at the base of the cylinder with a mesh wire separating the gravel from the sample (Figure 3.14). When the sample was compacted into the cylinder, a pin guide was punctured into the center of the sample creating a 2 mm size pinhole. The pin guide was left in the sample but the pin removed. A mesh was placed on top of the pin guide and more sand gravel placed above the mesh right up to the rim of the cylinder.

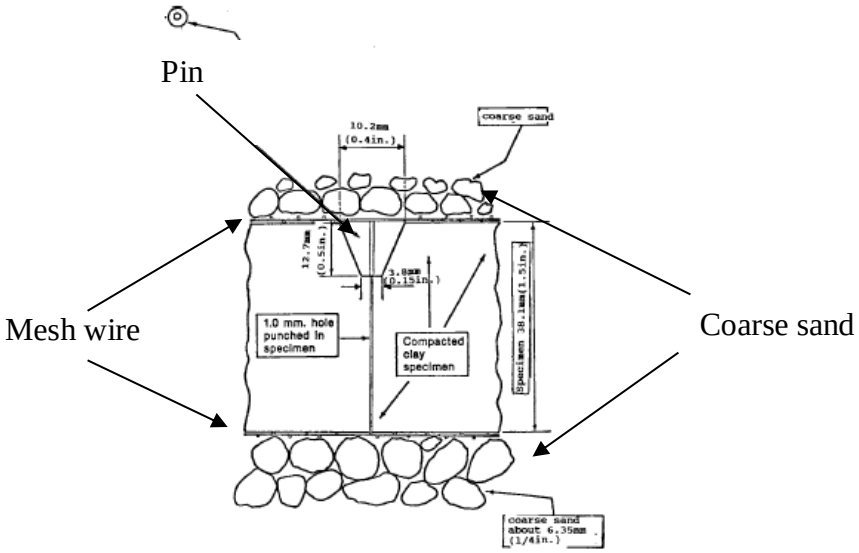

Figure 3.14: Cross section through pinhole test specimen (Sherard, 1976)

After the test was completed, the gravels were removed, and the sample pushed into a small container. The pin guide was removed and the pin hole observed for

any changes in the size of the pinhole. If the hole enlarged then the soil was classified as a dispersive soil. However, if the pinhole remained the same size as the actual pin then the soil would be classified as non-dispersive.

3.6.3 **Particle size analysis using laser sizer**

Grain size analysis was conducted on the samples taken from the soil piping structures at Plummers Point with the use of a laser sizer known as a Malvern Mastersizer 2000. It can detect particle sizes between the range of 0.02 µm – 2000 µm.

A small portion of the sample was placed in a glass jar and it was just enough to cover the base of the jar. Then about 5 g of the sample was subsampled and placed into the laser sizer using a spatula. The first set of samples were firstly tested without pretreatment. However, the second test involved the pre-treatment of samples. Pre-treatment involved adding 10% of hydrogen peroxide to the sample which was used to digest the organic material within the sample. Storage of the samples during the digestion process required having the samples placed in a fume cupboard on a hot plate. Weekly monitoring of the samples was made to observe if digestion had completed its course. This was confirmed when samples stopped bubbling. However, all samples were allowed to stand for a period of 4 weeks to fully digest the organic matter.

The laser sizer was set to run 20,000 measurements. The refractive index setting was 1.5 and the absorption setting was set at 0.2. Furthermore, the sampler settings were at 2500 rpm for pump speed, stirrer speed at 1000 rpm and continuous ultrasound. The pre-measurement delay was 15 seconds.

Chapter 4
DIGITAL SHORELINE ANALYSIS SYSTEM (DSAS) RESULTS

4.1 Introduction

The aim of this chapter is to determine the long term rate of coastal cliff retreat for the entire research area with the use of digital shoreline analysis system (DSAS) software. This chapter is organised firstly by outlining the methods used for analysing the data and assessing which method provided the best estimate for cliff recession rates. Secondly, it uses the best method chosen to determine if there is any relationship between the rate of cliff retreat to the underlying geology of the area. Thus, it tries to correlate rate of retreat with underlying geology.

4.2 DSAS data analysis

The data analysed was for the years 1943, 1982 and 2011. This is a period of 39 years between 1943 and 1982, and 29 years between 1982 and 2011, totaling to 68 years between the oldest and the most recent years. The data obtained from DSAS was analysed for each peninsula within the study area. This provided a better understanding of rates of cliff retreat around each peninsula. Furthermore, it also allowed the comparison of rates of the entire study area to distinguish any relationship between the data and give insight into the causes that may have produced observed variation in rates.

For each peninsula two sets of rates were calculated: one using the buffered baseline type, and the other using straight baseline (see Appendix 1). It was then determined if the rates were similar or different using these different baseline types. This took into account that the buffered baseline may have transect lines intersecting the shorelines at different angles in comparison to the straight baseline which generates transects intersecting in the same direction (Figure 4.1).

Figure 4.1: Straight and Buffer baseline comparison at Matakana Jetty

4.3 **Georeferencing**

The georeference accuracy is considered adequate for the 1943 and 2011 aerial photographs since they were professionally orthorectified and georeferenced by New Zealand Aerial Mapping. However, there was a need to correctly georeference Plummers Point and Matahui Point since the roads in the 1943 aerial photographs did not align with the 2011 aerial photograph. With the 1982 aerial

photograph some images were already available in digital form as they had previously been scanned during the GIS analysis in the report by Healy *et al.*, (2010). Conversely, other images for areas such as Matahui Point, Aongatete and part of Matakana Island had to be scanned prior to georeferencing.

4.4 **Data Analysis**

The results for each region were further analysed in particular locations within the research area (Table 4.1, Figure 4.1 - 4.4) while the raw data obtained from the analysis are shown as spreadsheets in Appendix 1. Each row in Table 4.1 describes the type of baseline used in the analysis and the number of transects that intersect the three shorelines to generate an average rate EPR and linear regression rate LRR calculated by DSAS.

Although EPR calculates the distance from oldest to youngest by the lapsed time, DSAS only calculates EPR values if all three shorelines (1943, 1982 and 2011) are intersected. The 1982 dataset is less compared to that of 1943 and 2011. Therefore, the EPR data generated by DSAS is limited by the points of intersection of 1982. Fewer points of intersection for 1982 correspond to fewer EPR data generated.

Therefore an additional EPR method was included in this analysis which involved manual intersection calculation. This method involves taking the difference of the distances between the baseline and the point of intersection of the oldest shoreline (1943) and the recent shoreline (2011). By calculating the difference in distance between both shorelines to the baseline, the distance between both shorelines can be determined which is the rate of cliff retreat. This method seemed more accurate since it calculated EPR for all 1943 and 2011 for data that intersected at a particular location. As a result, more data was obtained from this method.

Table 4.1: Summary of rates for erosion for regions specified within the research area. Accretion=+ve Erosion=-ve

				End – point rate (m.y^{-1})					Linear regression rate (m.y^{-1})					Manual intersection (m.y^{-1})	
Region	Location	Baseline type	No. of Transects	Min	Max	Mode	Average	Standard Error	Min	Max	Mode	Average	Standard Error	Average	Standard Error
Matahui Pt	West	Buffer	37	-0.22	+0.16	-0.14	-0.10	0.02	-0.22	+0.10	-0.13	-0.09	0.01	-0.06	
		Straight	33	-0.22	+0.09	-0.08	-0.10	0.01	-0.22	+0.10	-0.10	-0.10	0.01	-0.09	0.05
	East	Buffer	9	-0.17	+0.04	-0.17	-0.05	0.03	-0.16	+0.04	-0.01	-0.05	0.02		
		Straight	10	-0.19	+0.06	-0.02	-0.04	0.03	-0.18	+0.06	-0.02	-0.04	0.03	-0.02	0.14
Aongatete		Buffer	68	-0.14	+0.03	-0.04	-0.06	0.005	-0.13	+0.03	-0.03	-0.04	0.005	-0.05	
		Straight	63	-0.18	+0.04	0.00	-0.06	0.005	-0.18	+0.05	-0.07	-0.05	0.005	-0.05	0.004
Turners Pt		Buffer	6	-0.11	0.00	0.00	-0.03	0.02	-0.13	+0.01	0.00	-0.04	0.02	-0.04	
		Straight	3	-0.11	-0.15	-0.11	-0.12	0.02	-0.13	-0.18	-0.13	-0.15	0.02	-0.10	0.02
Pahoia	West	Buffer	21	-0.33	+0.05	-0.09	-0.12	0.02	-0.34	+0.02	-0.07	-0.12	0.02	-0.12	
		Straight	21	-0.22	+0.94	-0.07	+0.01	0.06	-0.22	+1.00	-0.07	+0.01	0.06	-0.04	0.05
	East	Buffer	12	-0.82	+1.14	+0.04	+0.07	0.12	-0.77	+1.19	+0.05	+0.05	0.12	0.07	
		Straight	8	+0.02	+1.19	+0.05	+0.18	0.13	-0.05	+1.23	+0.05	+0.17	0.14	+0.27	0.14
	Southeast	Buffer	22	-0.17	+0.03	-0.01	-0.03	0.009	-0.16	+0.02	-0.01	-0.04	0.009	-0.03	
		Straight	24	-0.10	+0.02	-0.02	-0.03	0.006	-0.11	+0.03	-0.02	-0.03	0.007	-0.03	0.007
Omokoroa	Southwest	Buffer	21	-0.09	+0.05	-0.03	-0.01	0.009	-0.08	+0.05	-0.04	-0.02	0.009	-0.02	
		Straight	18	-0.07	+0.05	-0.03	-0.01	0.01	-0.07	+0.06	-0.04	-0.01	0.01	-0.07	0.06

				End – point rate (m.y^{-1})					Linear regression rate (m.y^{-1})					Manual intersection (m.y^{-1})	
Region	Location	Baseline type	No. of Transects	Min	Max	Mode	Average	Standard Error	Min	Max	Mode	Average	Standard Error	Average	Standard Error
Omokoroa	West	Buffer	5	-0.21	+0.07	-0.21	-0.08	0.05	-0.21	+0.07	N/A	-0.08	0.05	-0.07	
		Straight	7	-0.29	+0.08	N/A	-0.11	0.05	-0.28	+0.07	N/A	-0.11	0.05	-0.08	0.03
	East	Buffer	8	-0.07	+0.07	-0.04	-0.02	0.02	-0.07	+0.07	-0.07	-0.02	0.02	-0.04	
		Straight	6	-0.05	+0.07	-0.03	0.002	0.02	-0.05	+0.06	-0.03	+0.002	0.02	-0.02	0.015
Plummers Pt		Buffer	17	-0.12	+0.01	-0.09	-0.08	0.01	-0.11	+0.02	-0.07	-0.07	0.01	-0.05	
		Straight	17	-0.15	0.00	-0.11	-0.08	0.01	-0.15	-0.01	-0.1	-0.08	0.01	-0.08	0.007
Waitui Reserve		Buffer	10	-0.12	+0.05	-0.03	-0.03	0.01	-0.12	+0.05	-0.01	-0.03	0.01	0.01	
		Straight	10	-0.12	+0.05	-0.02	-0.03	0.02	-0.12	+0.05	-0.02	-0.03	0.02	-0.093	0.01
Southwest Matakana		Buffer	34	-1.12	0.00	-0.16	-0.20	0.08	-1.06	+0.01	-0.07	-0.19	0.06	-0.20	
		Straight	26	-0.26	0.00	-0.05	-0.11	0.02	-0.26	+0.01	-0.19	-0.11	0.03	-0.11	0.05
Central Matakana		Buffer	13	-0.10	0.00	-0.01	-0.03	0.01	-0.09	0.00	-0.01	-0.03	0.01	-0.02	
		Straight	13	-0.11	-0.01	-0.01	-0.04	0.01	-0.10	+0.01	0.01	-0.03	0.02	-0.04	0.02
North Matakana		Buffer	53	-0.32	0.03	-0.16	-0.13	0.02	-0.3	+0.02	-0.14	-0.13	0.02	-0.20	
		Straight	30	-0.30	0.02	0.01	-0.11	0.02	-0.29	+0.02	-0.18	-0.11	0.02	-0.12	0.02

4.4.1 **Graphic results**

Since the EPR data generated by DSAS (Appendix 1) only produced a limited set of data, the manual calculated EPR data set was compared to the DSAS LRR set of data to determine which data set was the best method to use in the analysis. Each dataset consisted of both buffer and straight rate averages. Another comparison is made later in this section to determine which baseline type (buffer or straight) produced the best results.

4.4.2 **LRR and EPR Methods**

The graph illustrated in Table 4.1 shows that LRR datasets have a narrower distribution and a higher peak compared to EPR datasets which have a wider distribution and lower peak. LRR dataset considers all three datasets (1943, 1982 and 2011) while EPR only focuses on two datasets (1943 and 2011). The inclusion of the 1982 data has limited the LRR dataset generated by DSAS. This is because the 1982 shoreline only covered half the area of the other two datasets due poor resolution and georeferencing. The R^2 values for the first half of the dataset averages 0.52 which indicates a weak relationship between the data since it is not close to the regression line. Therefore the EPR data was chosen over LRR. However, the EPR will be further analysed to determine which EPR provides best estimates from either buffer or straight baselines.

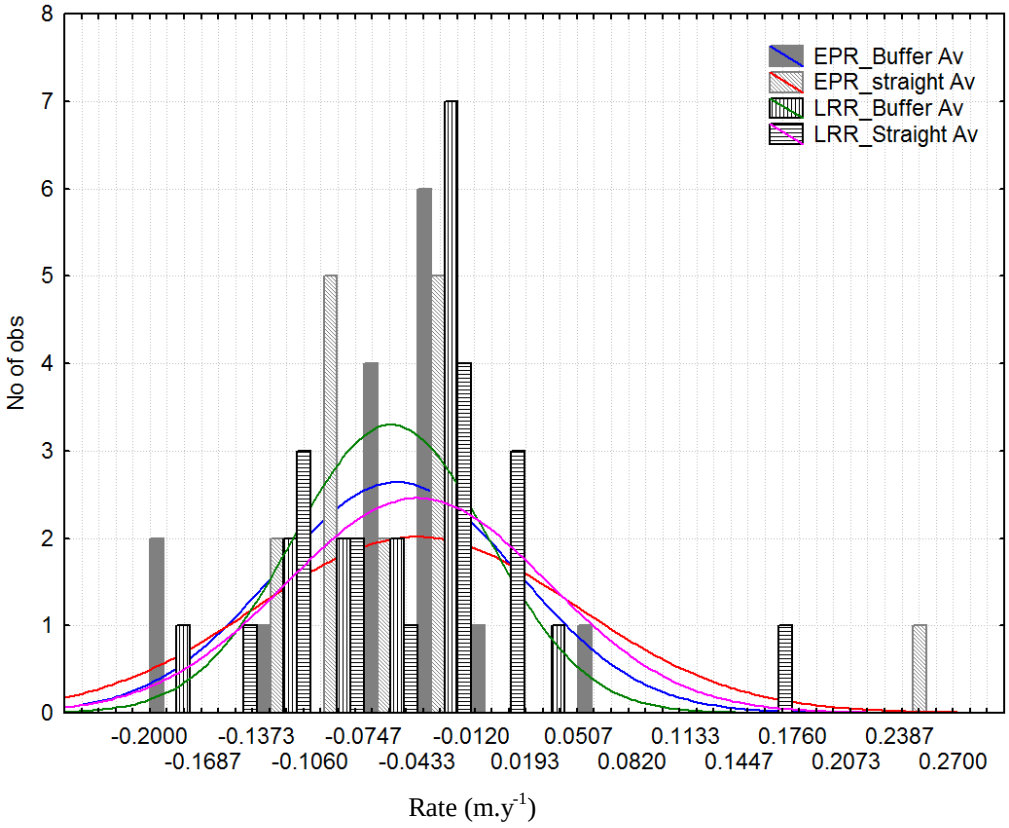

Figure 4.2: Graph of EPR datasets (buffer and straight) and LRR datasets (buffer and straight

4.4.2.1 **Buffer and straight baselines**

The EPR data for buffer and straight baselines was compared graphically (Figure 4.3) to determine which method to preferably use. The buffer method had a more negative peak therefore it is conservative compared to the straight method which has a less negative peak depicting less erosion in its dataset (Figure 4.3). The difference between both methods is that the buffer method has a more peaked distribution with fewer outliers compared to the straight method which has a more spread distribution. Therefore, it is from these results that the buffer method was determined as the best method to be used in this analysis to provide best estimates of erosion rates.

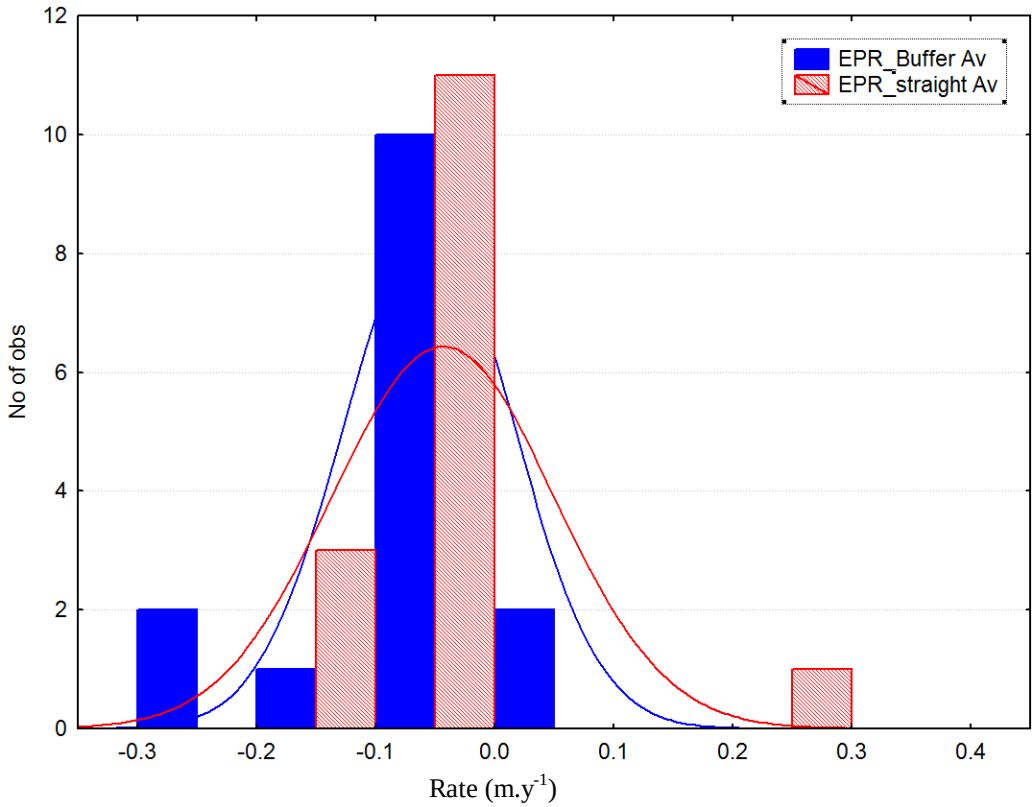

Figure 4.3: Graph of EPR Buffer versus EPR Straight baseline

The minimum EPR derived from buffer baseline is -0.2 m per annum located at Southwest Matakana. The mode EPR for this dataset is -0.05 m per annum located at Aongatete and Plummers Point. Furthermore, the average EPR for the dataset is -0.06 m per annum located at West Matahui.

4.4.3 **Analysis of Buffer baseline**

4.4.3.1 **Minimum average rate (erosion)**

The analysis for the buffer baseline shows a variation in the rates around the Harbour (Table 4.2). These average rate data (Appendix 1) have been overlain on a geological map to determine the relationship between the rate and the underlying geology (Figure 4.4). This information suggests that the highest rate of cliff retreat occurred in underlying geology dominated by Matua Subgroup and Te Puna Ignimbrite. There is the odd occurrence of high rates within the Matakana Basalt and Pakaumanu Group; however, this could be the result of poor

georeferencing. The highest rate of cliff retreat has occurred in Southwest Matakana followed by North Matakana. This is illustrated in Table 4.3.

Table 4.2: EPR buffer data

Region	Location	Minimum ($m.y^{-1}$)	Mode	Average ($m.y^{-1}$)	Standard Error
Matahui Pt	West	-0.23	None	-0.06	0.009
	East	-0.19	None	-0.03	0.009
Aongatete		-0.14	None	-0.05	0.004
Turners Pt		-0.12	None	-0.04	0.02
Pahoia	West	-0.12	None	-0.12	0.02
	East	-0.81	None	0.07	0.1
	Southeast	-0.17	None	-0.03	0.01
Omokoroa	Southwest	-0.09	None	-0.02	0.01
	West	-0.26	None	-0.07	0.03
	East	-0.13	None	-0.04	0.01
Plummers Point		-0.15	None	-0.05	0.006
Waitui Reserve		-0.12	None	0.01	0.05
Matakana	Southwest	-1.12	None	-0.2	0.05
	Central	-0.23	None	-0.02	0.02
	North	-0.44	None	-0.2	0.03

Table 4.3: Relationship between average rate and corresponding geological unit

Region	Location	Average ($m.y^{-1}$)	Standard Error	Geological Unit
Matakana	Southwest	-0.2	0.05	Matua Subgroup (mQam)
	North	-0.2	0.03	Pakaumanu Group (eQp), Alluvial gravel, sand silt and clays of modern rivers (Q1al), Matakana Basalt (IPwt),
Pahoia	West	-0.12	0.02	Matua Subgroup (mQam)
Omokoroa	West	-0.07	0.03	Te Puna Ignimbrite (mQu)
Matahui	West	-0.06	0.009	Matua Subgroup (mQam)

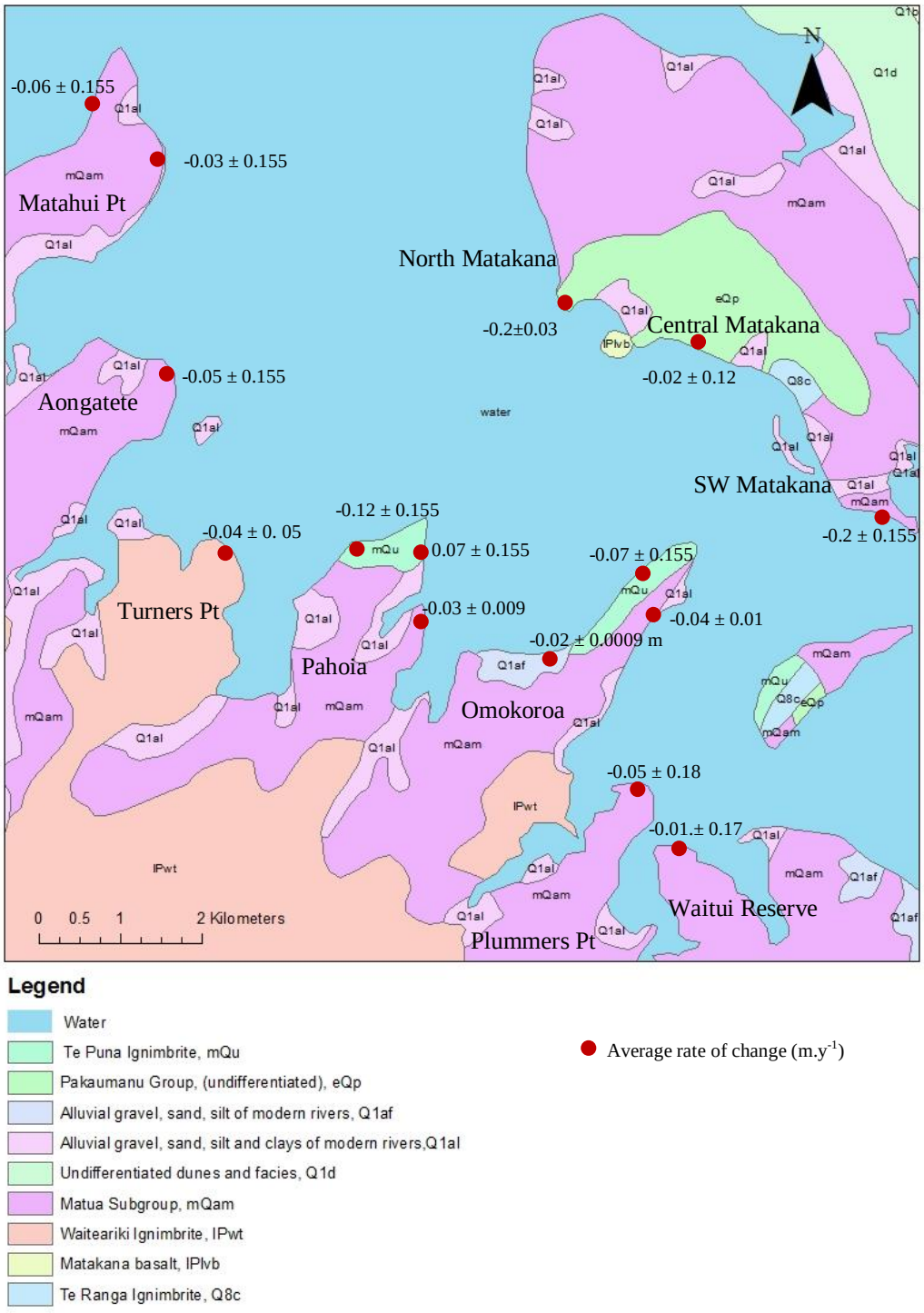

Figure 4.4: Geology map of Tauranga with average end-point rate for buffer baseline (Leonard et al. 2010; Briggs et al. 2005)

4.4.3.2 **Maximum average rate (accretion)**

There were also positive values representing accretion rates which are unlikely to have occurred since cliffs do not have the tendency to accrete but readily erode. This has occurred East Pahoia and Waitui Reserve (Table 4.4). These positive values have been caused by poor georeferencing of the aerial images which has distorted the shorelines from the exact position they should have been positioned.

Table 4.4: Summary table of maximum rates

Region	Location	Minimum	Mode	Average	Standard Error
Pahoia	East	-0.81	None	0.07	0.1
Waitui Reserve		-0.12	None	0.01	0.05

4.5 **Error Analysis**

The two ways used to calculate errors for the DSAS analysis were:

- standard error which is derived from the distribution of rates determined at each transect; and
- georeferencing error.

The georeferencing error was determined by identifying control points present on both 1943 and 2011 aerial photographs. The coordinates were then recorded and Pythagoras theorem used to determine the offset distance. Total error in the rates was calculated using the formula in equation 4-1 which is then divided by 68 to calculate the annual error:

$$error = \sqrt{2 \times (offset\ distance)^2} \qquad (4\text{-}1)$$

Comparing the two types of errors it shows that the georeferencing errors tabulated in (Table 4.5) are greater in value than the standard error in all cases. Therefore, the georeferencing error should be used as the best error estimate.

There is no better result that can be achieved from this data since the aerial photos and orthorectification was properly done by NZAM. Therefore, the errors calculated are still large with the best data made available. It can be concluded

that all rates derived from aerial photo interpretation should be treated with care, including those derived in other studies conducted using similar air photo sets.

Table 4.5: Types of Standard error and Georeference error and their values

Region	Location	Average rate ($m.y^{-1}$)	Standard Error	Georeference Error	Average Georeference Error
Matahui Pt	West	-0.06	0.02		0.155
	East	-0.03	0.03		0.155
Aongatete		-0.05	0.005		0.155
Turners Pt		-0.04	0.02	0.05	0.05
Pahoia	West	-0.12	0.02		0.155
	East	0.07	0.12		0.155
	Southeast	-0.03	0.009		0.009
Omokoroa	Southwest	-0.02	0.009		0.009
	West	-0.07	0.05		0.155
	East	-0.04	0.02	0.17	0.17
Plummer Pt		-0.05	0.01	0.3 0.14 0.10	0.18
Waitui Reserve		0.01	0.01	0.17	0.17
Southwest Matakana		-0.2	0.08		0.155
Central Matakana		-0.02	0.01	0.12	0.12
North Matakana		-0.2	0.02	0.03	0.03

4.6 **Summary**

Overall, the best method to be used to provide best estimates of cliff retreat is using the manual EPR calculations and not the DSAS calculated dataset. This is because there are more points available to be analysed in the manual calculations, whereas the DSAS data is limited to intersection points that include 1982 data. This is the same issue with the LRR dataset generated from DSAS therefore; the Manual EPR calculated dataset is the best method to obtain average rates of cliff retreat.

Further analysis of the EPR data confirmed that the buffer baseline generated EPR method produced better cliff retreat estimates compared to the straight baseline

generated method. The buffer baseline generated method is more conservative while the straight method produces less erosion in its dataset. Thus, the buffer method was chosen as the best method to use.

The buffer data was overlaid on a geological map and this analysis revealed that high rates of cliff retreat had occurred in geology underlain by Matua Subgroup. Other geological units that had considerable rates of erosion included Pakaumanu Group, Matakana Basalt and Te Puna Ignimbrite. However, the most common geological unit with high rates of erosion is the Matua Subgroup as discovered in this research.

Georeferencing errors are unavoidable in any analysis involving aerial photographs. Despite obtaining the best georeferenced photos available, georeferencing is clearly the greatest source of error in the analysis undertaken. Any analysis undertaken using these or similar aerial photographs will inevitably incorporate these errors. Despite this, no better data sources are available to determine long term erosion rates over large areas. Thus these rates represent best, the estimates of erosion rate, but for planning and management purposes it is important to consider the errors and incorporate the errors into any assessment of future erosion.

Chapter 5

FIELD AND LABORATORY RESULTS

5.1 Introduction

The aim of this section is to describe field assessments conducted at selected sites and present the results obtained. The information collected includes the purpose and justification for selecting the site, followed by a description of the geomorphology of each site, and a description of the stratigraphic column. The Bay of Plenty District Council carried out mitigation measures at each site at Omokoroa and this was considered during assessments. The first section describes three sites located on Omokoroa Peninsula. The last section describes a site located at Plummers Point, and includes laboratory results of samples corresponding to three of the selected sites; Pa site, Midway site and Back site.

5.2 Omokoroa Peninsula

The sites selected for field analysis were located at Omokoroa Peninsula and Plummers Point peninsula. Three sites were selected at Omokoroa: they include Bramley Drive landslip, South landslip and Ruamoana landslip located to the east of Bramley Drive (Figure 5.1). These sites were selected since they had visible coastal cliff exposures that revealed the underlying stratigraphy. Furthermore, by assessing these sites, the likely causes triggering these landslips could be determined.

Figure 5.1: Location and Geomorphic Map of Ruamoana landslip, Bramley Drive landslip and South landslip

Bramley Drive

5.2.1.1 Geomorphology

The Bramley Drive scarp located at (N5830855, E1868801 in New Zealand Transverse Mercator 2000) is approximately 60 m in width, with a vertical outcrop of almost 20 m, and the height of cliff top averages about 36 m (Wendt, 2013). In 1979 the scarp retreated 20 m and there was a further regression of 6 m after the 2011 landslip event. There was a further regression of approximately 1.5 m after the occurrence of the April and August 2012 slope failure events. Therefore, in total the volume removed from the cliff scarp was 59,400 m^3.

The main scarp has a circular shape resulting from a rotational landslip activated in 1979 and 2011 (Figure 5.2a). As a result of these landslips, several bench terraces were created extending out from the centre line of the landslip, and

indicated as concave slope breaks in Figure 5.1. The topmost bench is located at the foot of the cliff scarp (Figure 5.2b). At the base of bench 1 is a small bench referred to as bench 2 and below this is a wide-spread area of debris which is bench 3. The base of bench 3 is the high water mark and it comprises debris spread outward offshore resulting from the runout from the previous landslips. Bench 3 is visible as a 'spit' bulging out on the seaward point of the landslip.

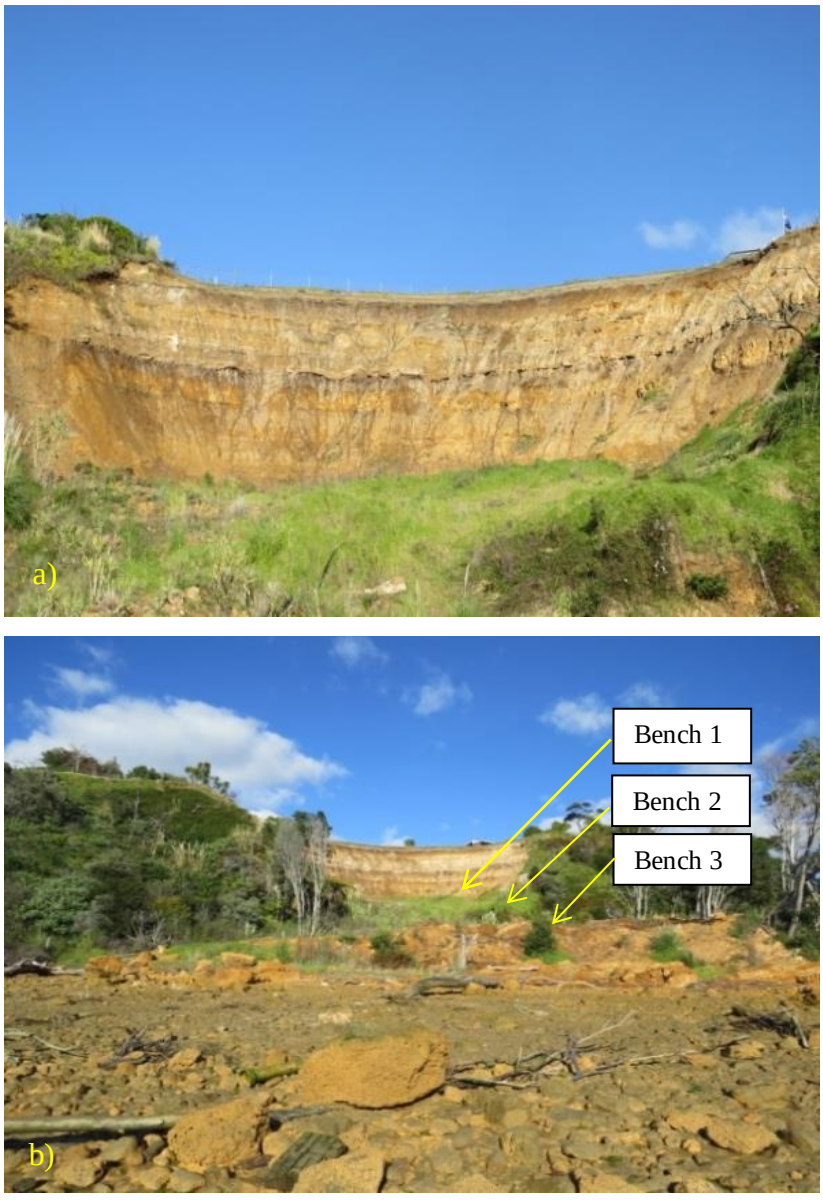

Figure 5.2: (a) Bramley drive scarp (b) Location of benches

The cliff face is still eroding at a small scale. That is, rills were observed on the face. These rills represent channels for water runoff. A paleosol divides the smaller rills in the upper part of the stratigraphy from the larger rills in lower half of the cliff face (Figure 5.3a).

At the base of the scarp, are talus piles (Figure 5.3b). These talus piles have accumulated as a result of debris transported by the rills, or that has fallen as a result of physical weathering conditions (wetting and drying or the effects of wind).

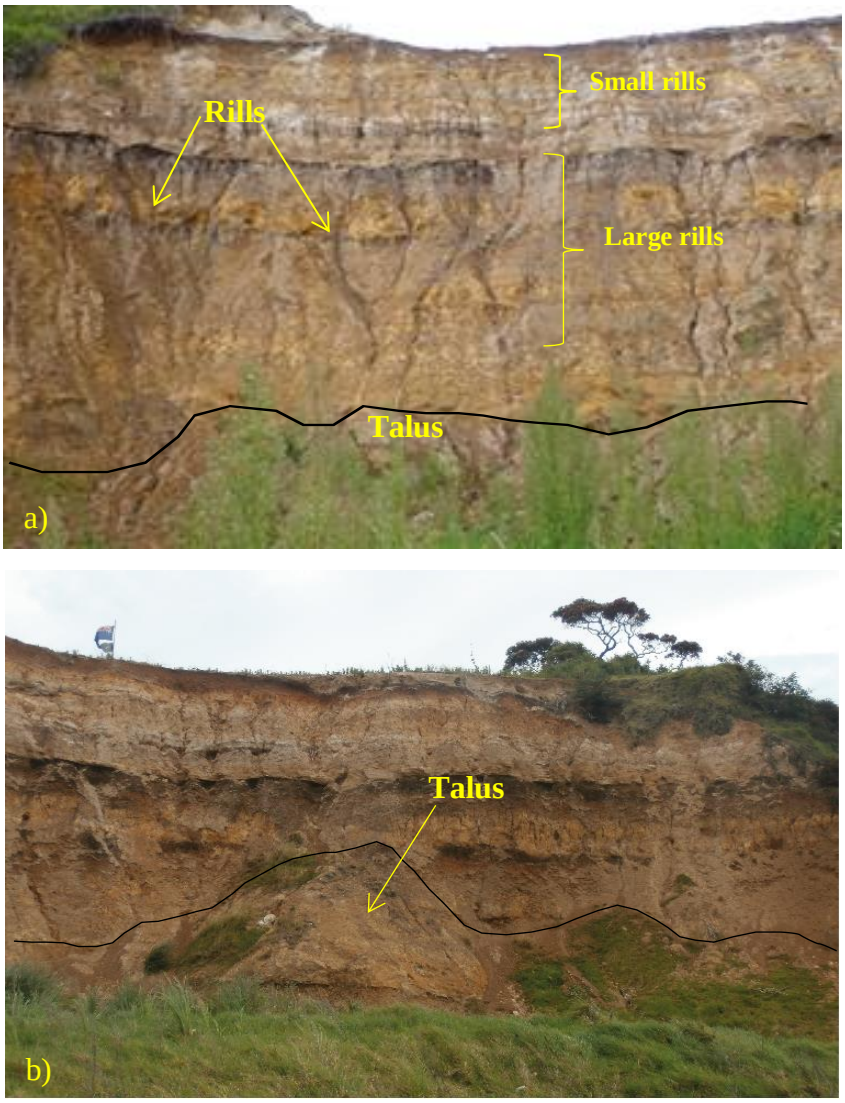

Figure 5.3: Photographs of Bramley Drive cliff , (a) central part of landslip, (b) eastern part of landslip

The western side of the cliff face shows an indication of erosion with fresh exposures on the cliff face, as observed on August 11 2014 (Figure 5.4a). There are no signs of rills on the surface indicating that the debris had presumably fallen as a result of topple failure. A large talus pile is located on its slope flank (Figure 5.4b).

Figure 5.4: Erosion and deposition on western side of cliffs

5.2.1.2 **Stratigraphic Column**

A stratigraphic column of the cliff scarp was previously drawn by (Wendt, 2013), which is reproduced in Table 5.1. The oldest layer positioned at the foot of the cliff scarp is covered with talus. This layer consists of two sequences of the Pahoia Tephra group separated by a distinctive paleosol horizon. The lowest profile comprises of four Pahoia layers while the more recent Pahoia sequence

consists of only two layers. Overlying the Pahoia sequence is the Hamilton Ash, which is comprised of six weathered layers with a distinctive dark brown paleosol on top. This sequence is further overlain by the Rotoehu Ash consisting of one tephra separated here into 2 units based on minor textural variations. Undifferentiated post-Rotoehu tephra deposits comprise the parent material for the modern soil (Figure 5.5) (Briggs *et al.*, 1996).

During site investigations, it was noticeable that at the eastern base of the first bench was an exposure of Te Puna Ignimbrite (Figure 5.6a). The Te Puna Ignimbrite was moist and dense with manganese oxide nodules/concretions. In the sequence it underlays the Pahoia Tephra. Te Puna Ignimbrite was also observed on the western cliff face (Figure 5.6c). Close examination of the layer showed the presence of large pumice clasts and manganese oxide nodules/concretions (Figure 5.6d). However, Te Puna Ignimbrite was absent from the base of the first bench along the central path of the runoff.

Table 5.1: Stratigraphic column of section at Bramley Drive (Wendt, 2013)

Stratigraphic Unit	Layer		Soil Description
	Topsoil	Dark brown	
Post-Rotoehu Ash	L1	Silty clay with sand Brown (7.5YR 4/6)	Columnar soil structure, low plasticity, gradual base, rootlets
Rotoehu Ash	L2	Sandy silt Yellowish brown	Friable, low plasticity, gradational base, shear vane conducted
	L3		Homogenous, loose, non-plastic, shear vane conducted
Hamilton Ash Paleosol	Paleosol	Dark brown	
	L4	Silty clay Very dark reddish brown (5YR 2/4)	Columnar structure, gradational base
	L5	Fine silty clay Orange (7.5YR6/8)	Homogenous, dry, rootlets
	L6	Silty clay with fine sand Grayish yellow (2.5Y7/2)	Homogenous, dry, desiccation cracks
	L7	Clay with some silt Bright yellowish brown (10YR7/6)	Shear vane conducted
	L8	Clay Light gray(2.5Y8/2)	15 cm thick, shear vane conducted
	L9	Clay with some silt Pale yellow(2.5Y8/4)	Homogenous, dry, shear vane conducted
Pahoia Tephra Paleosol	Paleosol	Chocolate brown	
	L10	Clayey silt Bright reddish brown(5YR5/6)	Hard, structured, gradational base, rootlets
	L11	Silty sand Yellowish brown(10YR5/	Homogenous
Pahoia Tephra	Paleosol	Dark Brown	
	L12	Silty clay Reddish brown (5YR4/6)	Hard, structured, gradational base, rootlets
	L13	Clayey silt with sand Yellowish orange(10YR7/8)	Homogenous,smooth,cohesive, slightly wet, gradual base, shear vane conducted
	L14	Sandy silt Bright yellowish brown (10YR6/8)	Homogenous, wet, Manganese (Mn) nodules, sharp base, shear vane conducted
	L15	Silty clay Bright brown (7.5YR5/8)	Homogenous, wet, Mn nodules, Mn rich layers
	End of profile	Debris talus	

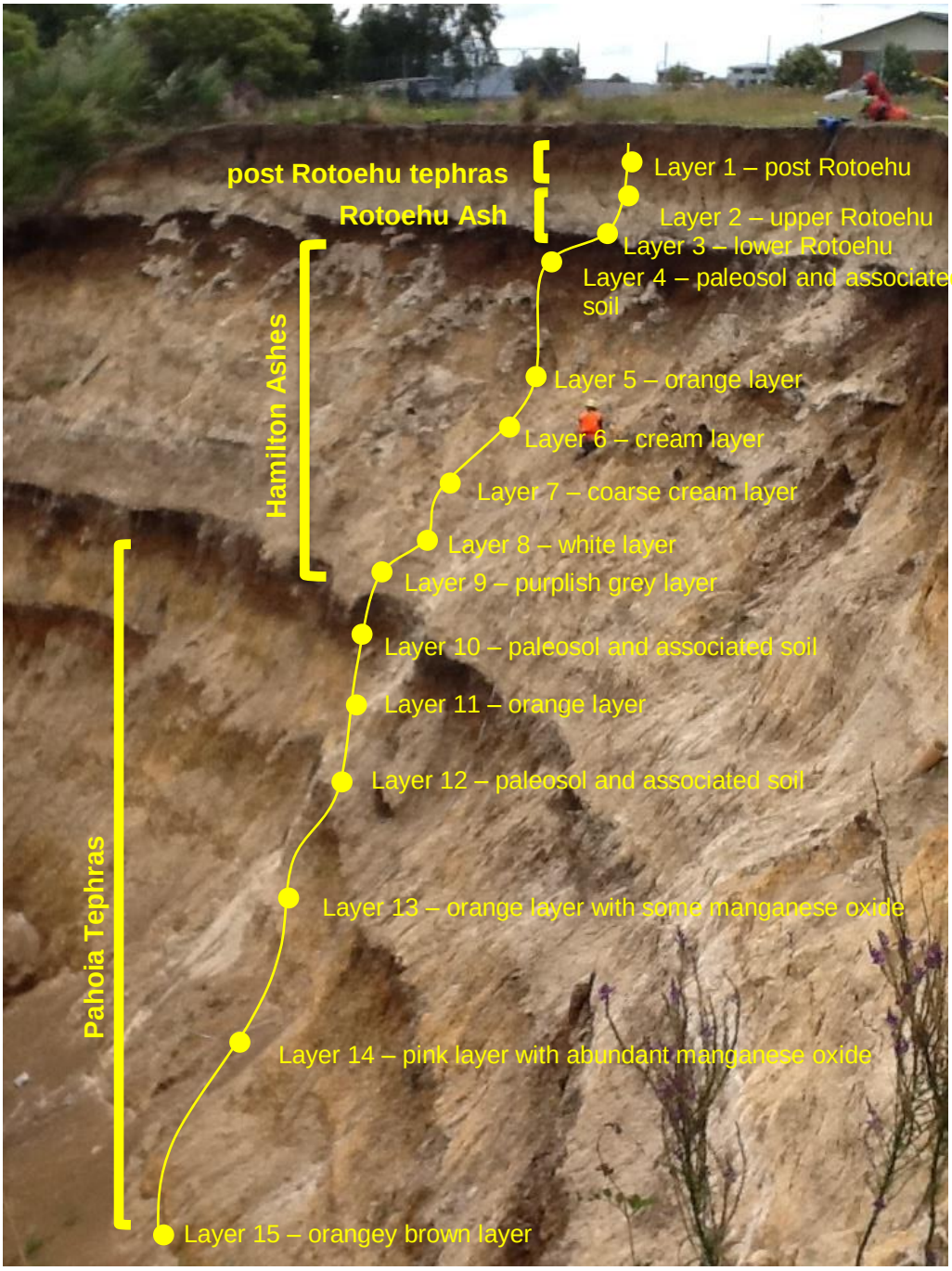

Figure 5.5: Stratigraphic column at Bramley Drive exposure (Moon *et al.*, 2013)

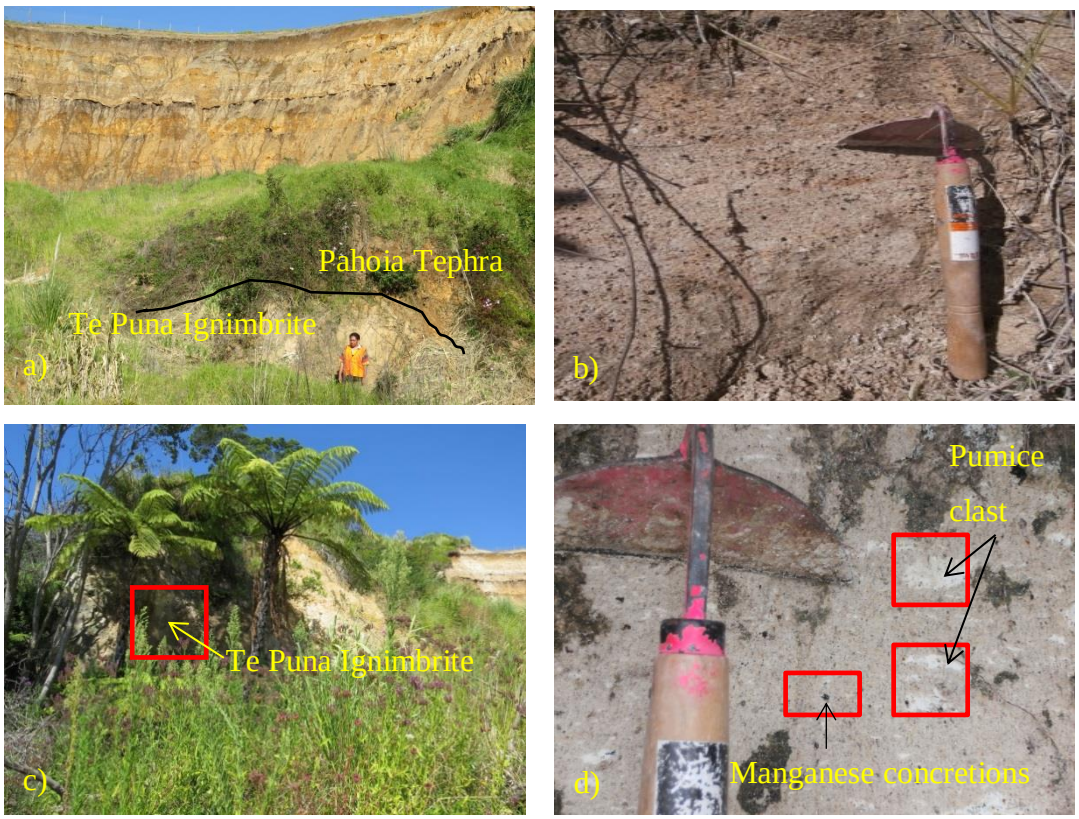

Figure 5.6: (a) Location of Te Puna Ignimbrite below Pahoia tephra (b) close up view of Te Puna Ignimbrite strata (c) Location of Te Puna Ignimbrite on western cliff face (d) close up view of pumice clasts and manganese oxide nodule/concretions in Te Puna Ignimbrite

5.2.1.3 **Engineering works**

During investigations it was noted that some sections of the first bench were quite saturated. Water was flowing out from sources at the base of the scarp, mostly around the central base of the scarp. Poly pipes were also visible at the base of the scarp having been inserted into the base of the cliff face (Figure 5.7). This pipe-work was done to reduce saturation of the Pahoia Tephra.

Figure 5.7: Poly pipes inserted into base of scarp

Plants had been grown to try to stabilise the layer. On the terraces, pohutukawa plants were planted (Figure 5.8). These plants, as suggested by Nautilus (2011), are important as they contribute to stabilising the soil since they have a strong deep root structure.

Figure 5.8: Pohutukawa plants planted on slopes

5.2.2 **South landslip**

This is a small scale landslip in comparison to the much larger Bramley Drive landslip. It is located south of Bramley Drive and is adjacent to 37 and 39 McDonnell Street at (N5830775, E1868699 in New Zealand Transverse Mercator 2000). The slip is situated further inland from the shoreline.

5.2.2.1 **Geomorphology**

This site had steep Te Puna ignimbrite bluffs about 5-6 m in height from the base with the outcrop extending over approximately 30 m. Debris eroded from the cliff face has accumulated at the base of the cliff (Figure 5.9). There are evidence of exposure of the cliff face, which indicating erosion has taken place and the cliff had retreated by topple failure. Although, the site only has a small exposure of coastal cliff retreat, it clearly reveals the underlying geology of the area, which could be identified in the stratigraphy.

Figure 5.9: Steep Te Puna Ignimbrite cliffs

5.2.2.2 **Stratigraphic Column**

The coastal cliff at this section has Te Puna Ignimbrite at the base of the sequence, which is densely packed and moist. This layer is overlain by Pahoia Tephra. In the field it is quite easy to distinguish between the two layers as they are different in colour (Te Puna Ignimbrite is yellowish brown while Pahoia Tephra is bright reddish brown in colour) (Figure 5.11 a, b.).

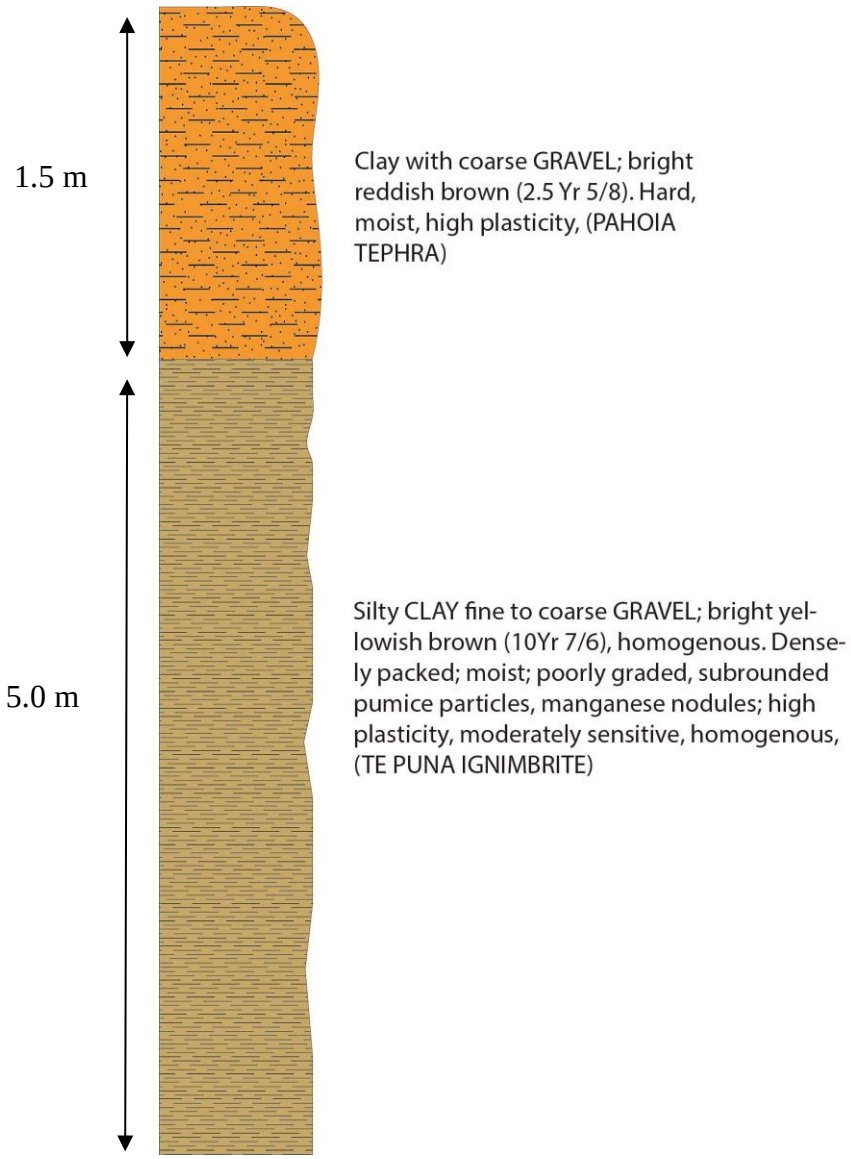

Figure 5.10: Stratigraphic column of section at South landslip

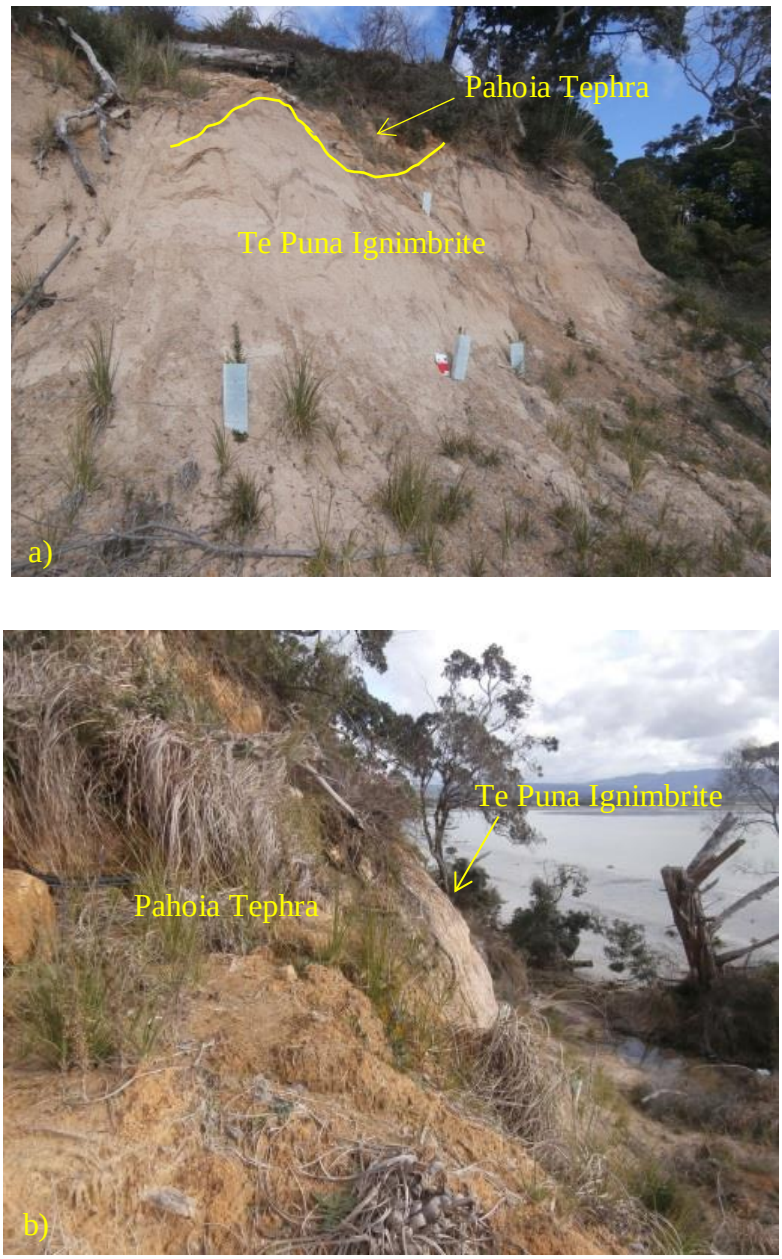

Figure 5.11:(a) Contact between Te Puna Ignimbrite and Pahoia Tephra, (b) view of the stratigraphy from the bench on the Pahoia layer looking down

5.2.2.3 **Engineering works**

Investigations of this site reveal that the base of the Pahoia Tephra layer is quite saturated and there is high water content within the stratigraphy. Water was flowing out from the Pahoia Tephra sequence and flowing over the Te Puna Ignimbrite, suggesting that the ignimbrite is of low permeability. Therefore, to prevent the excess water from triggering any further landslips, water pipes were installed by Waikato Bay of Plenty District Council (Tonkin & Taylor Ltd, 2014) within the Pahoia Tephra to remove water, which was then piped away from the cliff structure and allowed to discharge (Figure 5.12a). In addition to these

methods of stabilising the cliff face, such as plants were planted along the slope flanks and the base of the cliff of the Te Puna Ignimbrite (Figure 5.12b).

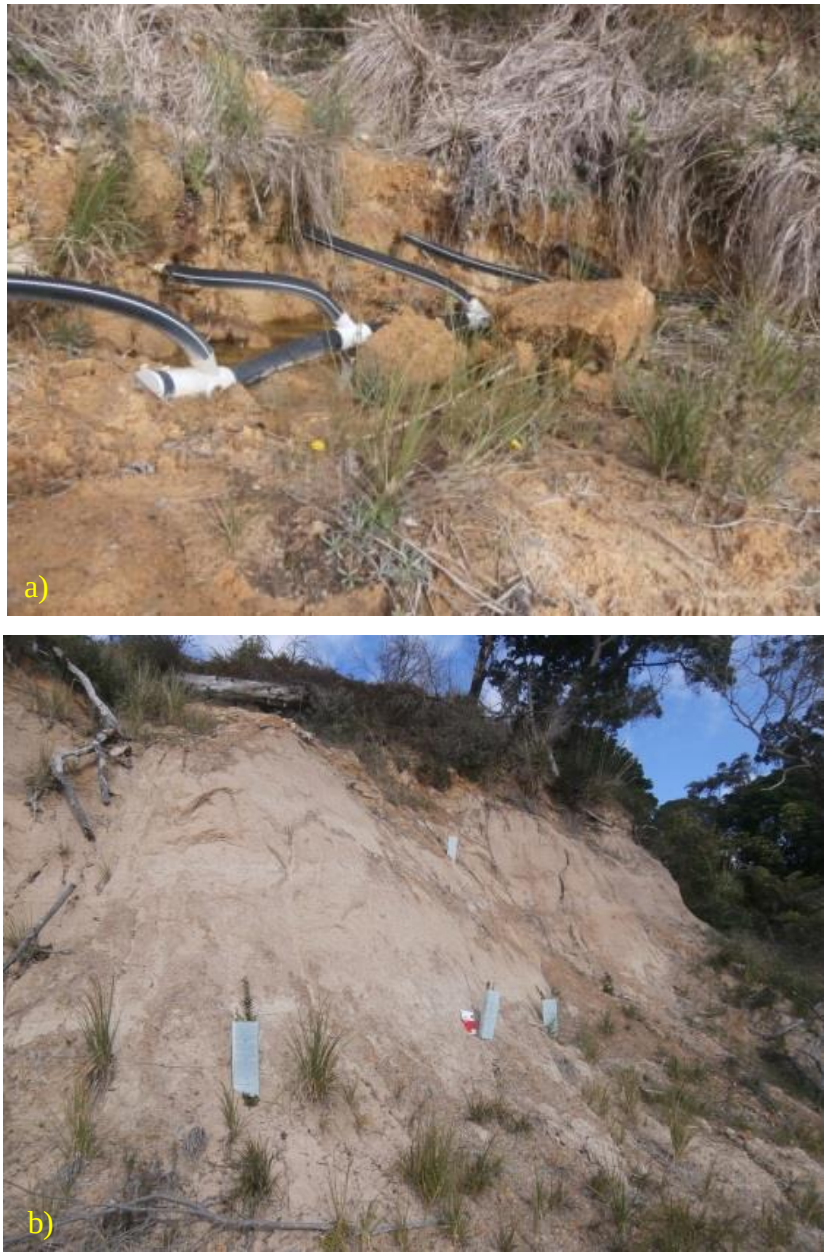

Figure 5.12: (a) Poly pipes inserted into base of Pahoia Tephra (b) plants grown on the slopes of the cliff scarp

5.2.3 **Ruamoana Drive**

This site is located to the north of Bramley Drive at (N5830963, E1868825 in New Zealand Transverse Mercator 2000) and is on the coastal cliffs adjacent to 21 and 28 Ruamoana Place (Keam, 2011), as shown in Figure 5.12. The landslip's location and distance close to residential homes poses a threat to residents close to the cliff edge.

5.2.3.1 **Geomorphology**

The cliff face slopes at an angle, with the upper part of the scarp eroded further inland compared to the face of the cliff which bulges outward. It has been subject to planar failure with talus piles accumulated at the base of the cliff (Figure 5.13a). Located offshore from the landslip are the remains of the run-out located on the coastal part extending a few metres out to the sea. This was caused by a landslip event in 2011.

Figure 5.13: (a) Cliff scarp, (b) run off from landslip

5.2.3.2 **Stratigraphic Column**

The stratigraphic column consists of steep Te Puna Ignimbrite at the cliff base with sequences of Pahoia Tephra, Hamilton Ash beds and Rotoehu Ash that overlie it. A good exposure is on the southern side of the cliff face with the stratigrahic column (Figure 5.14a, b). The ignimbrite contains manganese oxide concretions amidst fine pumice and large pumice clasts (Figure 5.16). Overlaying the ignimbrite is the Pahoia Tephra.

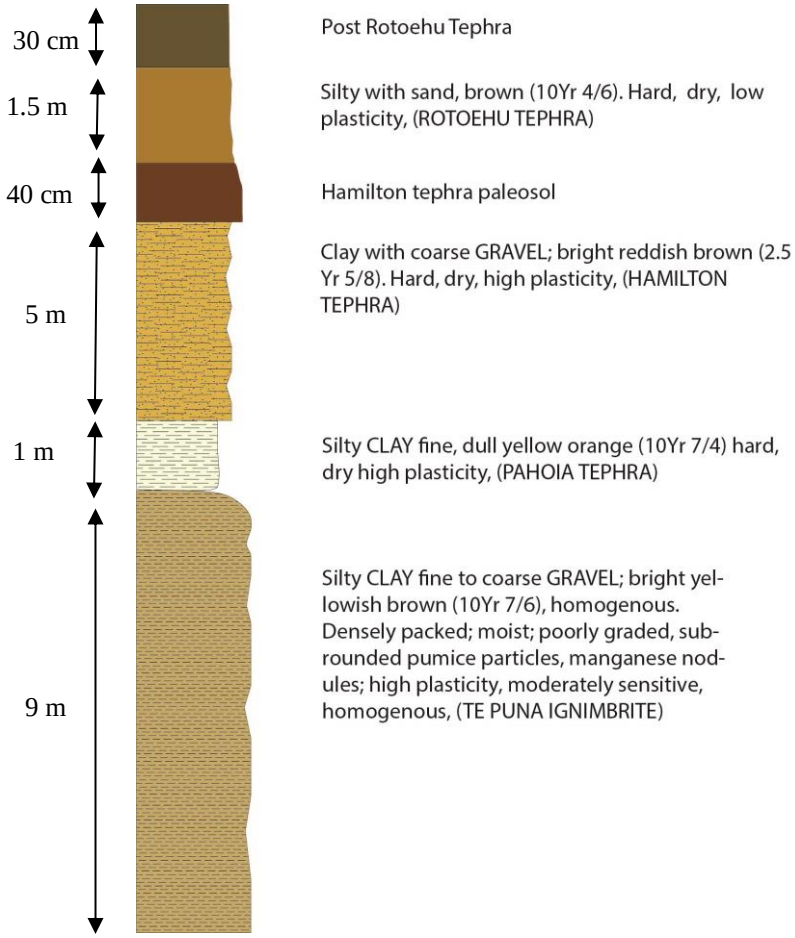

Figure 5.14: Stratigraphic column at Ruamoana

Shear vane tests were carried out for the Te Puna Ignimbrite layer. The shear strength measurements results were (34/25, 44/25, 69/10, 62/25, 66/27 kPa). These results were averaged and classified as moderately sensitive.

Figure 5.15: Location of stratigraphic section and position of the geological units

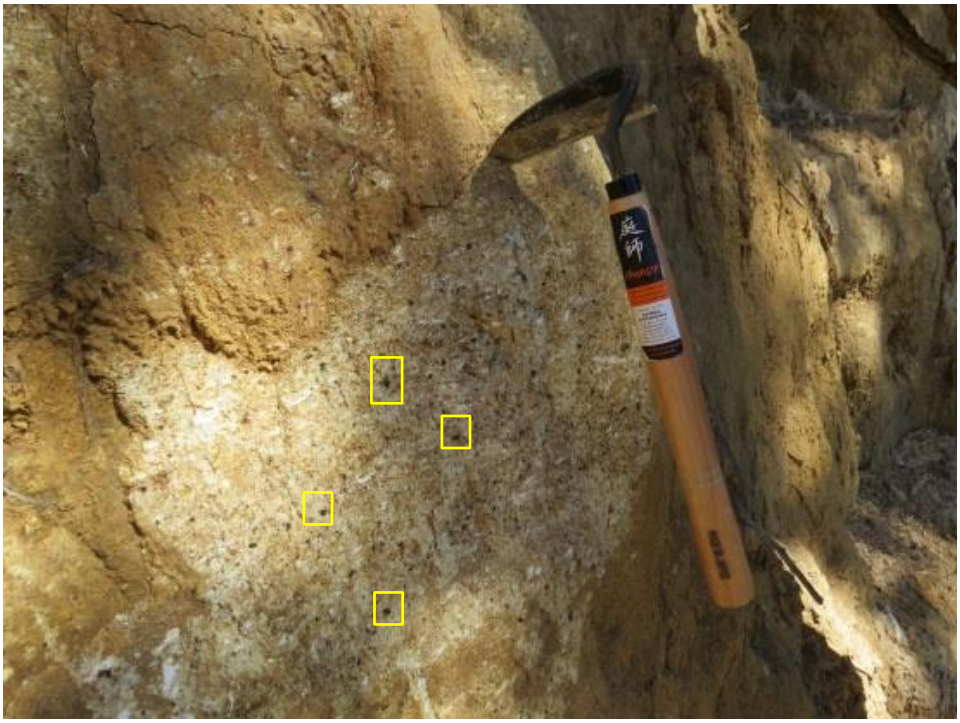

Figure 5.16: Close up view of Te Puna Ignimbrite with numerous manganese oxide concretions (wet-drying repeatedly)

5.2.4 **Engineering works**

In order to stabilise the cliff structure and minimise further erosion poly pipes have been installed to remove excess water that may saturate the layers in the stratigraphy (Figure 5.17). Furthermore, plants were also planted along the hill slopes to stabilise the cliff structure (Figure 5.17).

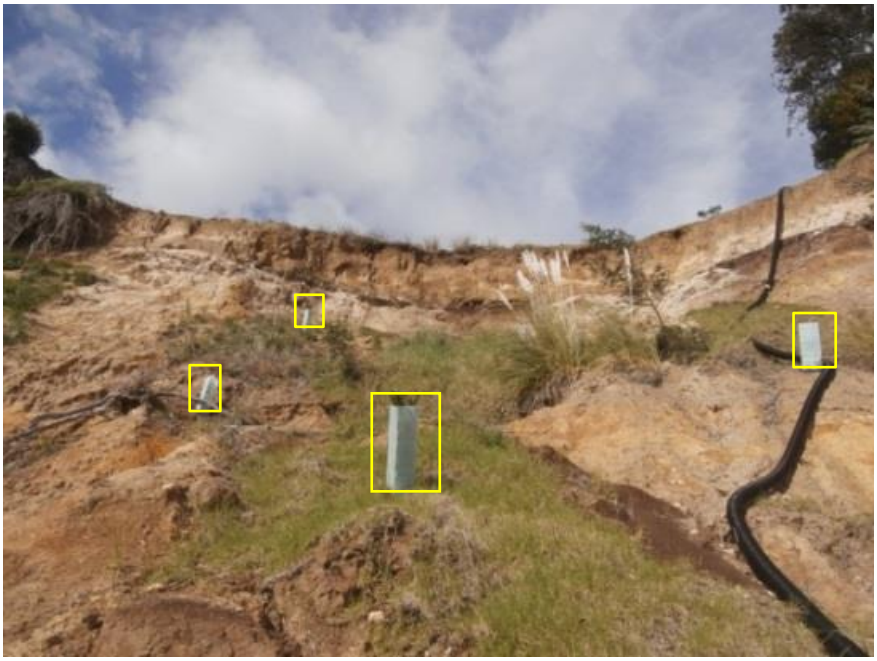

Figure 5.17: Poly pipes visible over the scarp and plants planted on the slopes of the scarp

5.3 **Plummers Point**

This site is located east of the Omokoroa Peninsula and is a peninsula itself with coastal cliffs that are retreating. A coastal cliff section with prominent exposures was investigated, referred to as Main site, along with three other sites that had piping structures. These site are known as Pa site, Midway site and Back site.

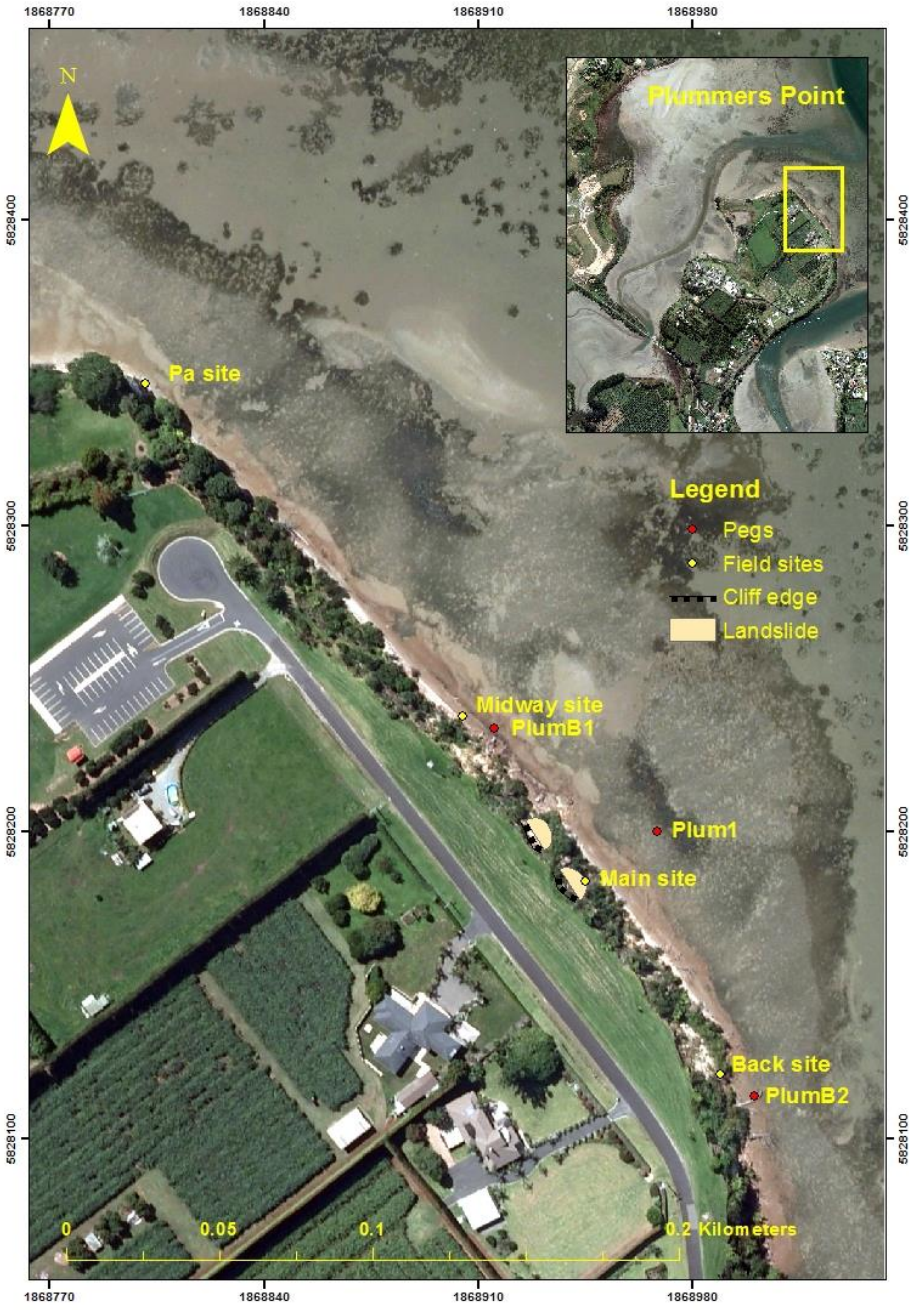

Figure 5.18: Location of field sites at Plummers Point

5.3.1 **Main site**

5.3.1.1 **Geomorphology**

The Main site is a coastal cliff section site located at (N5828184, E1868945 in New Zealand Transverse Mercator 2000). It has been subject to planar failure and is approximately 6.4 m in depth and 20 m in width with exposures indicating continuous erosion of the cliff scarp. Talus piles are located at the base of the scarp (Figure 5.19). The talus piles are quite visible in some sections, whereas in

other areas they are obscured and appear as vegetated benches consisting of historical talus piles.

Figure 5.19: Main site cliff section at Plummers Point with location of log

5.3.1.2 **Stratigraphy**

The stratigraphy at this site consists of eight layers (Figure 5.20). The total height of the cliff face is approximately 7 m (Figure 5.19). The stratigraphic column revealed interbedded with sandy SILT, clayey SILT and silty CLAY layers. These layers generally are dull yellow orange and yellowish brown in colour. The stratigraphy consists of three Pahoia layers and four undifferentiated layers. The layers close to the base of cliff are moist, while layers halfway up the cliff section are relatively dry. Photographs of the stratigraphic units are presented in Appendix 2.

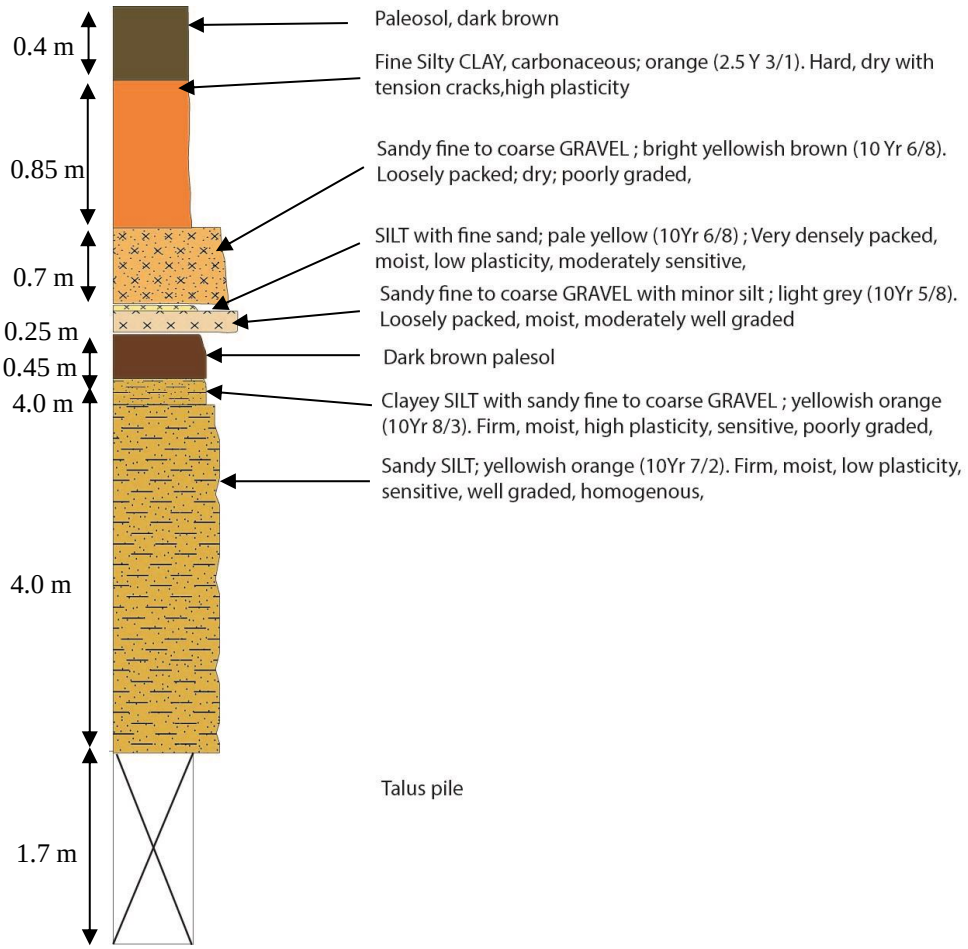

Figure 5.20: Stratigraphic column at Main section, Plummers Point

Shear vane results collected for the sandy SILT layer were 34/37, 53/22, 12/16, 37/12, 50/25 in kPa revealing moderate sensitivity. The clayey SILT layer had shear vane results of 37/6, 55/8, 47//6, 47/6, 50/6 in kPa. The average of these results indicates that the results are sensitive. The sandy fine to coarse gravel layer was also tested. The results obtained were 48/12, 56/9, 37/12, 50/16, 53/8 showing that the layer is sensitive.

5.3.2 **Piping**

Investigations of the surrounding areas in the proximity of the eroding coastal cliffs also reveal recent landslip exposures at the base of the cliff. Some of these sections (Pa site, Midway site and Back site) had the presence of piping structures (Figure 5.21 a, b, c). These features encouraged further analysis of the material, which is discussed in the crumb and Pinhole test section (5.3.5).

Figure 5.21(a) Pa site (b) Midway site (c) Back site

5.3.3 **Pa site**

This site is located at the northern point of Plummers Point, positioned at (N5828347, E1868802). The site is located below a Pa site. It is exposed as a coastal cliff at the western side of the peninsula. Furthermore, the site is located in close proximity to the shoreline.

5.3.3.1 **Geomorphology**

The Pa site consists of a cliff face approximately 9 m in depth. Although the cliff face is a relatively dense structure, joints on the cliff face may cause instability.
At the base of the cliff face is an eroded layer which may be the result of marine erosion or piping structures. The piping layer has a height of 69 cm and a depth of 65 cm.

This piping structure is located within the third layer from the base, and is comprised of clayey SILT layer. The presence of piping may induce instability as a result of reducing support from the base layer. It is for this reason that this site was selected to determine the susceptibility of the material to piping.

5.3.3.2 **Stratigraphic column**

The stratigraphy at the cliff exposures could be determined and tested based on field description. It consisted of six layers which could be reached and identified. These layers belong to sand, silt and gravel deposits of Holocene streams. As a result of the composition of the layers, shear vane tests for this site could not be carried out since the layers were either too hard for the vane to penetrate or too sandy/gravelly. The cliff face logging revealed that the layers comprised an alternating sequence of fine sandy SILTS and coarse grained clayey SILTS (Figure 5.22). The third layer from the base of the stratigraphy consisted of fine grained clayey SILT which had the presence of piping structures. The stratigraphy at the Pa site belongs to the Matua Subgroup. Photographs of the stratigraphic units are presented in Appendix 2.

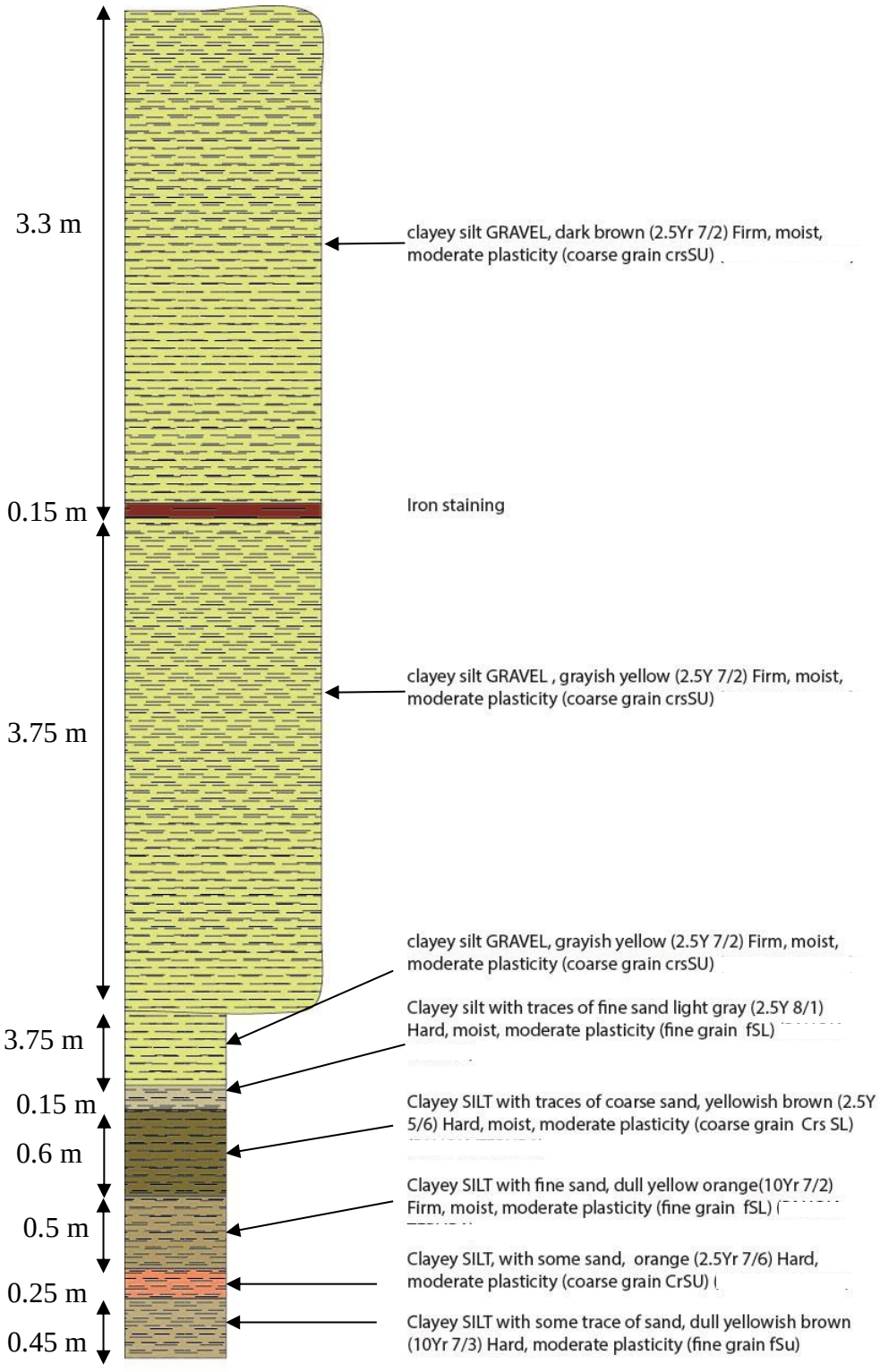

Figure 5.22: Stratigraphic column of the Pa site, Plummers Point

No shear vane tests were carried out for these samples since they were either too coarse grained or too hard. The base unit was too hard for the shear vane to penetrate through and other units were too granular.

5.3.4 **Midway site**

This site is located at this position (N5828238, S1868905 in New Zealand Transverse Mercator 2000) which is between the Main site and the Pa site (Figure 5.18). It is a recent exposure with the presence of piping. It is for this reason that it was analysed to try to determine the possible causes for the collapse of material.

5.3.4.1 **Geomorphology**

The landslip is about 2.25 m in depth. The exposure is a vertical cliff face with topple failure occurring in the lower units which resembles initial stage of piping. The piping structure was located within the layer one which is at the base of the stratigraphy. It is about 2-3 m from the mean high water mark level.

5.3.4.2 **Stratigraphic column**

The logging of this exposure was logged in a section line with the piping centred at the base of the stratigraphy. The cliff face logging (Figure 5.23) revealed from base to top interbedded sandy SILT, Paleosol, Clay, sandy CLAY, silty CLAY and silty SAND. These layers had a range of colours dull yellowish brown to light grey. A sandy CLAY layer was quartz rich with volcanic clasts. It consists of a sandy SILT layer with a height of 74 cm and depth of 60 cm. Photographs of the stratigraphic units are presented in Appendix 2.

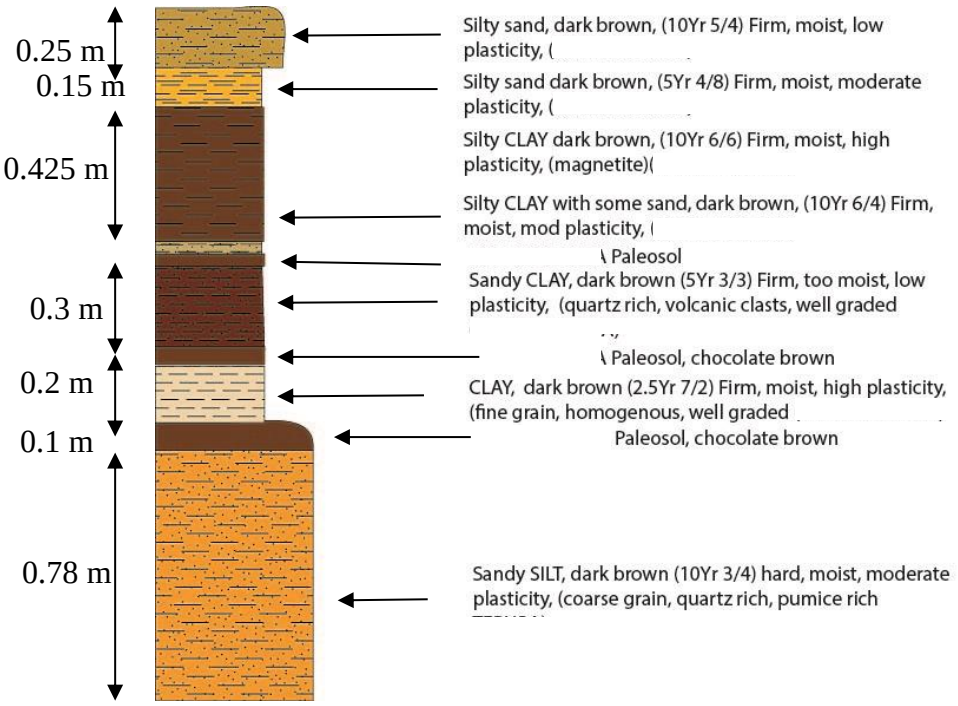

Figure 5.23: Stratigraphic column at Midway site, Plummers Point

5.3.5 **Back site**

This site is located east of the Main site at the following coordinates (N5828121, S186989 in New Zealand Transverse Mercator 2000). The exposure is relatively small in comparison to the other sites with piping. It has a depth approximately just over 2 m from the base of the cliff.

5.3.5.1 **Geomorphology**

The cliff exposure is subject to topple failure. Located at the base of the exposure it had the presence of a piping structure. The piping had a height of 45 cm, width of 88 cm and a depth of 60 cm (Figure 5.24).

5.3.5.2 **Stratigraphy column**

A stratigraphic column was generated from a straight line running directly through the piping structure. The total height of the cliff exposure is just over 2 m. Logging of this exposure revealed interbedded clayey SILT and SILT layers. It had colours from dark brown to red gray. The soils were relatively moist. The descriptions of the exposure are shown in Figure 5.25. Photographs of the stratigraphic units are presented in Appendix 2.

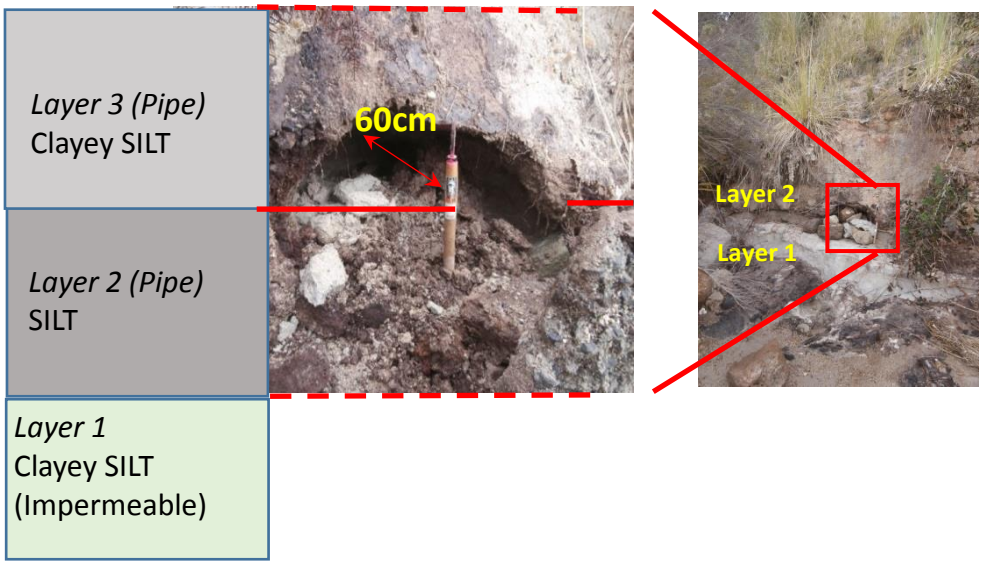

Figure 5.24: Stratigraphy of Back site

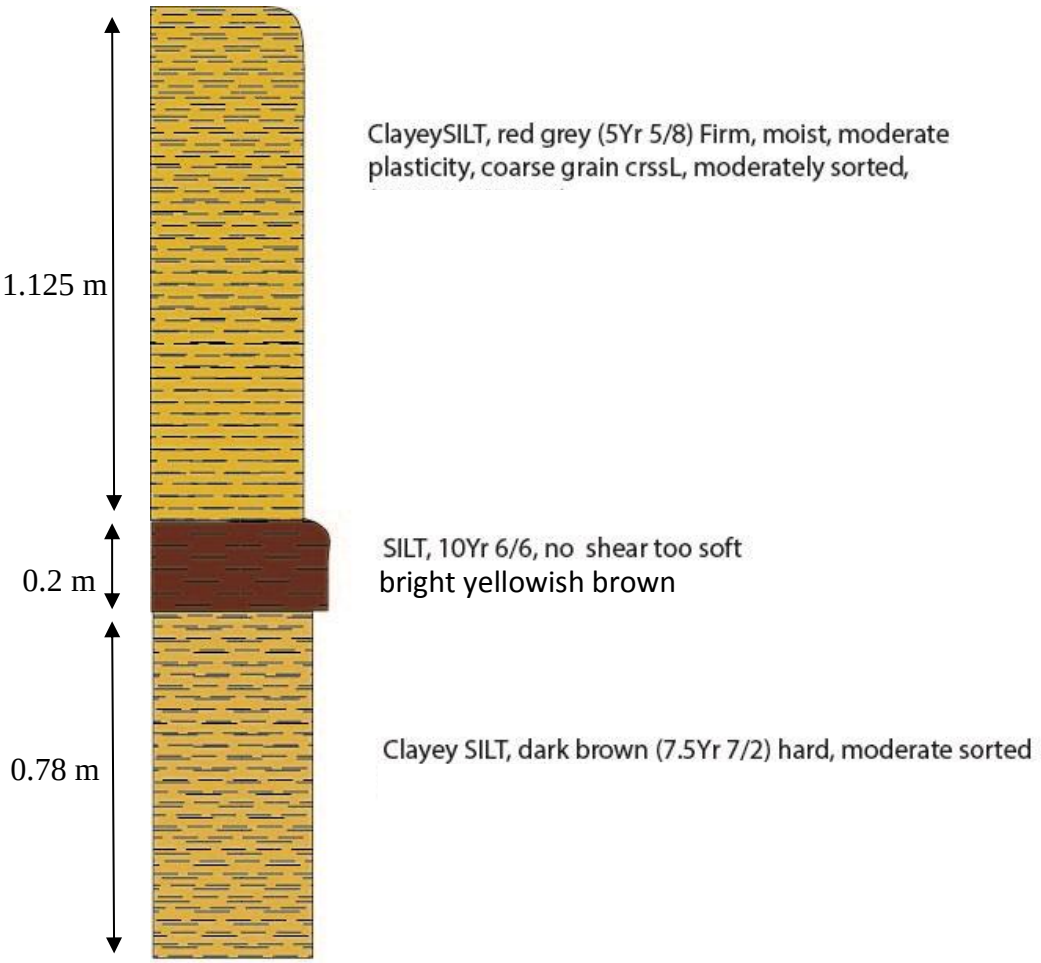

Figure 5.25: Stratigraphic column at Back site, Plummers Point

5.3.6 **Laboratory Tests – Pinhole Test, Crumb Test, Laser Sizer analysis**

The presence of piping structures within the coastal sections (Pa site, Midway site and Back site) caused further analysis to be undertaken. This was to determine if the layers are dispersive, generating the piping structures. The first test to be carried out was a crumb test followed by the pinhole test. Then a laser sizer analysis was conducted to determine the grain sizes for the layers in the stratigraphic columns located close to the piping structure.

5.3.6.1 **Crumb Test**

The crumb test was first undertaken prior to the pinhole test. This test reveals the dispersive character of the sample. When a crumb of soil is immersed in water (Figure 5.26), it has tendency to go into colloidal suspension and appear milky indicating that the sample is highly dispersive (Selby, 1993). The results obtained

from the crumb test in Table 5.2, layer 2 of Midway site and layer 2 of Back site were slightly dispersive. When the crumb was immersed in water it instantly dispersed creating a milky appearance. This is opposed to the other samples tested which had no change, indicating a non-dispersive characteristic.

Figure 5.26: Crumb test for Pa site layer 1

Table 5.2: Crumb test results

Soil Name	Test No.	Size of soil clod	Observation of crumb after 1 hour	Observation of crumb left overnight	Grade
Pa site layer 2	1	0.6 cm	No change	No change	Non-dispersive
Pa site layer 2	2	0.6 cm	No change	No change	Non-dispersive
Pa site layer 2	3	0.7 cm	No change	No change	Non-dispersive
Midway site layer 1	1	0.7 cm	Did not create cloudy water (1.5 cm spread)	No change	Non-dispersive
Midway site layer 1	2	0.6 cm	No change	No change	Non-dispersive
Midway site layer 1	3	0.8 cm	No change	No change	Non-dispersive
Midway site layer 2	1	0.6 cm	Disperses instantly when clod dropped. Spreads at the bottom of petri dish, 1 cm both directions	No change	Slightly Dispersive
Midway site layer 2	2	0.6 cm	Disperses instantly when clod dropped. Spreads at the bottom of petri dish, 0.5 cm both directions but a lump still observed at the centre of clod	No change	Slightly Dispersive
Midway site layer 2	3	0.6 cm	Spread 0.2 cm around the clod when dropped into water filled petri dish	No change	Slightly Dispersive
Back site layer 1	1	0.5 cm	No change Slight cloudiness below sample clod	No change Sample broke apart	Non-dispersive
Back site layer 1	2	0.5 cm	No change Little cloud dispersion under sample	No change	Non-dispersive
Back site layer 1	3	0.6 cm	No change Sample crumbled	No change	Non dispersive
Back site layer 2	1	0.8 cm	Did not create cloudy water (1 cm spread)	Did not change but clod spread 0.1 cm	Slightly Dispersive
Back site layer 2	2	0.6 cm	Dispersed as soon as clod dropped	No change	Slightly Dispersive
Back site layer 2	3	0.7 cm	Dispersed as soon as clod dropped	No change	Slightly Dispersive

5.3.6.2 **Pinhole Test**

The Pinhole test involves a small core sample inserted into the apparatus and piercing a hole using a pin to allow running water to pass through the hole. The water discharged through the core is collected and measured in a cylinder and observed for cloudiness which indicates dispersion. This test was carried out for all the layers tested previously in the crumb test. Full results are shown in Appendix 2, and summarised in Table 5.3. Some of the observations are shown in Figure 5.27a - d.

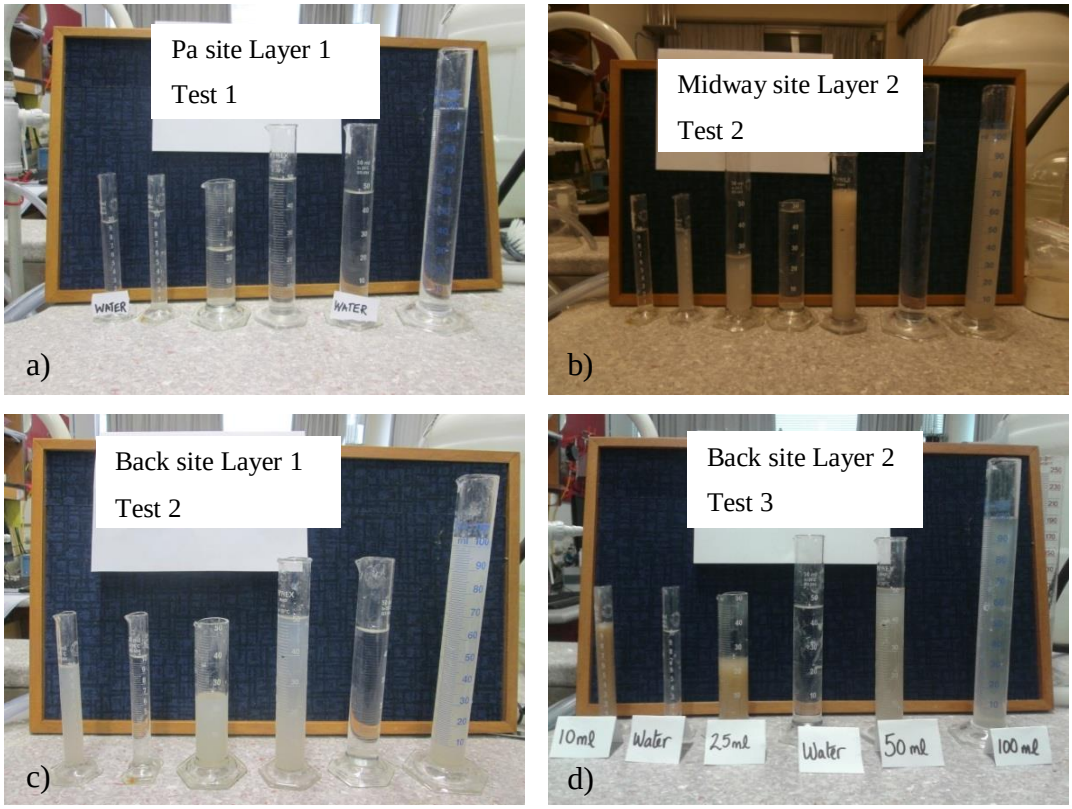

Figure 5.27: (a) Pa site Layer 1 test no observation – not cloudy, (b) Midway site Layer 2 test - cloudy, (c) Back site Layer 1 test – cloudy , (d) Back site Layer 2 test - cloudy

Although some tests revealed cloudy water indicating that the sample tested has a dispersive character, the results were compared to the core samples removed from the pinhole apparatus (Figure 5.28a) to determine if the sample showed any indication of erosion by the enlargement of the pinhole (Figure 5.28b).

At the Pa site, layers 1 and 2 both showed that the soil layers were not dispersive. This is evident by the clarity of the water sample in the pinhole test (Appendix 2)

as well as the size of the pin hole which remains the same size and shape (Figure 5.28 a, b).

At the Midway site layer 1, the water sample tests carried out indicated that the water was turbid with a colours ranging mainly from very dark to moderately dark (Appendix 2). Further, the core sample revealed that tests 1 and 3 had lost their strength and collapsed upon removal from the apparatus (Figure 5.29c). Although the pin hole seemed to have enlarged, this could be due to the enlargement as a result of the collapsed structure of the core. Test 2, on the other hand, withheld the core structure and the pinhole was clearly visible as remaining the same size and shape (Figure 5.29c). For the second layer, the three tests carried out revealed that when the water sample was initially observed it appeared as slightly dark (10 ml– 25 ml) and then darkened in 50 ml before gradually changing to a less turbid colour (Appendix 2). The core sample of test 1 revealed that the sample collapsed upon removal of the sample from the cylinder indicating that the sample had also lost its strength and the pinhole enlarged as a result of the collapsed structure (Figure 5.29d). Test 2 revealed that the sample pinhole remained the same size and shape (Figure 5.29d). In test 3, the pinhole dropped into the sample and therefore the sample had to be cut in half to reveal its interior. Although the pinhole remained the same size, the occurrence of the sample not being able to withhold the pin suggests that the sample had also lost its strength (Figure 5.29e). The pinhole test for Layer 2 confirms that the sample is dispersive and this finding agrees with that of the crumb test.

The general trend for Back site layers 1 – 3 for the water sample tests is an initial cloudy sample that is slightly dark, but which then changes to moderately dark to dark, followed by a less turbid solution ranging from moderately dark to slightly dark (Appendix 2). For Back site Layer 1 (Figure 5.29f) and Layer 3 (Figure 5.29g), the pinhole is the same size as the pin. However, Layer 2 shows indication of dispersion with test 1 showing a hole at the centre of the sample twice the size of the pinhole (Figure 5.29h). Test 2 revealed 2 rings around the centre of the hole indicating initial stage of erosion which is also the case with test 3, revealing a slightly enlarged pinhole also indicating initial stage of erosion (Figure 5.29h).

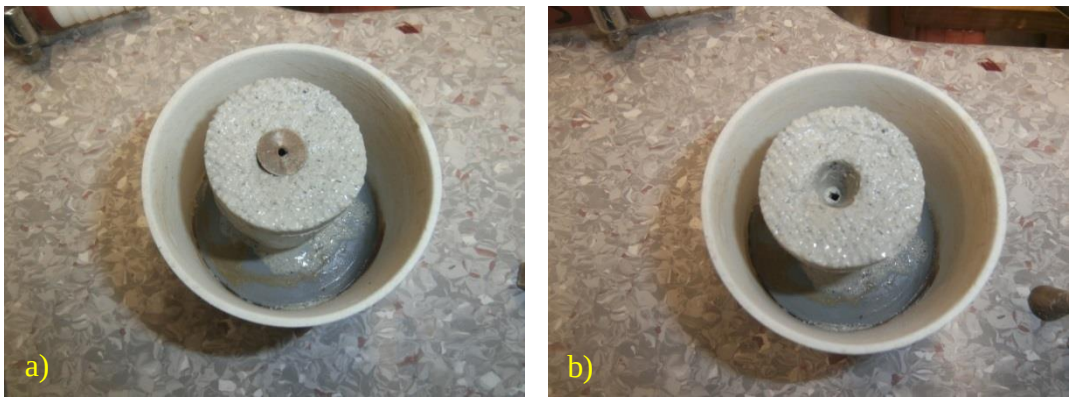

Figure 5.28: (a) Pa site core sample removed from pinhole apparatus (b) Pin removed from core sample to observe size of pinhole

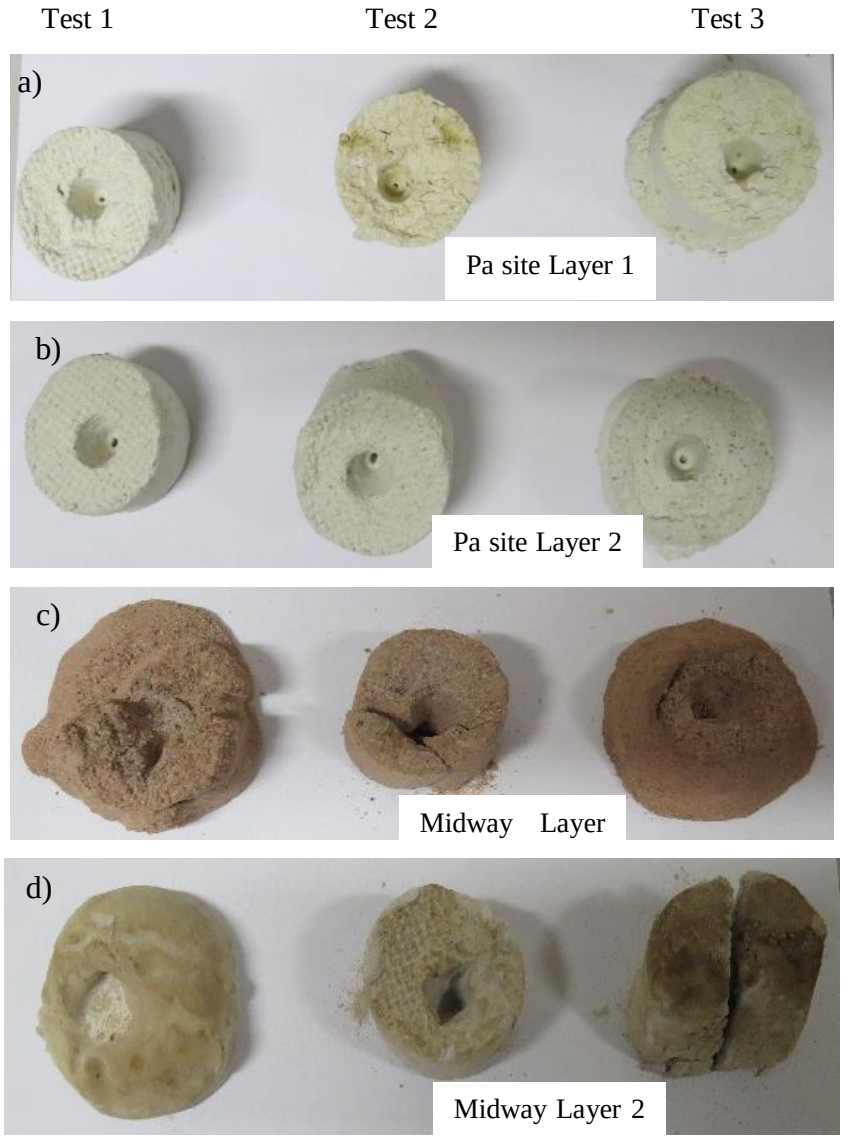

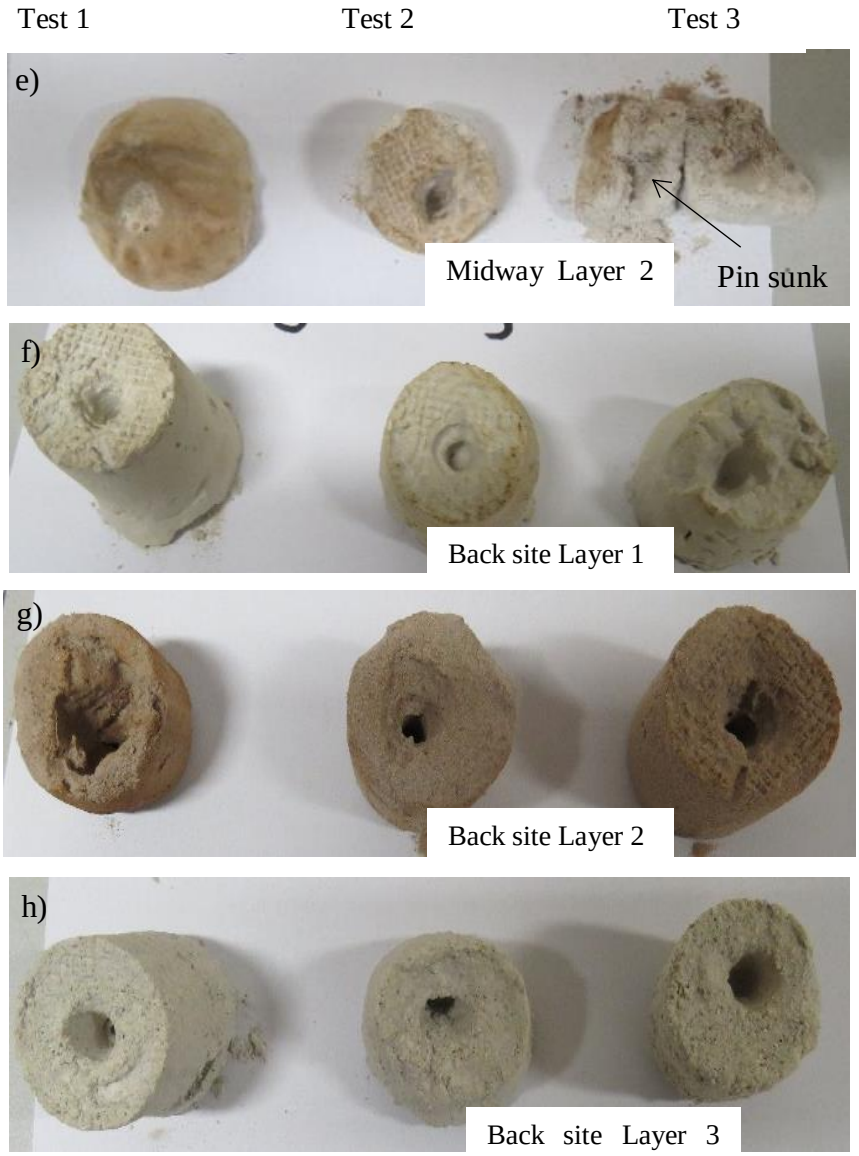

Figure 5.29: (a) Pa site cores layer 1 cores, (b) Pa site cores layer 2, (c) Midway site cores layer 1, (d) Midway site cores layer 2, (e) Midway site cores layer 2 with pinhole revealed, (f) Back site layer 1, (g) Back site layer 2, (h) Back site layer 3

5.3.7 **Grain size analysis using laser sizer**

Samples from each layer were analysed in the laser sizer. The first analysis was conducted by not pre-treating the samples prior to carrying out the test since it was suggested that there was probably no organic matter in the sample. The second test was carried out by pre-treating the samples to remove organic matter prior to conducting the analysis. Classification of the sediment for each layer was according to the Udden–Wentworth size classification for sediment grains (Udden, 1914; Wentworth, 1922), shown in Table 5.3, and the sediment sorting was classified based upon Folk (1968), shown in Table 5.4.

Table 5.3: Udden-Wentworth size classification (Udden, 1914; Wentworth, 1922)

	Millimetres	Millimetres	Microns	Phi (Φ) units	Wentworth size class
GRAVEL	4096			-12	boulder
	2048			-11	
	1024			-10	
	512			-9	cobble
	-----256-----	256	256000	-8	
	128	128	128000	-7	
	64	64	64000	-6	
	32	32	32000	-5	
	16	16	16000	-4	
	8	8	8000	-3	pebble
	4	4	4000	-2	
	2	2	2000	-1	granule
SAND	1	1	1000	0	very coarse sand
	0.5	½	500	1	coarse sand
	0.25	¼	250	2	medium sand
	0.125	1/8	125	3	fine sand
	0.0625	1/16	62.5	4	very fine sand
SILT	0.0313	1/32	31.25	5	coarse silt
	0.0156	1/64	15.6	6	medium silt
	0.0078	1/128	7.8	7	fine silt
	0.0039	1/256	3.9	8	very fine silt
CLAY	0.0020		2.0	9	clay
	0.00098		0.98	10	
	0.00049		0.49	11	
	0.00024		0.24	12	
	0.00012		0.12	13	
	0.00006		0.06	14	

Table 5.4: Classification for graphical sorting (Folk,1968)

Sorting	Sorting Classification
0.00 – 0.35	Very well sorted
0.35 - 0.50	Well sorted
0.50 – 0.71	Moderately well sorted
0.71 – 1.00	Moderately sorted
1.00 – 2.00	Poorly sorted
2.00 – 4.00	Very poorly sorted
>4.00	Extremely poorly sorted

The laser sizer tests reveal that the nontreated samples had similar results to the treated samples in terms of mean grain size and sorting (Table 5.5, Appendix 2). The presence of any organic matter did not affect the sediment texture. The textural results were compared to the results obtained from the pinhole test to indicate if there were any relationship between sediment texture and dispersive

character of the sample. According to the pinhole test results (Table 5.6), all the layers from all the sites were non-dispersive except for Back site layer 2, which showed signs of dispersion. This layer consists of about 90% sand (Appendix 2) and has a mean classification of fine sand that is poorly sorted with a silty sand texture. Therefore, the assumption is that these fine sand particles have been washed out from the sample during pinhole test trials producing the results obtained. There were other samples classified also as silty sand with similar size ranges as those of Back site Layer 2 such as Midway site Layer 1 and Layer 3, which were the collapsed samples from the Pinhole test. These samples (Layer 1, 3 from Midway site) did exhibit a slight dispersive character when tested. Therefore, soils within Plummers Point have a high probability of being dispersive.

Table 5.5: Laser sizer results for piping sites

Test	Site	Layer	Mean	Sorting
Nontreated	Pa	1	Medium silt	Very poorly sorted
Treated	Pa	1	Medium silt	Very poorly sorted
Nontreated	Pa	2	Coarse silt	Very poorly sorted
Treated	Pa	2	Coarse silt	Very poorly sorted
Nontreated	Pa	3	Medium sand	Poorly sorted
Treated	Pa	3	Medium sand	Poorly sorted
Nontreated	Midway	1	Fine sand	Very poorly sorted
Treated	Midway	1	Medium sand	Poorly sorted
Nontreated	Midway	2	Coarse silt	Very poorly sorted
Treated	Midway	2	Very fine sand	Very poorly sorted
Nontreated	Midway	3	Fine sand	Very poorly sorted
Treated	Midway	3	Fine sand	Very poorly sorted
Nontreated	Midway	4	Coarse silt	Very poorly sorted
Treated	Midway	4	Coarse silt	Very poorly sorted
Nontreated	Midway	5	Coarse silt	Very poorly sorted
Treated	Midway	5	Coarse silt	Very poorly sorted
Nontreated	Back	1	Coarse silt	Very poorly sorted
Treated	Back	1	Medium silt	Poorly sorted
Nontreated	Back	2	Fine sand	Poorly sorted
Treated	Back	2	Fine sand	Poorly sorted
Nontreated	Back	3	Fine sand	Very poorly sorted
Treated	Back	3	Very fine sand	Very poorly sorted
Nontreated	Back	4	Very fine sand	Very poorly sorted
Treated	Back	4	Very fine sand	Very poorly sorted

Table 5.6: Dispersion results N/D=Non Dispersive D=Dispersive N/T=Not Tested SD=Slightly Dispersive

Test	Site	Layer	Dispersive
Nontreated	Pa	1	N/D
Treated	Pa	1	N/D
Nontreated	Pa	2	N/D
Treated	Pa	2	N/D
Nontreated	Pa	3	N/T
Treated	Pa	3	N/T
Nontreated	Midway	1	S/D
Treated	Midway	1	S/D
Nontreated	Midway	2	S/D
Treated	Midway	2	S/D
Nontreated	Midway	3	N/T
Treated	Midway	3	N/T
Nontreated	Midway	4	N/T
Treated	Midway	4	N/T
Nontreated	Midway	5	N/T
Treated	Midway	5	N/T
Nontreated	Back	1	N/D
Treated	Back	1	N/D
Nontreated	Back	2	D
Treated	Back	2	D
Nontreated	Back	3	N/D
Treated	Back	3	N/D
Nontreated	Back	4	N/T
Treated	Back	4	N/T

5.4 **Summary**

Field observations were collected from sites that were subject to erosion as a result of failure. At Omokoroa, Bramley Drive was subject to rotational failure, while Ruamoana and South landslip were planar failures. These failures were most likely triggered by prolonged rainfall, and were also associated with the basal units that may have created a perched water table.

At Plummers Point, the four sites investigated consisted of the Main site which is an exposed coastal cliff section subject to planar failure. Other sites investigated were newly exposed cliff sections (Midway site, Back site) and a historical site (Pa site). These three extra sites were studied in detail as they had the presence of piping structures. Samples were collected from the piping and adjacent layers to determine if the layers were dispersive. The Crumb Test and Pinhole Test produced results suggesting that the piping layers are dispersive to slightly dispersive. As a result, it is proposed that the landslip failures at Plummers Point

are most likely initiated by piping structures within the units. The pipes are located near the base of the stratigraphy and create instability within the overhanging cliff face after they have eroded. As a result, the cliff retreats because of this. Since piping is associated with the flow of water through the layer, installing horizontal drains to reduce the water content may increase the extent of piping.

Chapter 6

LASER SCAN RESULTS

6.1 Introduction

The aim of this chapter is to determine the shape and volume changes of two cliff sections located at Bramley Drive, Omokoroa, and at Plummers Point. This chapter presents the data analysis obtained from laser scan points collected over the years 2011, 2012, 2013, and May – November 2014. Laser scan (Terrestrial LiDAR) is a method used to determine short term cliff retreat. The laser scan analysis for Bramley Drive is firstly presented with surface volume changes tabulated, followed by a presentation of the DEM images. These reveal the surface volume changes and how the material has moved along the cliff scarp. The results from the laser scan analysis are also presented for Plummers Point using the same format.

6.2 Bramley Drive analysis

Scanning at this site was focused on the main landslip section (Figure 6.4) and also included the cleared sections on the sides. Laser scanning was previously carried out at this location in 2012 and 2013. This earlier laser scan data and LiDAR points acquired from a LiDAR survey conducted in 2011 were used to compare surface volume changes. A summary of the dates of the scan are presented in Table 6.1 and a map showing the locations is presented in Figure 6.1.

Table 6.1: Summary table of Laser scan data and position of setup

Date	Method	Person conducting scan	Laser scan setup location
09 09 11	LIDAR survey	NZAM	
20 09 12	Laser scan	Dean Sandwell	Top of Cliff (BrmlyC and BrmlyD)
25 07 13	Laser scan	Dean Sandwell	Top of Cliff (BrmlyC and BrmlyD)
10 11 05	Laser scan	Dr Willem de Lange and Camillia Garae	Brm1
11&18 08 14	Laser scan	Dr Willem de Lange and Camillia Garae	Brm1 and Brm2
07 09 14	Laser scan	Camillia Garae	Brm1
23 10 14	Laser scan	Camillia Garae	Brm2
22 11 14	Laser scan	Camillia Garae	Brm2

Figure 6.1: Location of Bramley GPS Pegs used as position for laser scan setup

Laser scans over the past years (September 2012-November 2014) as summarised in Table 6.1 as well as LiDAR data flown from September 2011 can determine if there are changes occurring at the cliff face. The surface changes can be illustrated using Digital Elevation Models (DEMs) produced by Aspect tool in Arc GIS. This shows the slope direction (Figure 6.2) and indicates that the main central part of the scarp is facing the northwest. In November 2014, the surface of the central scarp partially comprised of material dipping to the north and northwest direction. There was also a slight change in the slope angle of the scarp from September 2011 to November 2014 from a range of 54 - 72 degrees in slope angle to 65 - 85 degrees in slope angle. This confirms that erosion of the cliff face has occurred between that time interval. These DEMs (Aspect and Slope) also show that

Bramley Drive site was subject to rotational landslip failure represented by the circular pattern of erosion.

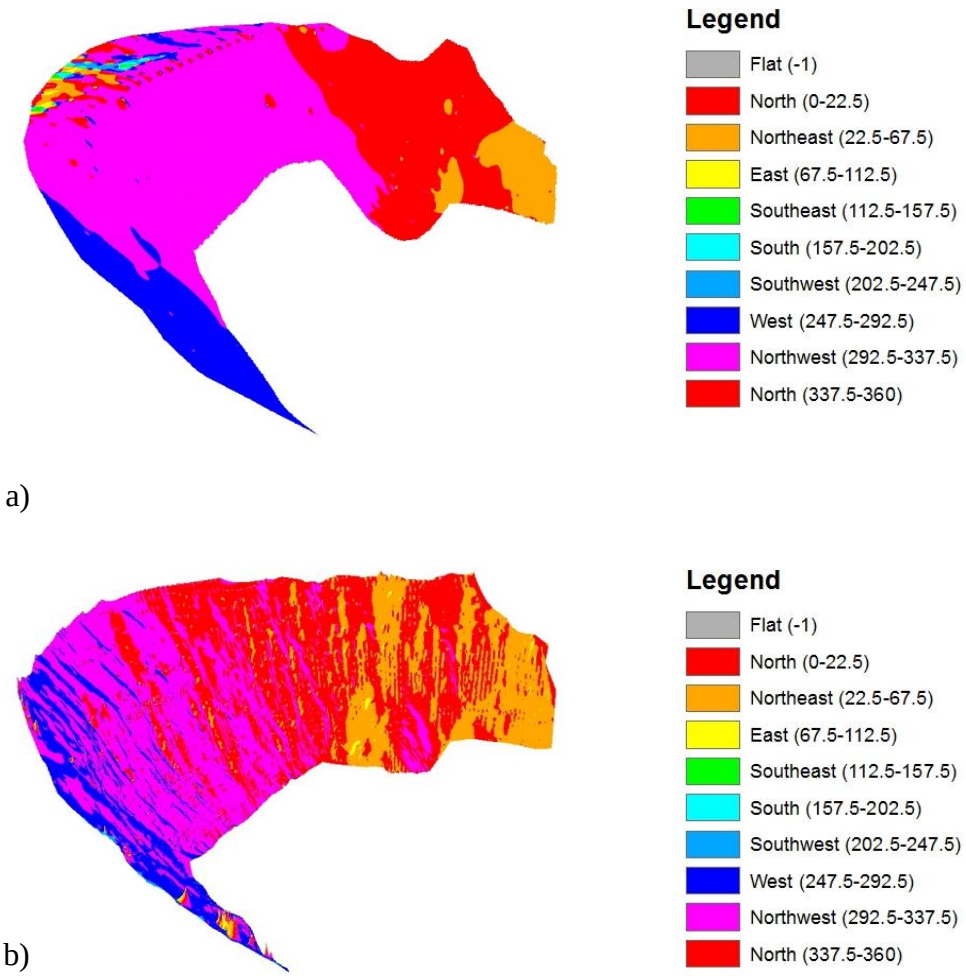

Figure 6.2:Aspect images showing the direction the cliff face is facing (a) 2011 aspect DEM, (b) November 2015 aspect DEM

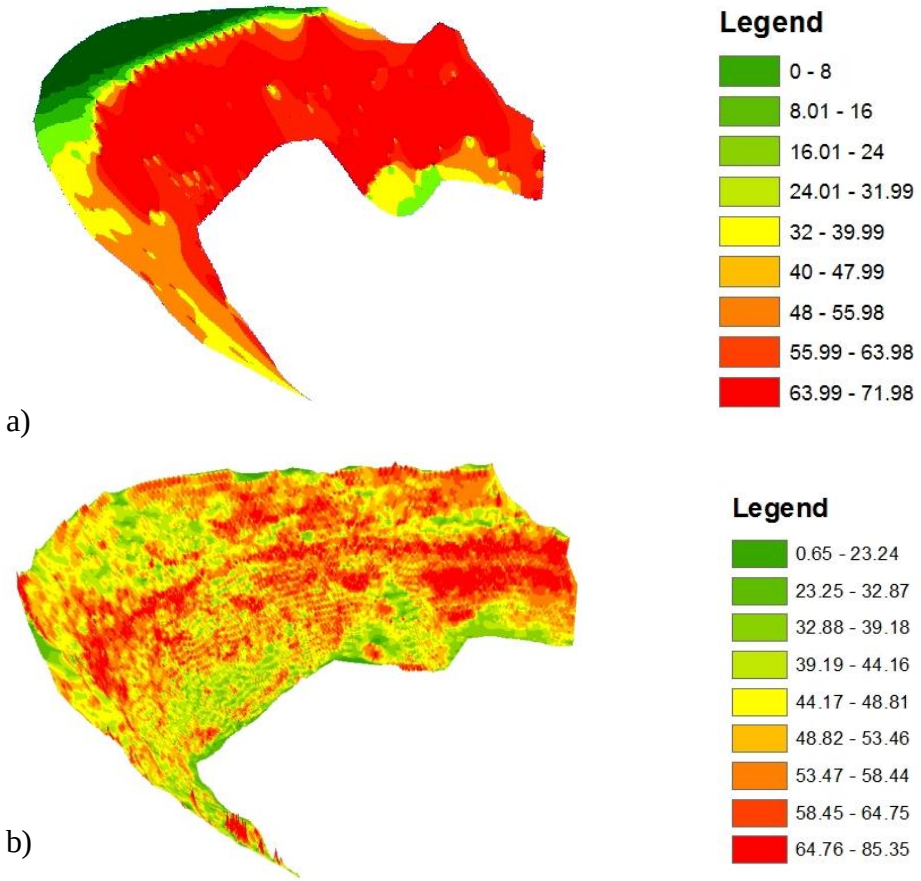

Figure 6.3: Slope images showing the slope angle of the cliff face in degrees (a) 2011 slope DEM, (b) 2014 slope DEM

Some vegetation covered sections near the base and on the side edges had to be avoided as the scanner cannot accurately locate the ground surface under dense vegetation. The area scanned was large, therefore, the exposed cliff face was divided into three sections with each scan taking approximately 1.5 hours. The procedure for scanning the cliff face changed over time in order to improve the data quality. The earlier months had the scanner first positioned at Brm1 and then the scan setup was shifted to the peg closest to the base (Brm2). This was carried out to infill areas not visible from the lower site.

The closer the scan was positioned to the cliff face the better the results were. This was because when positioned away from the cliff face at Brm1, some vegetation from bench 1 in Figure 6.4 (located at the base of the cliff face) extended in the air covering the base of the cliff face. However, when the scan setup was close to the cliff face the vegetation cover could be avoided since the peg is located at a higher elevation near the base of the cliff face. Unfortunately, the entire landslide was not

visible from the closest site. Hence it was necessary to combine surveys from at least two sites to get complete coverage.

Figure 6.4: Bramley Drive landslip showing the central part of the cliff face

6.1.1 Surface volume changes

To obtain surface change volumes, a raster image has to be generated from the scan data points. When the raster image has been generated then the surface volume (3D Analyst) tool is selected. This tool calculates the surface volume and 3D area for the selected raster. The surface volume difference is then manually calculated for selected raster images from different time intervals. These surface volume changes have been calculated and are presented in Table 6.2 and rate of cliff recession is given in Table 6.3. To aid with the interpretation of the data, DEMs have been created to determine elevation changes shown in Figure 6.5 - 6.8. The elevation images use dark shading representing high elevation and yellow shading represent low elevation. Another DEMs developed was the surface change images (Figure 6.9 - 6.12) and Appendix 3. These images describe the movement of debris along the cliff face. On the image, red shading represents net gain, blue shading denotes erosion and grey shading means that no surface change occurred.

From Table 6.2, it is apparent that the highest volume eroded between September 2011–September 2012 was 3037 m^3 (Table 6.2). This net loss of material was related to the landslip failures that occurred from 2011 - 2012 with an average recession rate of 8 m^3/day (Table 6.3). The rate eroded per day on average for this time period is about -0.01 m. This result is presented in the DEM in Figure 6.5a which shows that erosion is focused on the central part of the scarp as represented by the yellow shade. The sides of the scarp had darker shades indicating that there was less erosion occurring in that part of the scarp. The surface changes during that period was supported by the DEM in Figure 6.9a indicating that erosion occurred in the central part of the scarp.

As evident in Table 6.1, the LiDAR scans were taken by different operators and, more importantly, from different locations. Furthermore, the density of scans varied, with later scans containing more measurements than the earlier scans. Finally, the vegetation coverage varied with time. All these factors mean that the specific locations of individual measurements varied overtime, and were not consistent.

As far as possible, the GIS analysis was confined to the same region of the landslide. However as shown by the 3D - area analysed (Table 6.2), this region varied from 1011 to 1513 m^2 in surface area. This variation affects the volume determined from the differences between DEMs. The volume can be normalised by dividing by the 3D-area (Table 6.2) to allow the average volume change per unit square metre to be estimated.

Comparing the normalised volumes between surveys (Table 6.2) indicates that the high density recent scans are very consistent. However, the earliest scans show larger fluctuations (-4.39 to 5.99 m^3/m^2). In part, some represent volume changes due to landslide events (September 2011 to September 2012) and minor erosion of cliff edges (May 2014 to August 2014).

Overall, it appears that the volume determination involves significant errors from a range of sources. Therefore, the DEMs were used to plot location specific changes. This ensured that only areas common to both surveys were processed,

and allowed areas of erosion and accretion to be identified. This approach is considered more useful than overall volume change.

The next highest volume of material eroded off the cliff face from July 2013–May 2014 with a volume change of 435 m^3 (Table 6.2). The DEM reveals that erosion occurred along the cliff scarp and was concentrated particularly in the rills (Figure 6.6c). However, the image showing the surface changes and movement of debris (Figure 6.10a), indicates that there is erosion (net loss) in the entire cliff scarp, and this material has been deposited at the base.

The third highest volume change occurred from September 2012–July 2013 with a change of 122 m^3 (Table 6.2). During this period, erosion occurred along the whole cliff scarp as represented by the yellow shading in the image Figure 6.5b. This is supported by the surface changes in Figure 6.9b, which illustrates that erosion occurred in the entire cliff scarp. However, debris from this period accumulated in small piles as it travelled down the scarp. Larger volumes of debris that were transported down the scarp accumulated as talus piles at the base.
Apart from the significant volume changes presented in the table, minor volume changes were also recorded (Table 6.2). From September 2014 – October 2014 minor changes were evident, indicating erosion had occurred in the rills along the scarp as well as at the two ends of the scarp. Positive volume differences representing accretion was found from August to October 2014 data. This is represented by the dark shades in the elevation change DEM (Figure 6.7a, b). The same representation is shown in Figure 6.11a, b indicating that there is net gain of debris across the scarp. As discussed earlier, minor volume changes may mostly represent survey errors. However, the DEM data do indicate changes consistent with direct observations.

For October 2014–November 2014 the DEM reveals that erosion had occurred over the entire scarp (Figure 6.7b, 6.8). This is also supported by additional surface change (Figure 6.11b, 6.12) which illustrates net loss over the entire scarp with net gain on the eastern edge side of the scarp. There were also minor rates of accretion in the time interval from May 2014–August 2014 and August 2014 – September 2014 (Table 6.2). The DEMs in Figure 6.6b, 6.7a indicate that these

accretion rates are the talus piles as well as debris that had accumulated along the rills. This is also portrayed in the DEMs in Figure 6.10b, 6.11a.

Table 6.2: Summary of Bramley Drive surface volume change

Survey date	Method for data collection	3D-area [m^2]	Area difference [m^2]	Volume to reference plane [m^3]	Volume difference [m^3]	Volume / Area [m]	Volume / Area Difference [m]
09 09 2011	LIDAR	1297		21,650		16.69	
Difference			**216**		**-3037**		**-4.39**
20 09 2012	Laser scan	1513		18,613		12.30	
Difference			**-502**		**-122**		**5.99**
25 07 2013	Laser scan	1011		18,491		18.29	
Difference			**166**		**-435**		**-2.95**
10-11 05 2014	Laser scan	1177		18056		15.34	
Difference			**76**		**27**		**-0.91**
11 & 18 08 2014	Laser scan	1253		18083		14.43	
Difference			**-47**		**76**		**0.63**
07 09 2014	Laser scan	1206		18159		15.06	
Difference			**-26**		**-94**		**0.25**
23 10 2014	Laser scan	1180		18065		15.31	
Difference			**-3**		**-64**		**-0.02**
22 11 2014	Laser scan	1177		18001			

Table 6.3: Rate of cliff retreat

Survey date	Method for data collection	Volume difference [m^3]	Number of days	Average rate [$m^3.d^{-1}$]	$\frac{\text{Volume}}{\text{Area}}$ Difference [m]	Average rate per day [m]
09 09 2011	LIDAR					
Difference		-3037	377	-8	-4.39	-0.01
20 09 2012	Laser scan					
Difference		-122	308	-0.4	5.99	0.02
25 07 2013	Laser scan					
Difference		-435	290	-1.5	-2.95	-0.01
10-11 05 2014	Laser scan					
Difference		27	92	0.3	-0.91	-0.01
11 & 18 08 2014	Laser scan					
Difference		76	27	2.8	0.63	0.02
07 09 2014	Laser scan					
Difference		-94	46	-2.0	0.25	0.005
23 10 2014	Laser scan					
Difference		-64	30	-2.1	-0.02	-0.00067
22 11 2014	Laser scan					

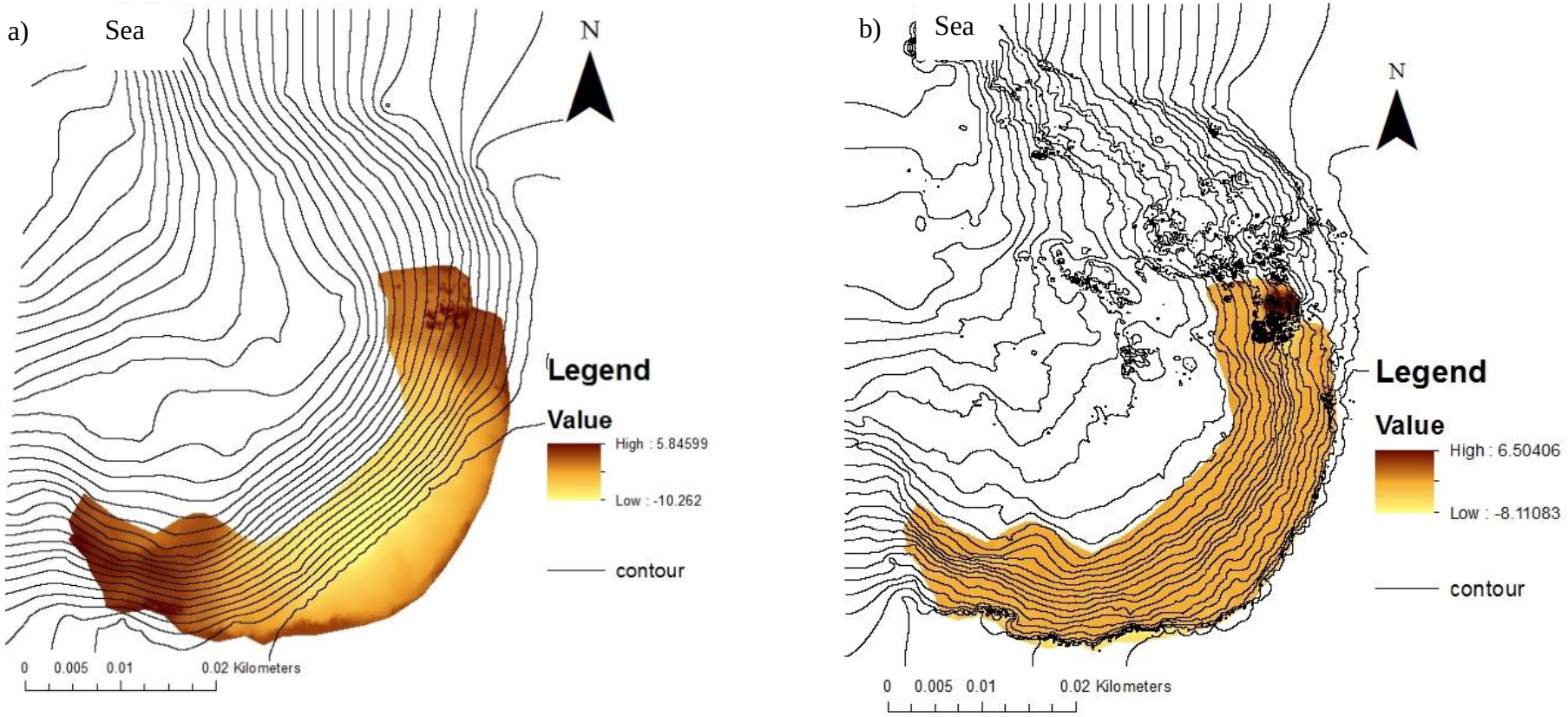

Figure 6.5: Elevation changes showing relative surface changes and soil volume loss for time interval (a) September 2012 – September 2011 and (b) July 2013 – September 2012

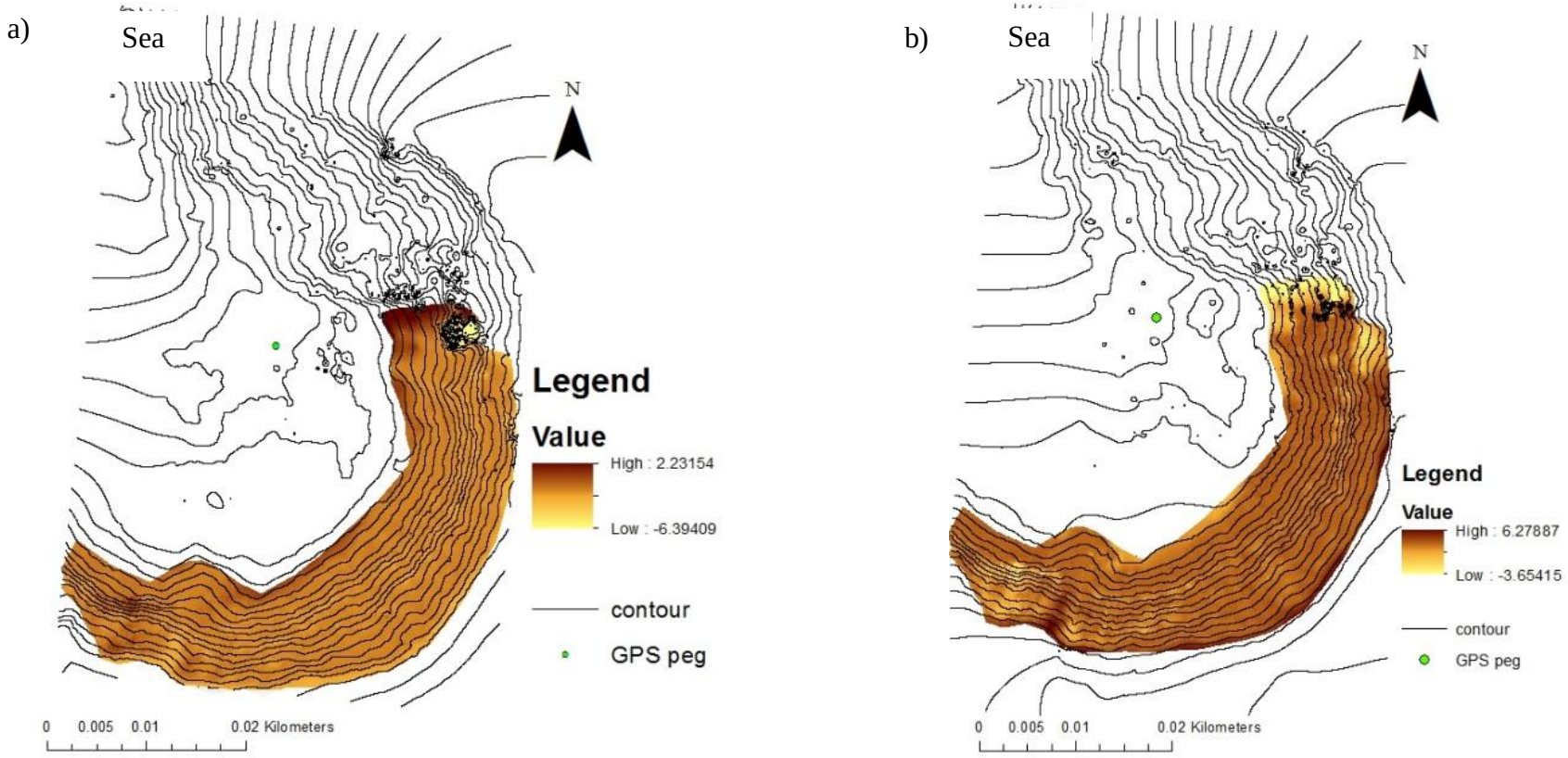

Figure 6.6: Elevation changes showing relative surface changes and soil volume loss for time interval (a) May 2014 – July 2013 (b) August 2014 – May 2014

a)

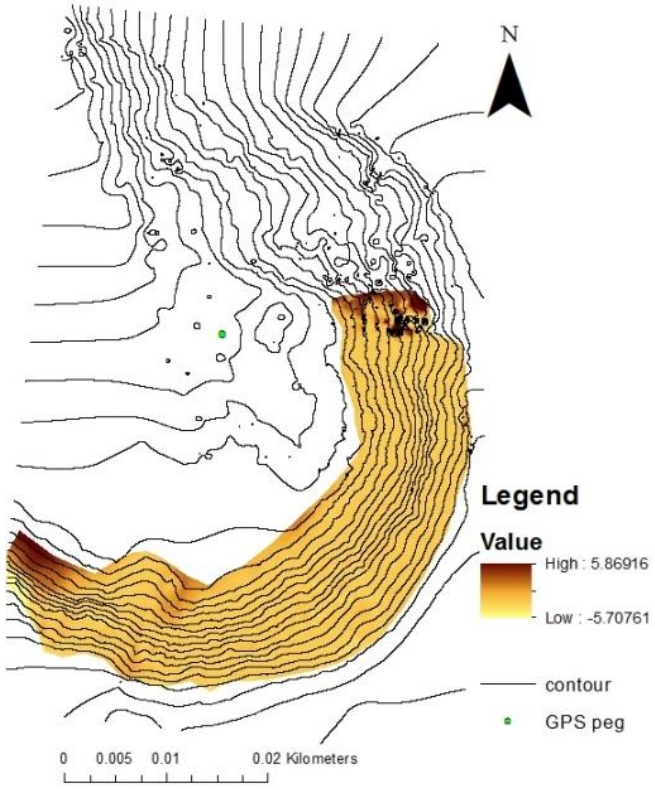

b)

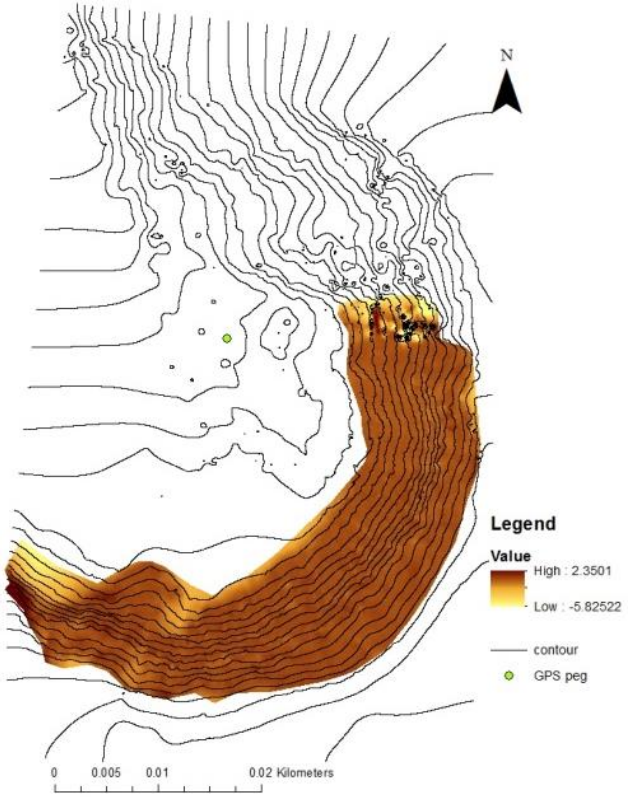

Figure 6.7: Elevation changes showing relative surface changes and soil volume loss for time interval (a) September 2014 – August 2014 (b) October 2014 – September 2014

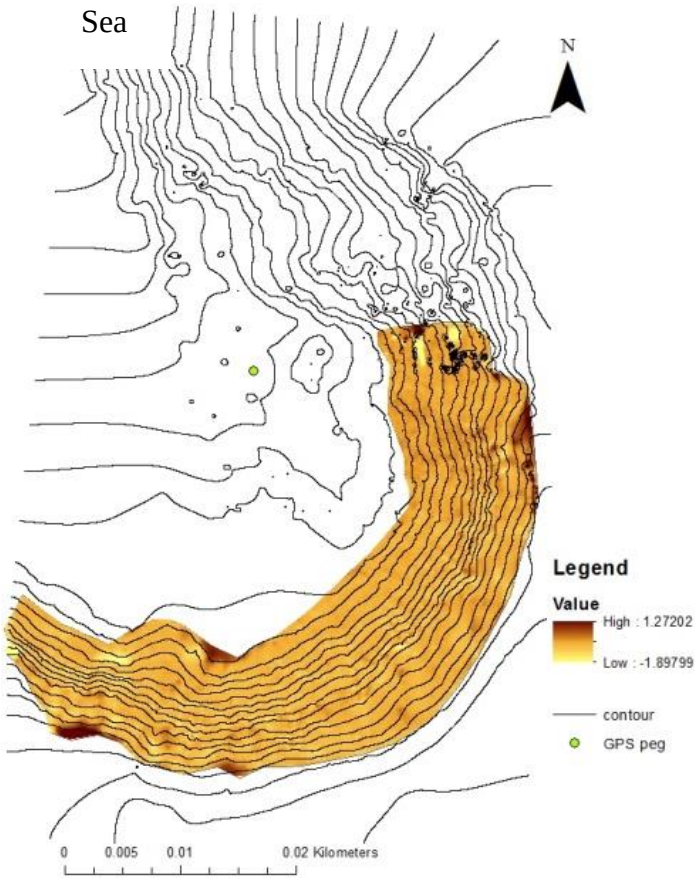

Figure 6.8: Elevation changes showing relative surface changes and Soil volume loss from November 2014 – October 2014

a)

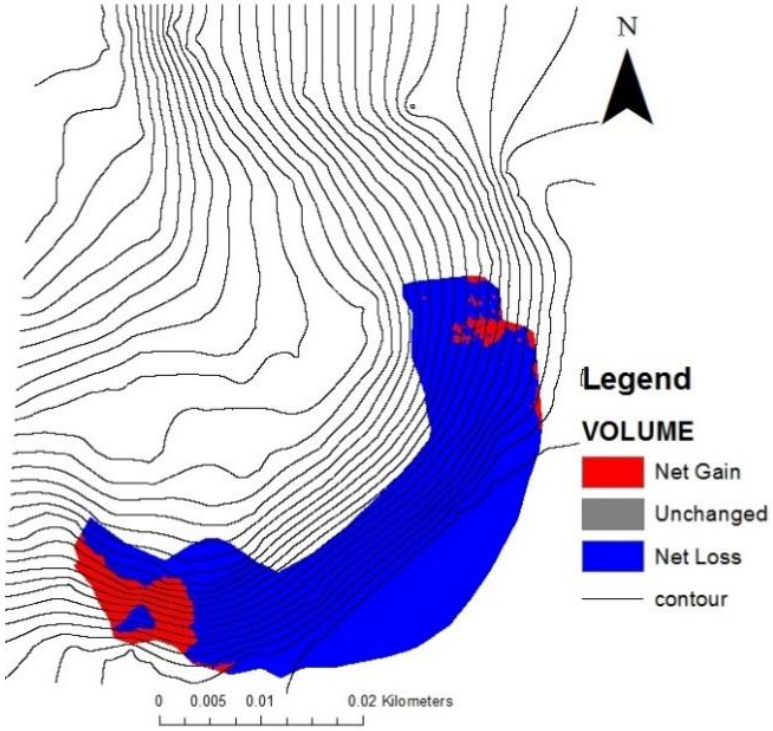

b)

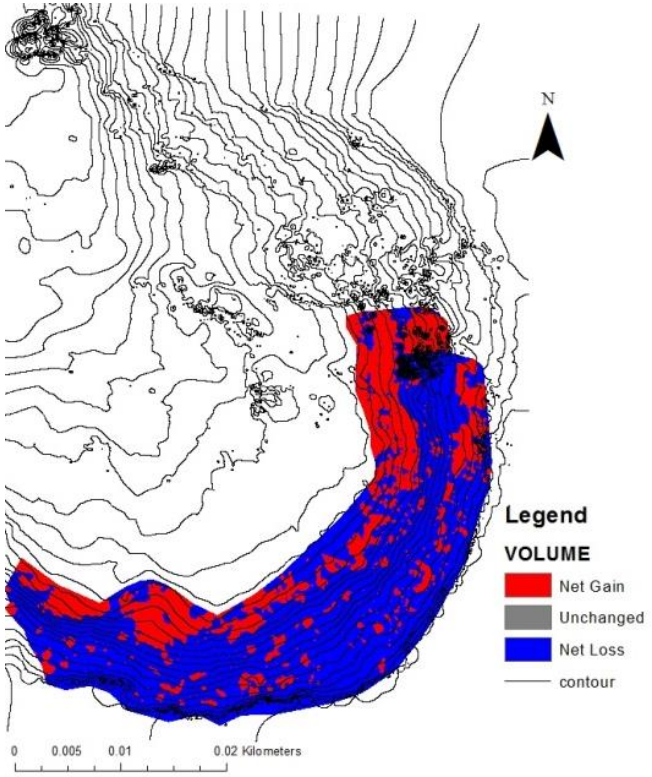

Figure 6.9: Surface changes for time intervals for (a) September 2012 – 2011, (b) July 2013 - September 2012

a)

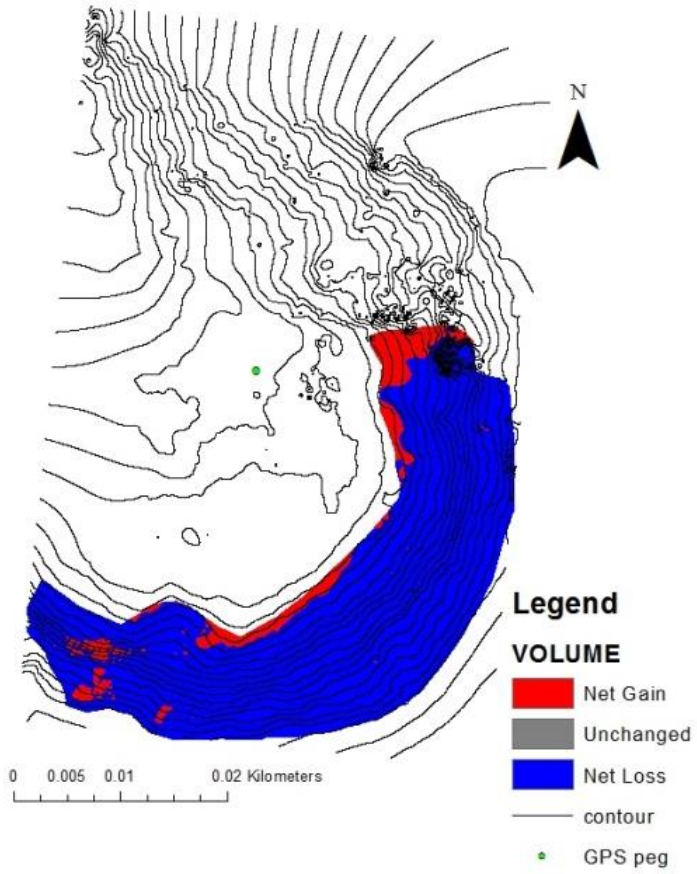

b)

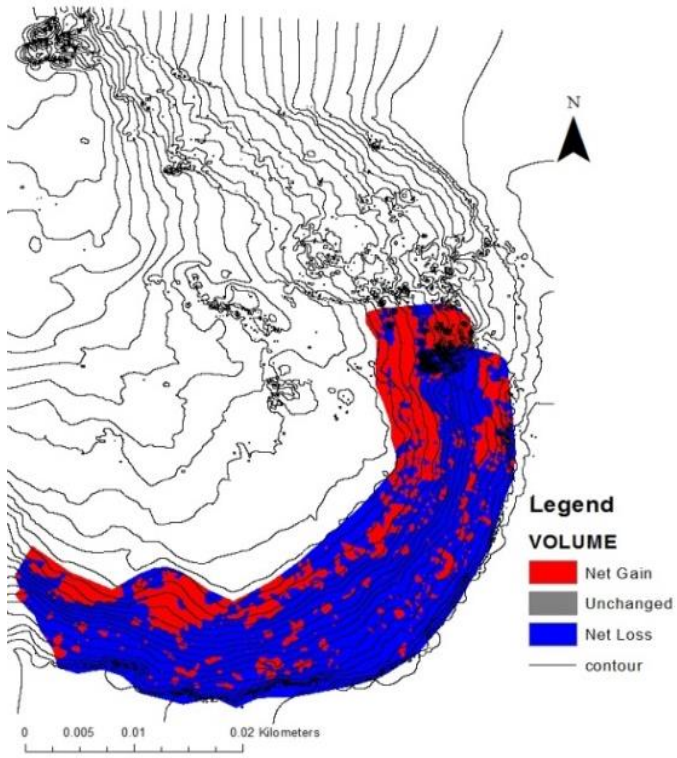

Figure 6.10: Surface changes for time intervals for (a) July 2013 – May 2014, (b) August 2014 – May 2014

a)

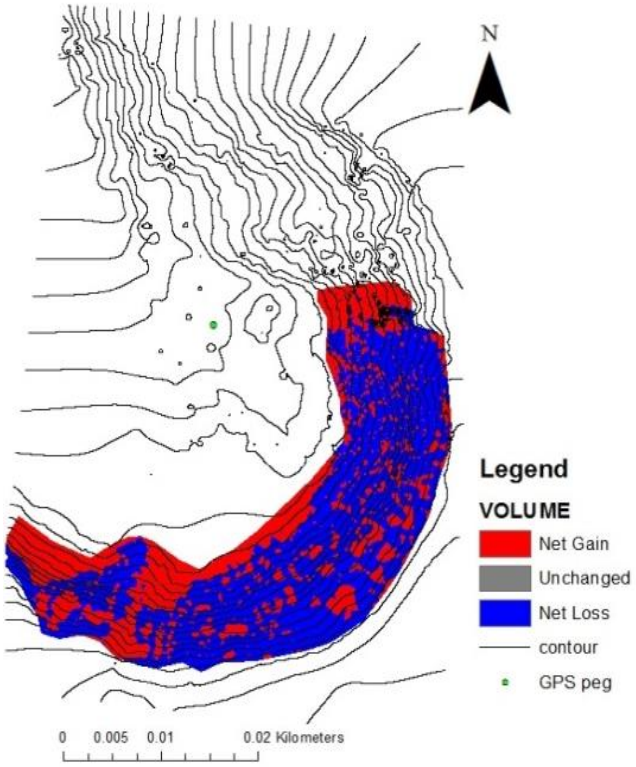

b)

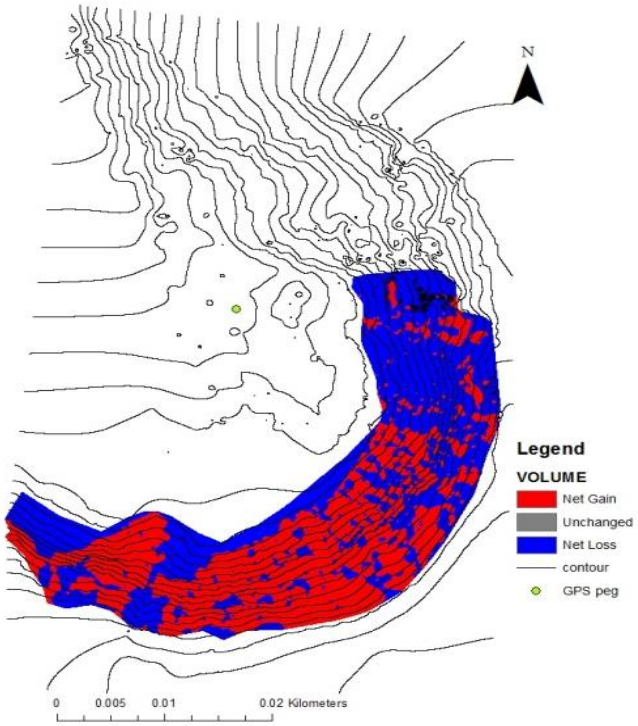

Figure 6.11: Surface changes for time intervals for (a) September 2014 – August 2014, (b) October 2014 - September 2014

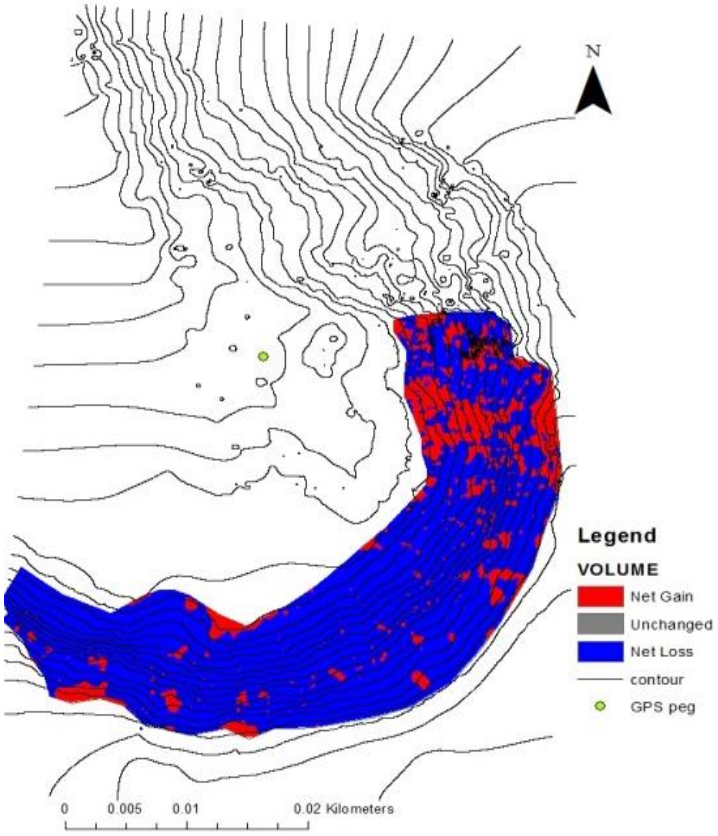

Figure 6.12: Surface changes for time intervals November 2014 – October 2014

6.2 Plummers Point analysis

This site was divided into three sections (north, central and south). These areas are shown in Figures 6.13, 6.14a, b. Scanning of these sections was restricted to the slope between the top edge of the scarp and the base of the scarp just above the talus pile. Areas with thick vegetation cover were avoided and not included in the scan. Consequently, there was a large vegetative patch that was left out from scanning located between the central and northern side of the cliff section. This is located between Figures 6.14a and b. Although the scans were conducted as three consecutive separate scans the scan cloud points were combined to generate images referred to as north and south which represent the northern and southern section of the area of study.

Figure 6.13: South section of cliff face

Figure 6.14: (a) Central face of cliff face (b) northern side of cliff face

DEMs using Aspect 3D analyst on Arc GIS were generated to display the differences of surface changes between September 09 2011 and November 10 2014. The images show that in 2011 the cliff was facing the north direction as illustrated in Figure 6.15. In November 10 2014, portions of the cliff were facing North, Northeast, East and Southeast as shown in Figure 6.16. Therefore, over time there seems to be a change in the direction the cliff is facing as a result of surface changes caused by erosion. To aid with the interpretation of the surface changes affecting the cliff face, DEM images generated from Slope 3D analyst on Arc GIS were created. However, the steepest slope angle from both DEM images in Figure 6.17 and 6.18 remained the same at 89 degrees but the frontal part of the cliff in November 2014 image Figure 6.18 had a slope angle of 0.2–62 degrees which is less steep than in September 2011.

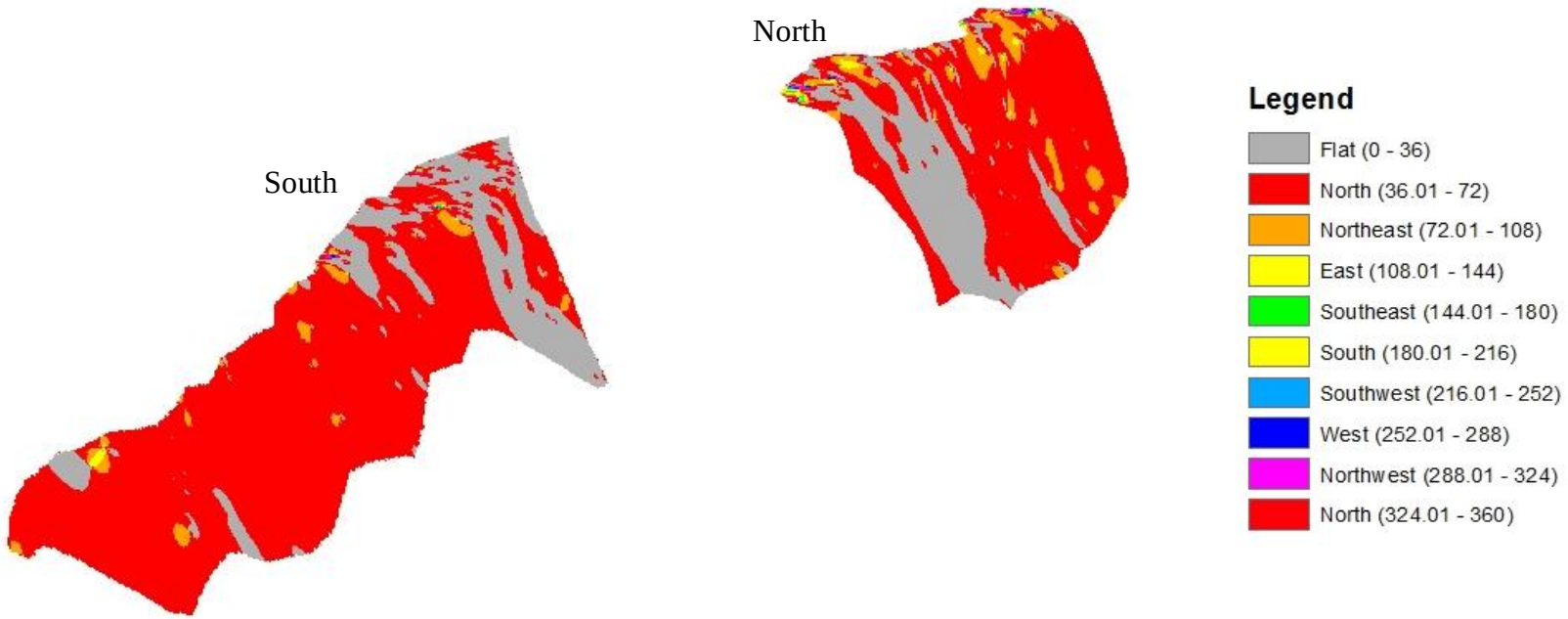

Figure 6.15: September 2011 aspect image showing direction cliff face is facing

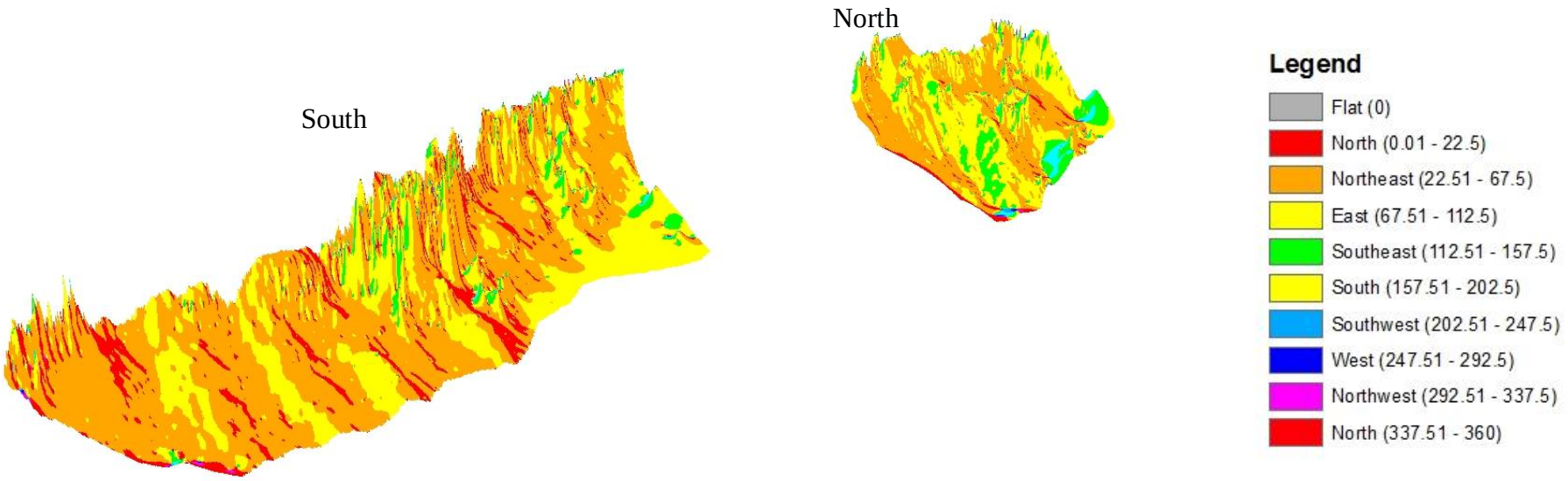

Figure 6.16: November 2014 aspect image showing direction cliff face is facing

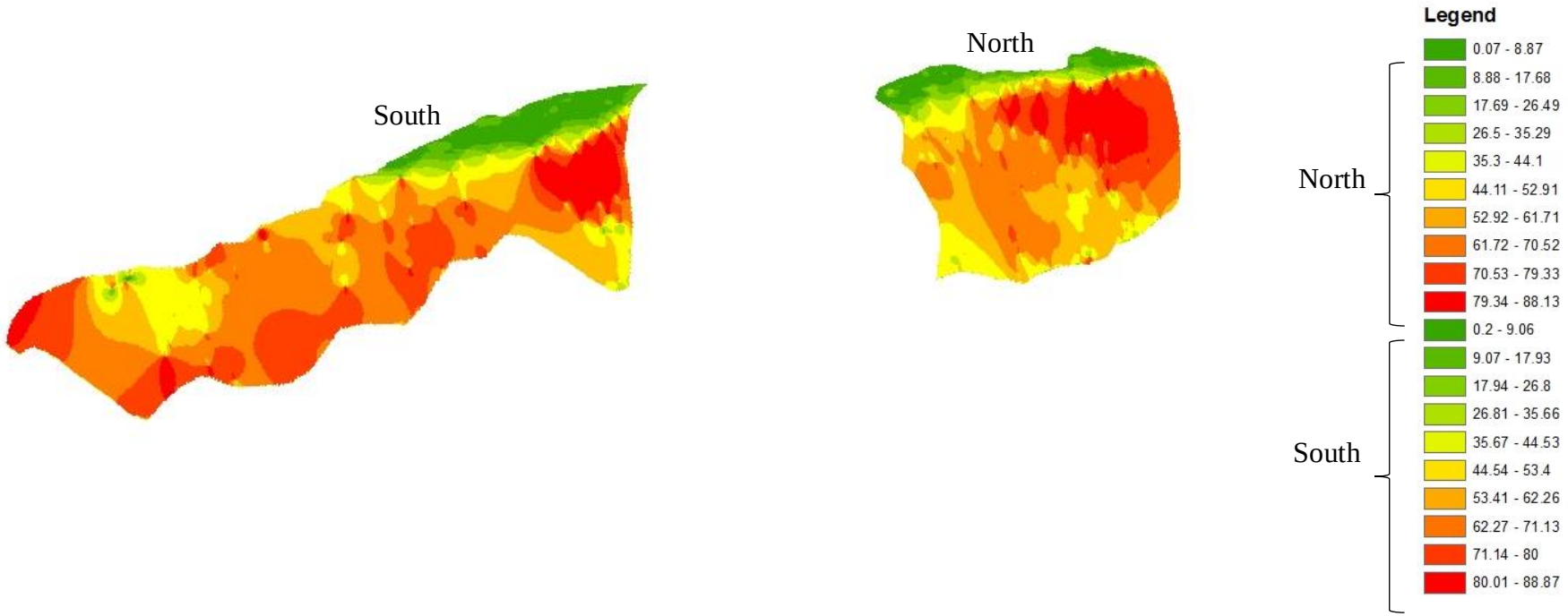

Figure 6.17:September 2011 slope image showing slope angle (degrees)

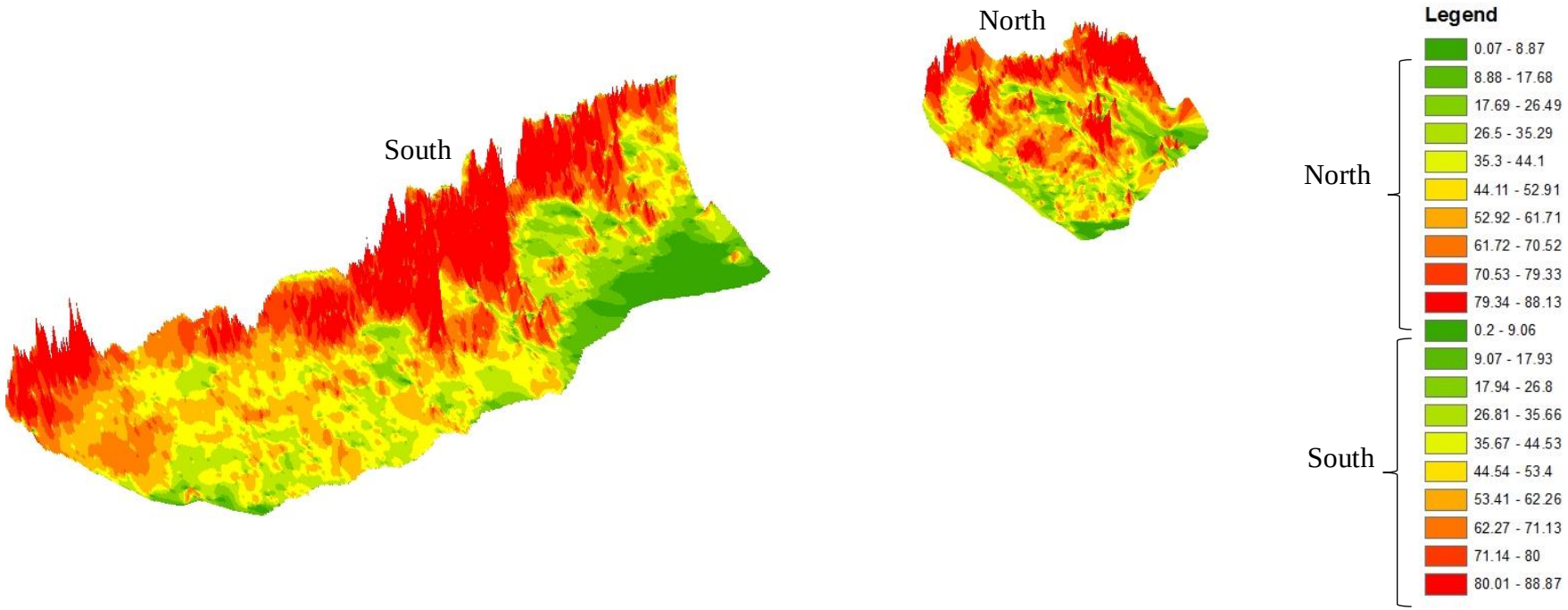

Figure 6.18: November 2014 slope image showing slope angle (degrees)

6.2.1 Surface volume changes

The data for this analysis was collected from airborne LiDAR survey in September 2011 as well as laser scan surveys obtained from May 14 2014 and July 29 2014 – November 08 2014 (Table 6.4). The DEM images are presented in Appendix 3. The highest volume change was between the time intervals of September 2011 and May 2014 with a volume difference of -466 m^3 for the south section having a rate of -0.2 m^3/day and -223 m^3 volume change for the northern section with at a erosive rate of -0.5 m^3/day. This is displayed in the image (Figure 6.19a) with lighter shades that depict erosion. The surface change image for this time period shows a similar trend to the elevation image showing that erosion had occurred in front of the scarp extending offshore (Figure 6.21a).

The second highest erosion rate was between September 09 2014 and October 11 2014 which had a volume difference at the north section of -34 m^3 and a rate of -1.1 m/day (Table 6.4). The DEM image (Figure 6.19b – d) and Figure 6.20a and Figure 6.20b reveals that erosion had occurred further offshore from the cliff face within the talus. This is similarly shown in the surface changes DEM images (Figure 6.21b – d & Figure 6.22a, b).

The third highest rate was between October 2014 and November 2014 with a volume difference of -21 m^3 with a rate of -0.8 m/day on the north section This is presented in the DEM image (Figure 6.20b) revealing a lighter shade near the base of the cliff in soil representing erosion. The same erosional trend is portrayed in the DEM showing surface change. It reveals that erosion next to the scarp with debris being transported from the cliff face offshore (Figure 6.22b).

There were also considerably high positive volumes (accretion) identified in the data. This was seen in the period from August 2014 to September 2014 (43 m^3) for the northern section of the cliff and 13 m^3on the western section of the cliff in both elevation DEM images (Figure 6.19d) and surface DEMs (Figure 6.21d). These models suggest a high volume of debris had accreted in the offshore direction. It was apparent from field observation that these results were not correct and this could have been caused by technical problems with setting up the scanner

over the period of August. Therefore, a comparison of data was taken to evaluate changes from July to September 2014 and confirm that August data set was not correct. This produced results indicating that the north section was subject to erosion with a change of -45 m^3 (erosion), while the south was subject to a minor change of 7 m^3 (accretion). Thus, it is evident that the August dataset is not accurate and this may have occurred as a result of technical issues related to the laser scanner setup. There was also minor accretion recorded from changes from May to July 2014 with rates of 8 m^3/day. The DEM model (Figure 6.19b) illustrates that at the southern section there is erosion occurring at the top edge of the cliff. At the northern section there is erosion occurring at various places along the face, but mainly concentrated on the far east of the section. The likely cause for these positive values is due to fewer scan points overlapping each other between surveys. As a result, some points are left on their own without any corresponding points to overlap them creating misinterpretation of results such as accretion when in actual fact this is not the case.

Table 6.4: Rate of retreat

Survey date	Method	North Volume difference	South Volume difference	Number of days	Rate [m/day]
09 09.2011	LIDAR				
Difference		-233		978	-0.2
Difference			-466	978	-0.5
14 05 2014	Laser Scan				
Difference		8		76	0.1
Difference			8	76	0.1
29 07 2014	Laser Scan				
Difference		2		25	0.08
Difference			-6	25	-0.2
07 08 2014	Laser Scan	-			
23 08 2014					
Difference		43		17	2.5
Difference			13	17	0.8
09 09 2014	Laser Scan				
Difference		-34		32	-1.1
Difference			-12	32	-0.4
11 10 2014	Laser Scan				
Difference		-21		28	-0.8
Difference			11	28	0.4
08 11 2014	Laser Scan				

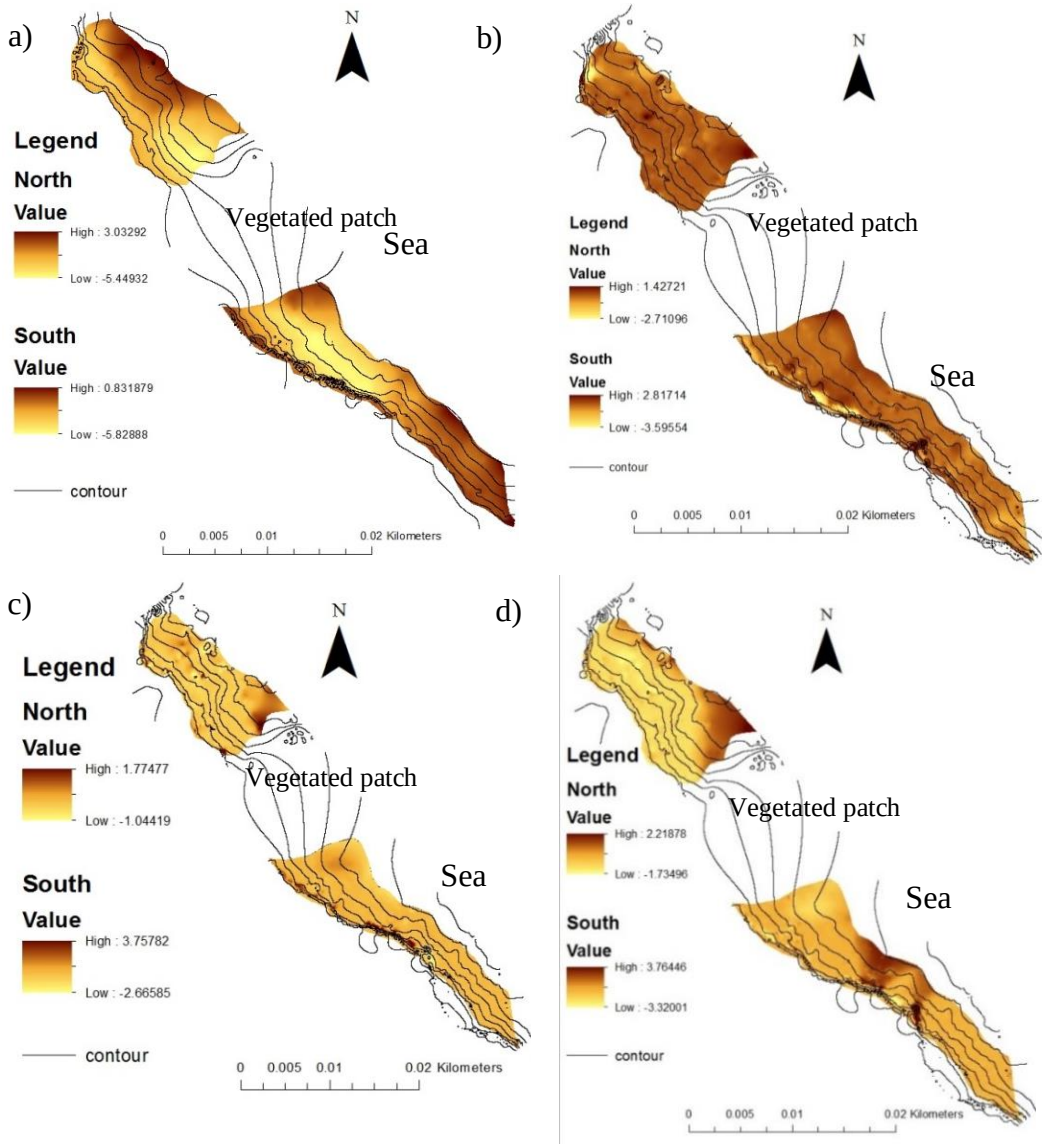

Figure 6.19: Elevation changes showing relative surface changes and Soil volume loss for time intervals (a) May 2014–September 2011 (b) July 2014–May 2014 (c) August 2014–July 2014 (d) September 2014–August 2014

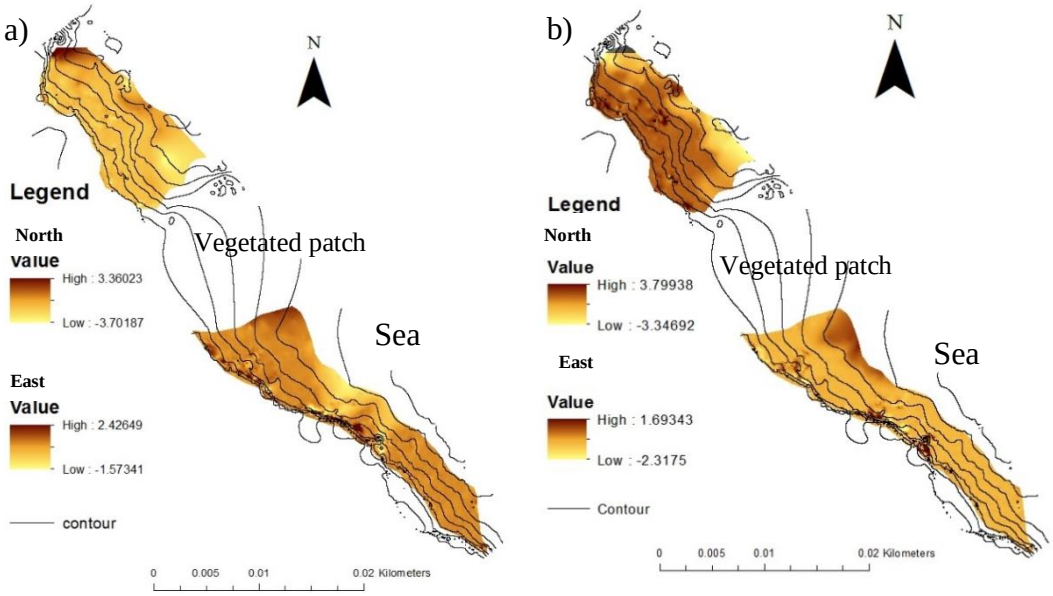

Figure 6.20: Elevation changes showing relative surface changes and Soil volume loss for time intervals (a) October 2014–September 2014 (b) November 2014–October 2014

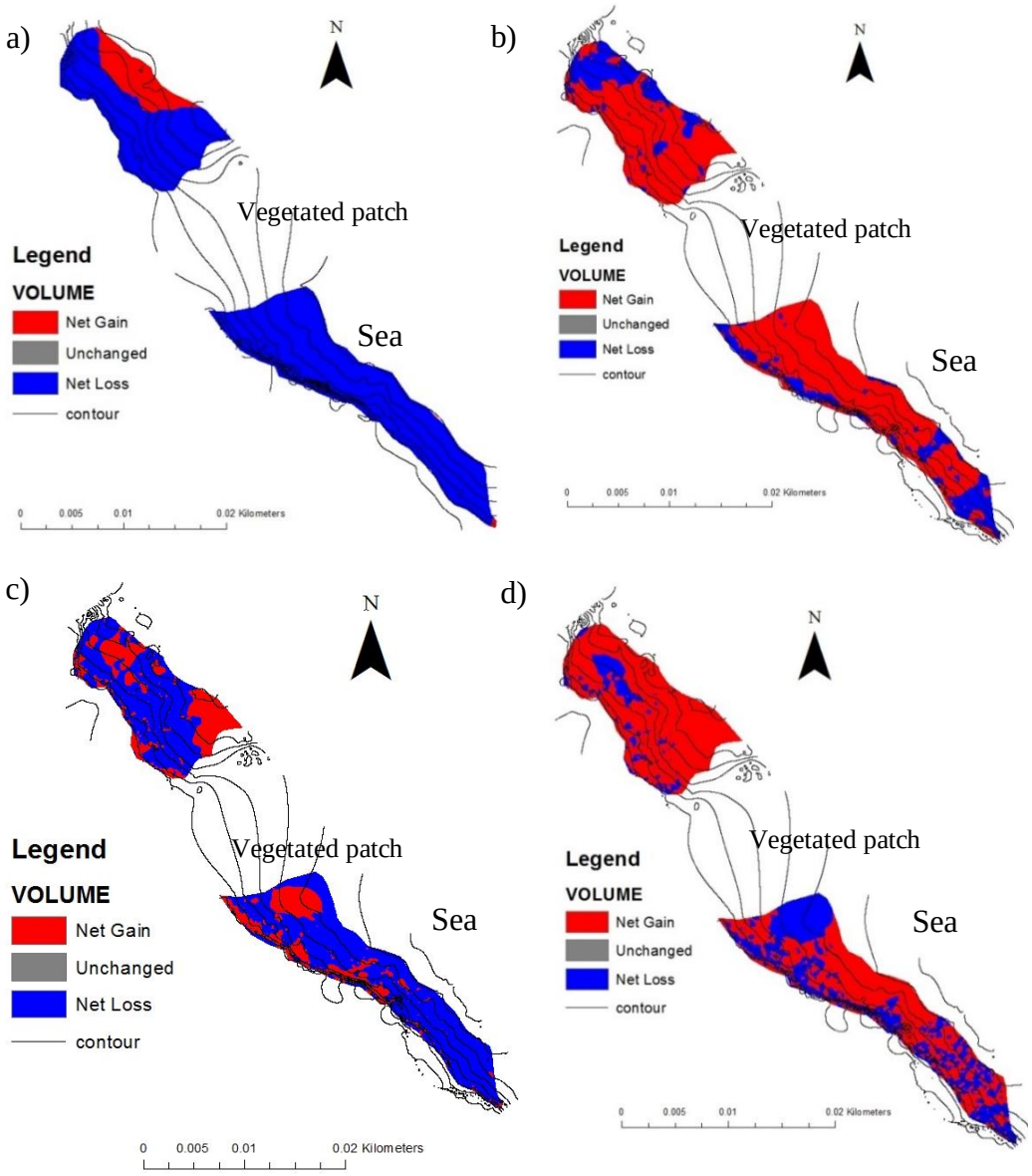

Figure 6.21: Surface changes and Soil volume loss for time intervals (a) May 2014 – September 2011 (b) July 2014 – May 2014 (c) August 2014 – July 2014 (d) September 2014 – August 2014

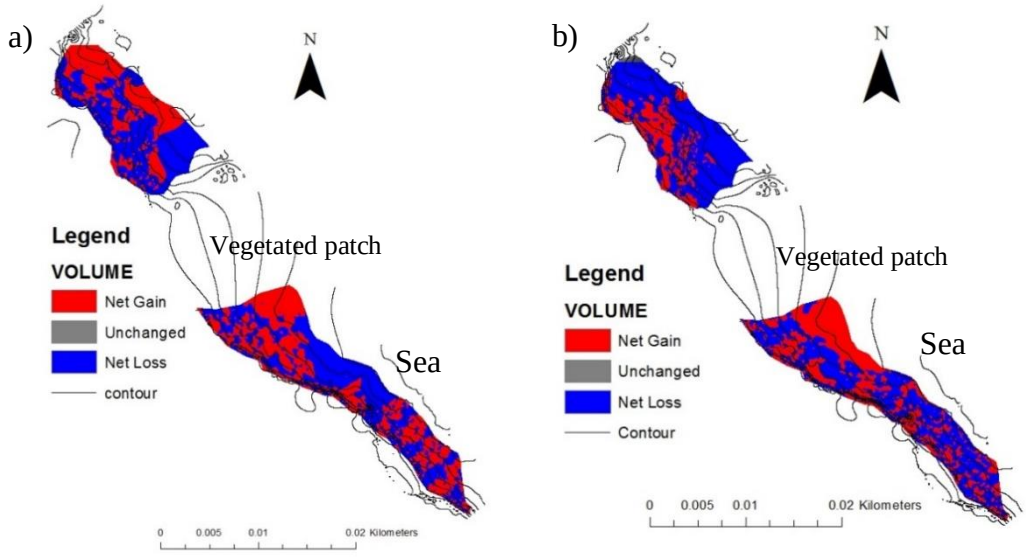

Figure 6.22: Surface changes and Soil volume loss for time intervals (a) October 2014 – September 2014 (b) November 2014 – October 2014

6.3 Summary

Overall, laser scanning is a method that is useful for determining short term cliff retreat. In particular, the DEMs track changes in a more detailed way than simple volumetric analysis and linear rates of shoreline movement. This method of scanning exposed cliff section such as Bramley Drive and Plummers Point over a period of time has enhanced understanding of the evolution of the cliff. The laser scan was conducted from May, August to November 2014 at Bramley Drive and from May, July to November 2014 at Plummers Point. These results were compared to earlier data to identify if there were any trends in the data. It was evident from the results generated, that the highest volume loss was from September 2011 to September 2012 for both Plummers Point and Bramley Drive. It was evident, that there were also positive values in the surface volume changes between the months of May to November for both sites. This is most likely caused by not having enough scan points overlapping each other between surveys. When a point is left isolated without another dataset overlapping it, it produces misleading results such as accretion when in actual fact it is not the case. The generated elevation DEM shows clearly areas of erosion or accumulation of debris while the surface changes DEM shows how debris is transported from the cliff edge down the slopes and re-deposited. Further, it is possible to compare the DEM changes with the underlying density of data points in order to assess the validity of results.

Chapter 7
DISCUSSION

7.1 Introduction

The aim of this chapter is to determine the probable causes for the long term cliff retreat rates acquired from aerial photos and short term rates based on laser scan data. These rates are then discussed in relation to the geology of Tauranga according to the field assessments carried out in this research.

7.2 DSAS analysis

7.2.1 Determination of best method for calculating cliff retreat

From the results obtained from this research, it is suggested that the best method used to estimate rate of cliff retreat is the EPR rates as opposed to the LRR rates. This contradicts Chand and Acharya (2010), who stated that EPR only considers two shorelines therefore it is only a suitable method for determining short term cliff retreat, whereas LRR was supported for determining long term cliff retreat since it considers multiple shorelines. However, the results obtained by this study indicate that the EPR method produced the best estimate for calculating rate of retreat compared with LRR. The reason for this is that the dataset for this study is comprised of three shorelines (1943, 1982 and 2011) of which 1982 has only limited data with poor georeferencing, therefore the EPR is proposed as the best method to be used.

7.2.2 Rate of cliff retreat in Tauranga

The rates acquired from the research undertaken range from accretion of 0.07 ± 0.155 m to erosion of -0.2 ± 0.155 m around the Tauranga Harbour. This range of rates was basically for soft cliffs comprised predominately of Matua Subgroup, Te Puna Ignimbrite, Waitеariki Ignimbrite or materials, with some sections including alluvial gravel, sand, silt and clays of modern rivers. On inspection, these rates seem quite high, particularly for the maximum rates, however cliff retreat is

temporally high variable, so rates differ each year depending on if there is a landslide and if there is, the size of the landslide.

Healy *et al.* (2010) conducted a survey in Tauranga and estimated rates of retreat around the eastern Tauranga Harbour by analyzing datasets from 1943, 1982,1996 and 2002, and their rates were very high. The study covered Te Puna Beach, Western and Southern Rangiwaea Island, Northern and Southeastern Motuhoa Island, Southern and Western Motuhoa Island. The study area covered by Healy *et al.* (2010) did not have any overlap with this thesis study area. Furthermore, the method used to obtain data included printing aerials, scanning aerial photographs at high resolution, then georeferencing aerials using selected control points which had good visibility. These points were located in the upper beach or at a cliff location. About 22 aerial images were used for this study (five aerials for 1943, four aerials for 1996, one aerial for 1982 and ten aerials for 2002). Only the 2002 aerial was obtained already orthorectified, the other aerials had to be orthorectified manually.

The total average range of shoreline change rates obtained by Healy *et al.* (2010) for the period of 1943–1996 was -0.01 to -0.39 m. The maximum rate of retreat was -1.73 $m.y^{-1}$ and the lowest rate was 2.95 $m.y^{-1}$ (Appendix 4). Almost half of the dataset within the period of 1996-2002 were positive values therefore the dataset was left out and only two sets of data (1943-1982 and 1982-1996) were averaged and used. These rates have been averaged and placed in Appendix 4 and graphed in Figure 7.1, together with the rates measured in this study.

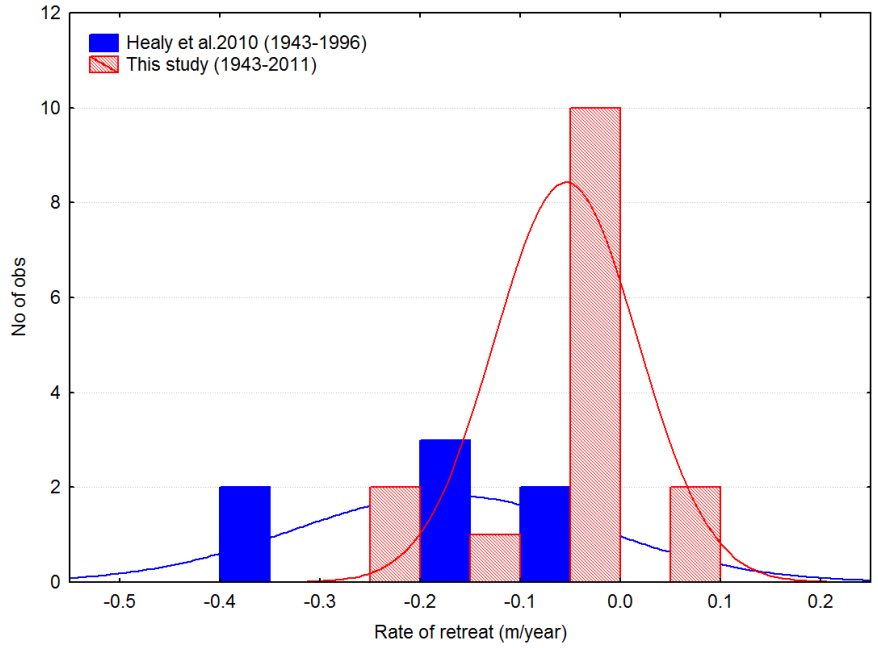

Figure 7.1: Graph comparing rates obtained in this research with those of Healy *et al.* (2010).

The Figure 7.1 shows that both datasets cover a similar range. This was supported by the statistical T-test which revealed that the groups were from the same population since they had a probability of 0.08. However, data from this study is more tightly clustered with a higher peak of low values compared with Healy *et al.* (2010) which had high rates that were outliers.

The rates obtained from this research were lower than the rates estimated by Healy *et al.* (2010). This could be due to georeferencing errors in the Healy *et al.* (2010) data which they have referred to. Another cause of the lower rate of retreat could be that the study area subject to cliff recession considered by Healy *et al.* (2010) may be subjected to greater marine action as the location is closer to the Harbour entrance. Gibb (1978) stated that the rate of cliff recession in New Zealand is between 0.25–1.0 m.y $^{-1}$. He identified sea cliffs eroding at a net rate of 0.3 m.y $^{-1}$ and 1.5 m.y $^{-1}$ with maxima of 2.3 m.y $^{-1}$ for mudstone at Cape Turnagain, while conglomerate material retreated at a rate of 2.0 m.y $^{-1}$ (Gibb, 1979). The rates from Healy *et al.* (2010) and Gibb (1978) and those obtained from this thesis research suggest that rates vary with different lithological units, and that the surrounding environment also contributes to the rate of cliff recession. That is, areas exposed to strong gusty winds and marine action, such as that of

Gibb (1979), are most likely to have a higher rate of cliff recession than sheltered areas such as in the Tauranga Harbour.

Soft volcanic cliffs of the Tauranga Group are located in Auckland harbours (Auckland and Manukau). Although the cliffs are sheltered in the harbour, these cliffs are also subject to erosion. A research assessment was undertaken by Tonkin & Taylor (2006) to determine the rate of cliff retreat. This data is summarised in table 7.1.

Table 7.1: Rate of cliff retreat of Tauranga Group cliffs in Auckland

Location	Formation	Average retreat rate ($m.y^{-1}$)	Maximum retreat rate ($m.y^{-1}$)
Hobsonville, Auckland Harbour	Puketoka	0.14	0.27
Conifer Grove, Manukau Harbour	Puketoka	0.33	
Wattle Downs, Manukau Harbour	Puketoka	0.1-0.25	
Hingaia Peninsula, Manukau Harbour	Puketoka	0.05-0.25	

Table 7.1 shows that the Auckland rates are slightly higher than the rates obtained from this research for Tauranga Harbour. This is evident with the highest rates found at Conifer Grove in Manukau Harbour being -0.33 $m.y^{-1}$ and moderate rates located at Wattle Downs and Hingaia Peninsula with maximum rates reaching 0.25 $m.y^{-1}$. These rates show that even in sheltered regions, the cliffs within Tauranga Group are still susceptible to erosion.

7.2.3 **International rates of cliff retreat**

Rate of cliff retreat depends on the resistance and structure of a rock (Bird, 2008). This also relates to rocks impacted by wave energy. Sunamura (1992) estimated the rate of cliff recession of volcanic ash on coastal cliffs to be at least 10 $m.y^{-1}$. However, Brooks and Spence (2013) stated that soft cliffs typically retreat at a rate over 1 $m.y^{-1}$, and rarely reach a rate of 10 $m.y^{-1}$. The high rate of 10 $m.y^{-1}$ is a high rate as it considers cliff recession as a result of episodic events caused by strong marine action. The rate data summarised in Figure 7.2 from several studies

(Brooks & Spencer, 2012, 2013; Del Rio *et al.*, 2009; Lee & Clark, 2002) is compiled in Appendix 4 and summarised in Table 7.2.

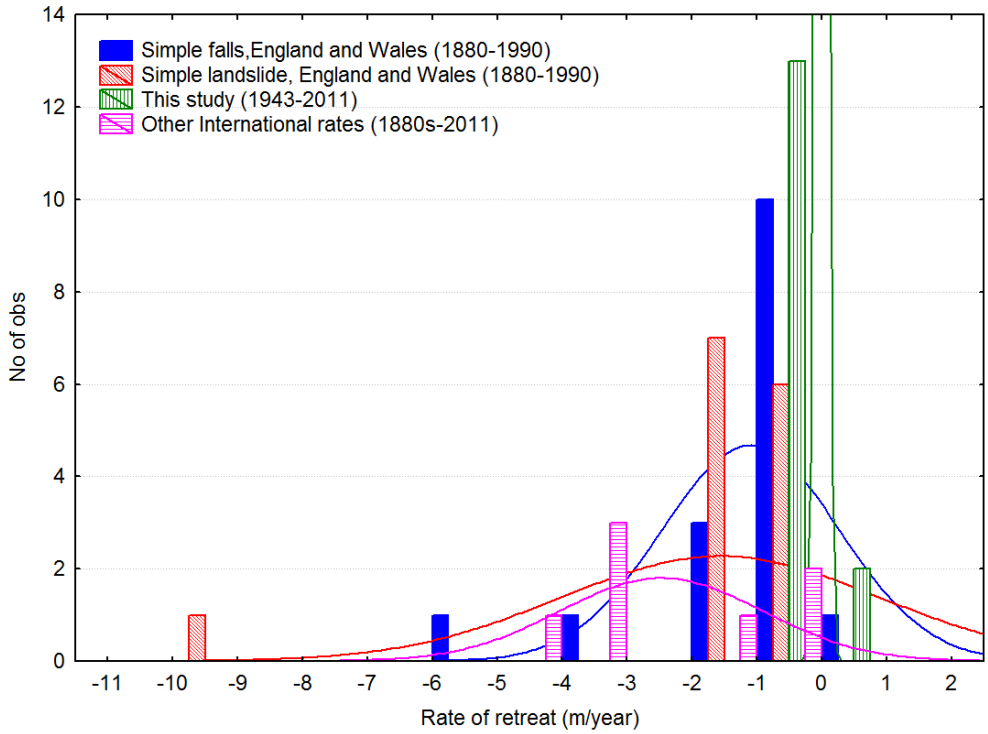

Figure 7.2: Comparison of thesis cliff recession rates to international rates

The rates obtained from this thesis research were compared with international rates from various soft rock literature and it revealed that the results obtained from this study did not have a wide distribution while other rates had a wider distribution with more outliers (Figures 7.2 & 7.3). These international rates were then grouped and compared to the thesis rate to determine if the mean was from the same population or different using the statistical method (T-Test) (Figure 7.3). It resulted in a probability of 0.00003 which indicates that the means of the two groups are different since $p \leq 0.05$. Another difference obvious from the graph (Figure 7.3) is that this study suggests very slow rates compared with international rates.

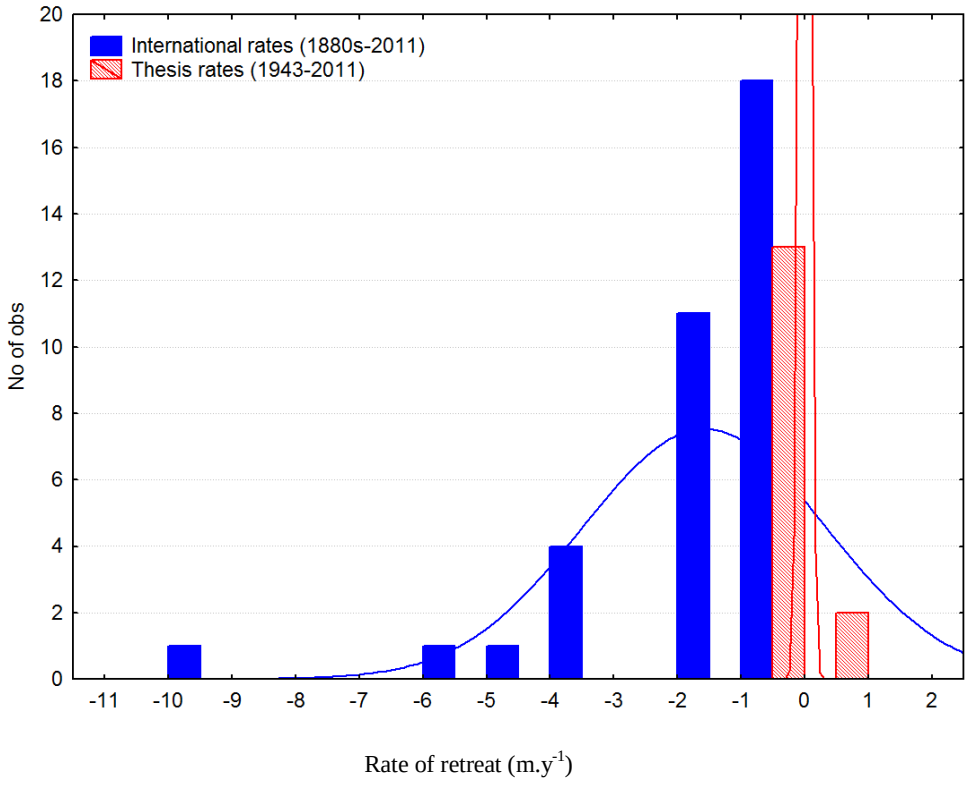

Figure 7.3: Comparison of thesis cliff recession rates to combined international rates

Table 7.2: : International literature with rates of soft rock cliffs

Study	Method	Site	Lithological unit	Year	Rate
Del Río *et al.*, (2009)	GIS analysis, rate of change calculation	Atlantic coast of Cadiz province, SW Spain	Soft detrital deposits (Pliocene-Pliestocene sands, clays, marls and conglomerates)	1956-2005	-0.2 – -1.6 ±0.10 m.y^{-1}
Kuhn and Prüfer, (2014)	Terrestrial laser scanning	Rugen, Germany	Cretaceous chalk with flint bands, Pleistocene glacial till and sand deposits	2007-2011	-3.46 m.y-^{1}
Brooks and Spencer, (2010)	DSAS (Digital Shoreline Analysis System)	Suffolk coast, UK	Pliocene and early-mid Pleistocene marine deposits.	1883-2010	-3.5 ±0.4 m.y-^{1}
				1993-2010	-4.7± 0.55m.y-^{1}
Brooks and Spencer, (2013)	DSAS (Digital Shoreline Analysis System)	Weybourne-sheringham	Glacial tills containing clay sized material but also mixed sands and gravels as well as silt.	1880s-2010	-1.2 m.y-^{1}
		Benacre-Southwold			-3.1 m.y-^{1}
		Walton-on-the-Naze			-0.75 m.y-^{1}

7.3 **Laser scan analysis**

The DEMs produced from the periodic laser scans at Bramley Drive and Plummers Point clearly revealed changes in the surface of the cliff face. The analysis showed areas subject to erosion, as well as areas of debris accumulation that had created talus piles or benches at the base of the cliff scarp. When this was compared to field assessments, there seemed to be some correlation with the laser scan data. That is, some areas subject to erosion were identified by the data obtained from the scan. This section will now focus on describing the analysis of laser scan data.

7.3.1 **Bramley Drive**

The laser scan data was compared to rainfall data from Waipapa Goodwall Road (Appendix 4) (Regional council of Bay of Plenty, 2015) for rainfall data predating July 2013. For rainfall postdating July 2013 the data is taken from Waikato University weather station located at Bramley Drive, Omokoroa. This is shown in Table 7.3 for Bramley Drive in Omokoroa. The data summarised in the table show that volume change on the slope correlates with rainfall data. Therefore, the higher the rainfall, the higher the volume eroded from the cliff scarp. This is because rainfall creates surface runoff which generates the rills on the surface, thus eroding debris. Another contributing factor to erosion is the process of wetting and drying. The alternation of drying in dry weather and wetting by rainfall as well as salt spray triggers erosion (Bird, 2008).

Although the laser scan produced some positive rate values (Table 7.3) indicating there was accretion, in actual fact this is impossible since cliffs have the tendency to erode and not accrete. Therefore, during that period (August 2014) there could have been some erosion but due to technical problems with the laser scanner it was generating incorrect results. This could also be the errors which will be discussed.

Table 7.3: Rate of cliff retreat and Rainfall data for Bramley Drive, Omokoroa

Survey date	Method for data collection	Volume difference [m^3]	Number of days	Rate [m/day]	Rainfall data [mm]
09 09 2011	LIDAR				
		-3037	377	-8	2989
20 09 2012	Laser scan				
		-122	308	-0.4	1509
25 07 2013	Laser scan				
		-435	290	-1.5	1599
10-11 05 2014	Laser scan				
		27	92	0.3	305.8
11 & 18 08 2014	Laser scan				
		76	27	2.8	107.4
07 09 2014	Laser scan				
		-94	46	-2.0	150.6
23 10 2014	Laser scan				
		-64	30	-2.1	45.4
22 11 2014	Laser scan				

A comparison of the DEM aspect images (Figure 7.4) from September 2011 and November 2014 was made. It reveals that in 2011 the southern part of the cliff faced the north while the central section dominantly faced the northwest direction while the northern section faced the west. A similar trend is followed for November 2014, however, there are more changes occurring on the cliff face showing the central section influenced by the sections on either side (south and north) curving into the cliff face from the top of the cliff. This implies that there is an external factor such as runoff or rain eroding the cliff face.

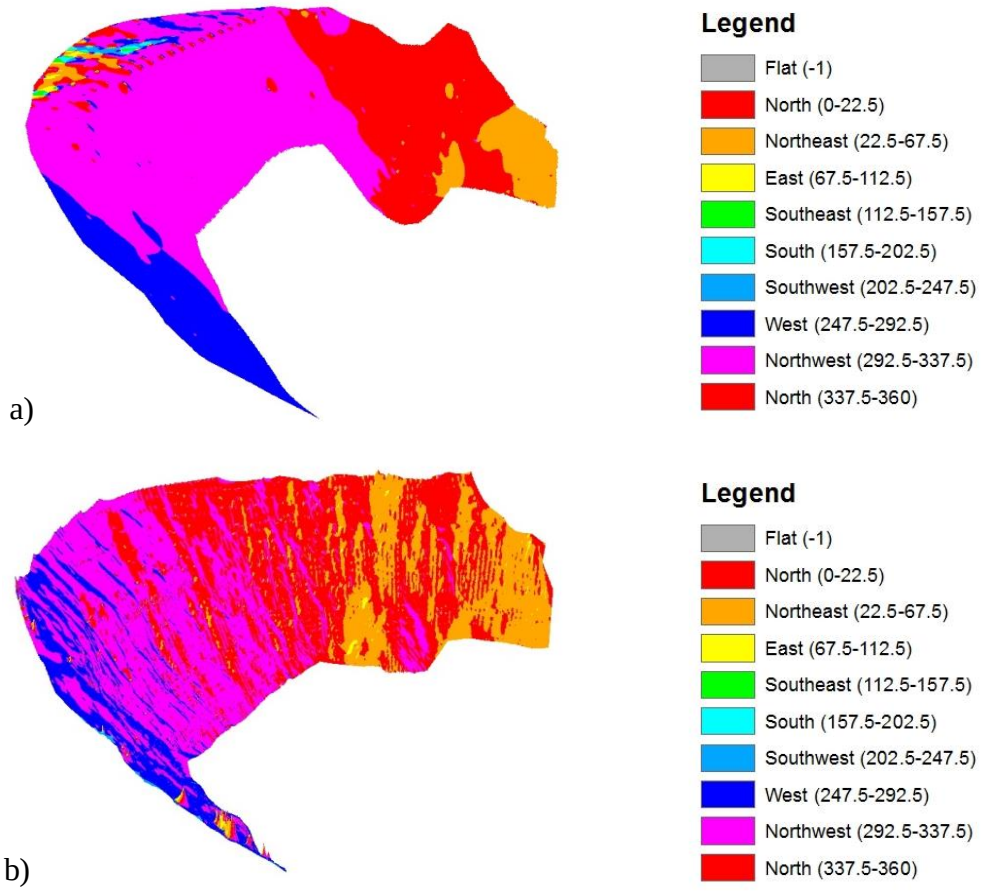

Figure 7.4: Comparison on aspect images of Bramley Drive a) September 2011 image, b) november 2014 slope image

Slope analysis was undertaken to evaluate the changes in the cliff face that were observed in the aspect analysis. The slope DEM images from September 2011 and November 2014 (Figure 7.5 a, b) were compared. The analysis revealed an increase in slope angle from September 2011 being 72 degrees to 85 degrees in November 2014. An interesting observation from the November 2014 slope image is that the central part of the cliff face has a high angle compared to the top of the cliff and the base of the cliff. This suggests that the middle layer is resistant and is bulging out from the cliff.

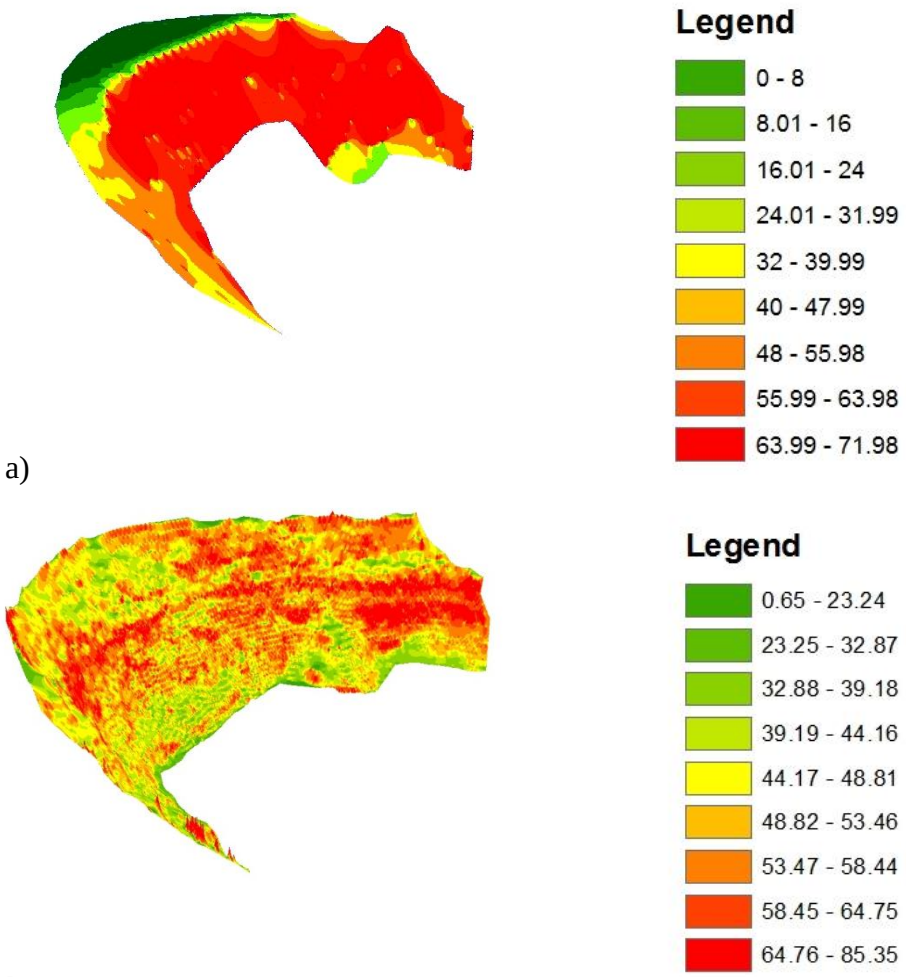

Figure 7.5: Comparison of Bramley Drive slope angle images (a) September 2011, (b) november measured in degrees

A field observation during wet conditions identified water seepage just at the boundary between the Pahoia paleosol layer and the Hamilton Ash at Bramley Drive (Figure 7.6). This indicates that this layer is partly impermeable. Therefore, the surface runoff is responsible for creating the larger rills and a contributing factor to cliff recession at the site.

Figure 7.6: Water seepage above Pahoia paleosol layer at Bramley Drive (source: de Lange 2014)

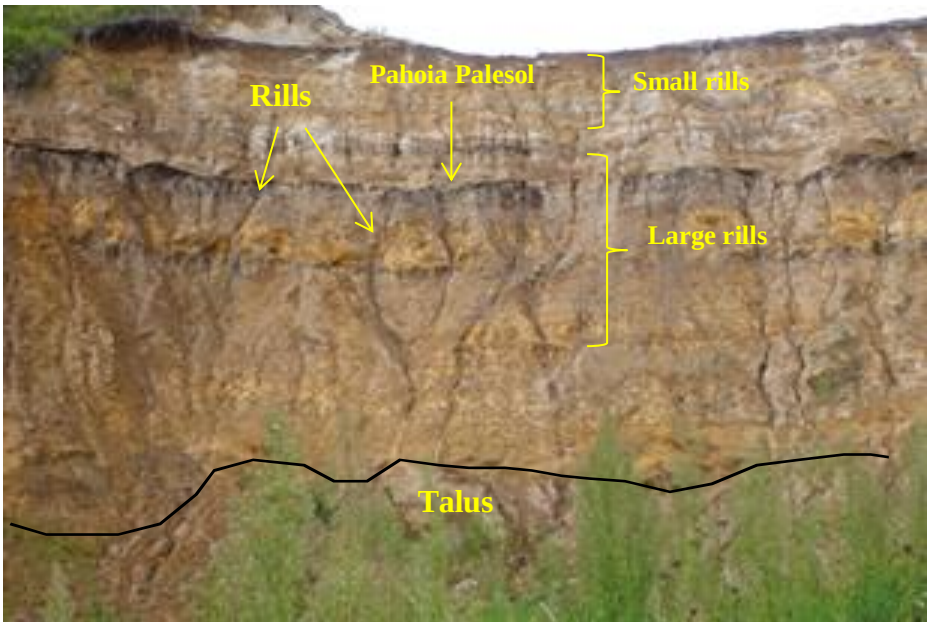

Figure 7.7: Large rills positioned below Pahoia paleosol

This Bramley Drive site has been previously subject to rotational landslip failure. However, small scale rate of retreat as evident from field observations has confirmed that weather conditions such as rainfall have contributed to shaping the cliff face and eroding material by surface water and creation of large rills on the cliff face.

A summary of the results is reproduced in Table 7.3. It shows that the rate of retreat was highest from September 2011 to September 2012. This corresponds to the high volume of rainfall during that period of about 2989 mm. High rainfall was also evident between July 2013 and May 2014 however the volume was less and the time interval between the dates was long therefore it generated a smaller rate of retreat. There were also some unrealistic values generated from the laser scanning from the period of May to November. The rates were too large compared to the rainfall and there was not much activity visible on the site during field surveys, therefore it is likely that this could have resulted from technical instrument errors during scanning.

7.3.2 **Plummers Point**

At Plummers Point, a comparison of the cliff face scanned was made to observe the changes from September 2011 and November 2014 (Figure 7.7, 7.8). This comparison shows that the slope angle at the edge of the cliff edge in both images is as steep as 88 degrees. However, the September 2011 image has steep drop at the cliff during that period but with the November image there is a gradual decrease in the slope angle seaward. This could be due to the accumulation of debris from landslips and talus piles.

The aspect data for the cliff exposure as measured in the November 2014 analysis using the laser scanner shows that the dominant direction the cliff is facing is east to northeast. Dominant wind directions are northwest and southwesterly. Therefore, this suggests that wind does not play a significant role in the wetting and drying effect.

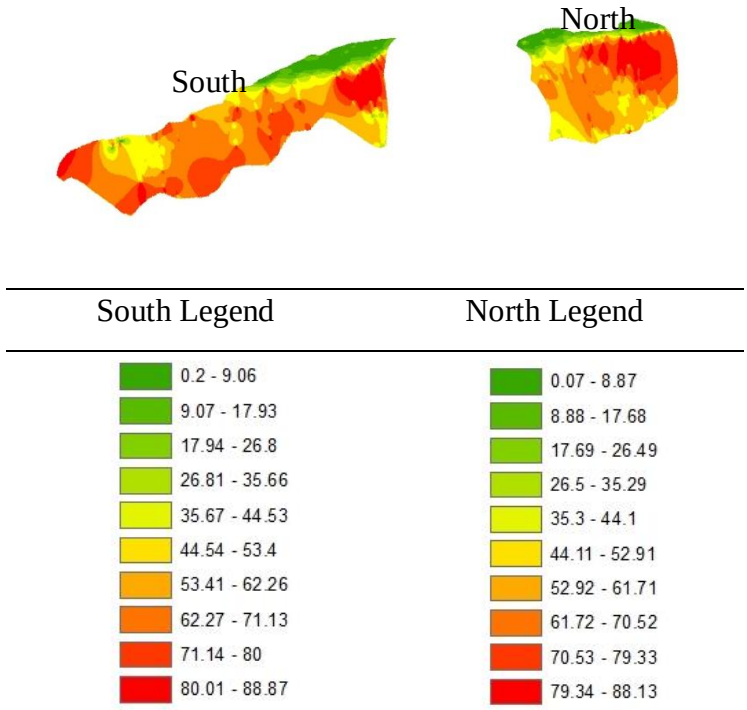

Figure 7.8: September 2011 Slope angle DEM of Plummers Point in degrees

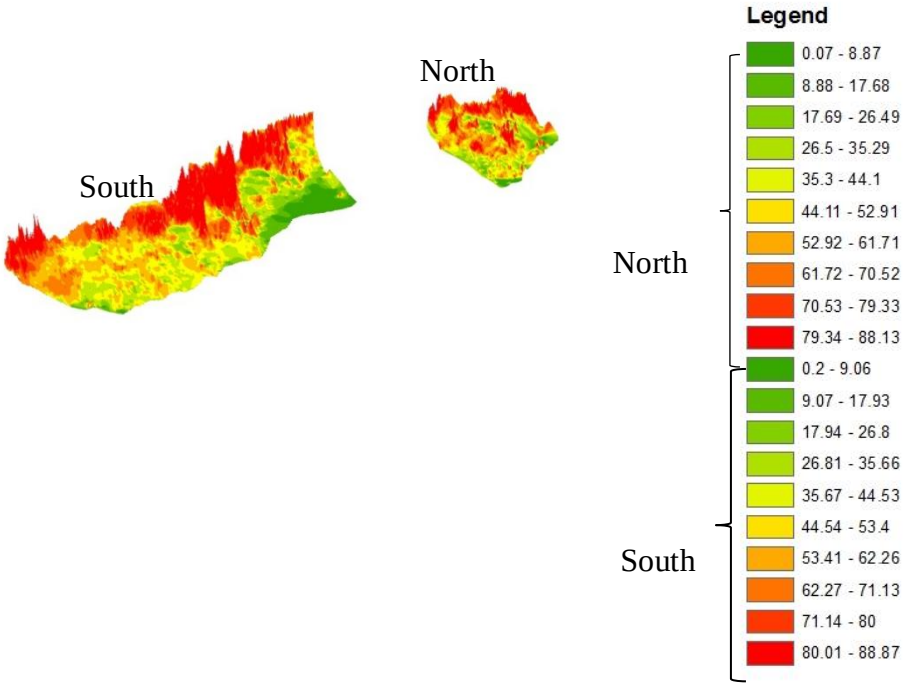

Figure 7.9: November 2014 Slope angle DEM for Plummers Point in degrees

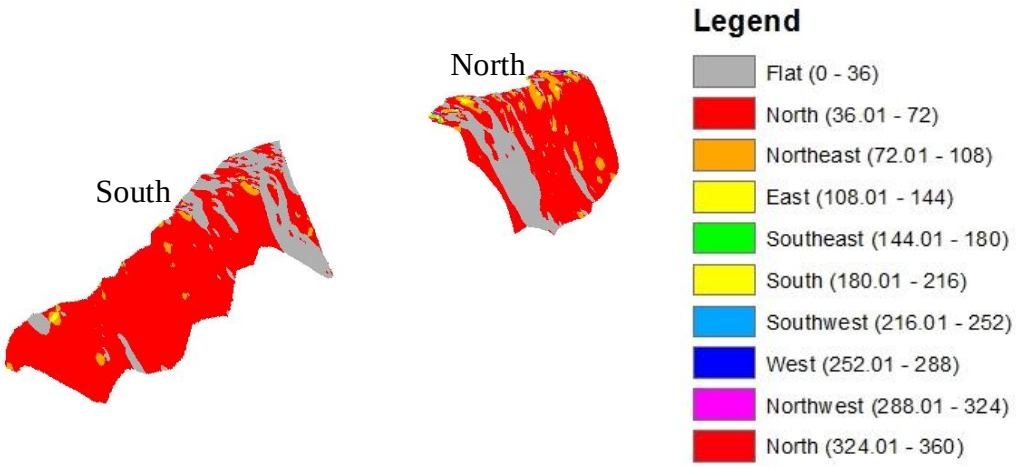

Figure 7.10: September 2011 Aspect DEM for Plummers Point

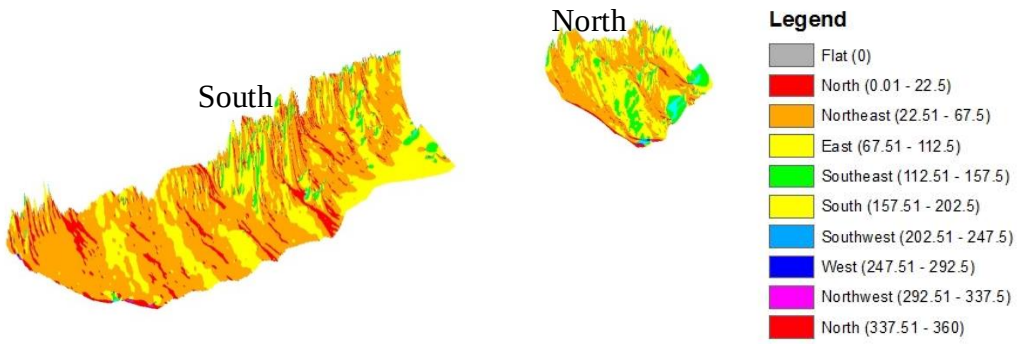

Figure 7.11: November 2014 Aspect DEM for Plummers Point

For Plummers Point, a similar pattern to Omokoroa was observed. There is only one set of data for the interval September 2011-May 2014 that indicates that scan data correlates to rainfall data (Table 7.4). Otherwise, with the other data from May 2014 to November 2014 there is no relationship to rainfall. The rainfall records are low but they are generating high positive values. This is likely to be caused by technical errors associated with the setup of the laser scanner which is evident in the data during that period.

Table 7.4: Rate of cliff retreat and rainfall data for Plummers Point

Survey date	Method	North Volume difference	South Volume difference	Number of days	Rate [m/day]	Rainfall data
09 09.2011	LIDAR					
						6097
Difference		-233		978	-0.2	
Difference			-466	978	-0.5	8874
14 05 2014	Laser Scan					
Difference		8		76	0.1	513.4
Difference			8	76	0.1	
29 07 2014	Laser Scan					
Difference		2		25	0.08	
Difference			-6	25	-0.2	110.6
07 08 2014	Laser Scan	-				
23 08 2014						
Difference		43		17	2.5	
Difference			13	17	0.8	42.4
09 09 2014	Laser Scan					
Difference		-34		32	-1.1	123.6
Difference			-12	32	-0.4	
11 10 2014	Laser Scan					
Difference		-21		28	-0.8	
Difference			11	28	0.4	72.4
08 11 2014	Laser Scan					

The rate of retreat has been determined for Plummers Point based on the time interval between the laser scan surveys. The highest rate of retreat should be between September 2011 and May 2014 since this had the highest volume eroded from the cliff face. However, this was not the case. Higher negative values appeared between October and November laser scan surveys. This period was subject to minimal rainfall and there was no prominent cliff recession at the site.

7.3.3 **Wind Climate and Wave Effect**

Bear (2009) stated that wind speed and direction are the main mechanisms that generate waves. In the Harbour there are two entrances Bowentown entrance (Figure 7.11) and Mount Maunganui entrance (Figure 7.13). The area of study (Plummers Point and Omokoroa Peninsula) are located at the central part of the Harbour. For Plummers Point the closest entrance is Mount Maunganui and this part of the Harbour has deep waters.

Fetch is the extent of open water that a wind blows over (Bird, 2008). The fetch from Mount Maunganui to Plummers Point is approximately 14.962 km ~ 15 km (Figure 7.13), while Omokoroa has a fetch of 23.952 km ~ 24 km (Figure 7.12) but is limited by the intertidal flats that lie between Matahui Point and Matakana Island so during normal weather conditions or low tide the waves break at this point. However, during stormy weather conditions wave heights increase and take the extent of the fetch. de Lange (1988) stated that two factors limit wave development in the harbour: the fetches which are limited by width and length, and the shallow waters which cover a vast area in the Harbour.

de Lange (1988) proposed that the most dominant winds in Tauranga are the north to northeast airstreams and the disturbed west to southwest airflows. The northeasterly winds carry humid air that generates rainfall and it produces wind speeds <8.5 ms^{-1}. As for the west to southwest flows they are associated with cold fronts which travel east to northeast over Tauranga with wind speeds >8.5 ms^{-1}. Recent study conducted by Christophers (*in prep*, 2015) at Tauranga Harbour identified that wave heights increase with strong winds and water depths.

The weather station at Omokoroa recorded the stormy conditions of Cyclone Luci in March 14 2014. The cyclone produced northwesterly winds with speeds >4 m/s and southwesterly winds with wind speeds <2 m/s. The data is provided in Appendix 4. The wind data correlated with wave heights displaying wave heights during that period between 0.15 – 0.2 m.

With regard to Plummers Point, the fetch is also lengthy to the Stella Passage channel in deep waters but the location of the area scanned is sheltered from the northwesterly winds by the Omokoroa Peninsula. Furthermore, the location is also sheltered from the southwesterly winds. However, if there are easterly winds it could have an impact on the site in terms of eroding the cliff face by the effect of wetting and drying since the cliff face faces the eastern direction.

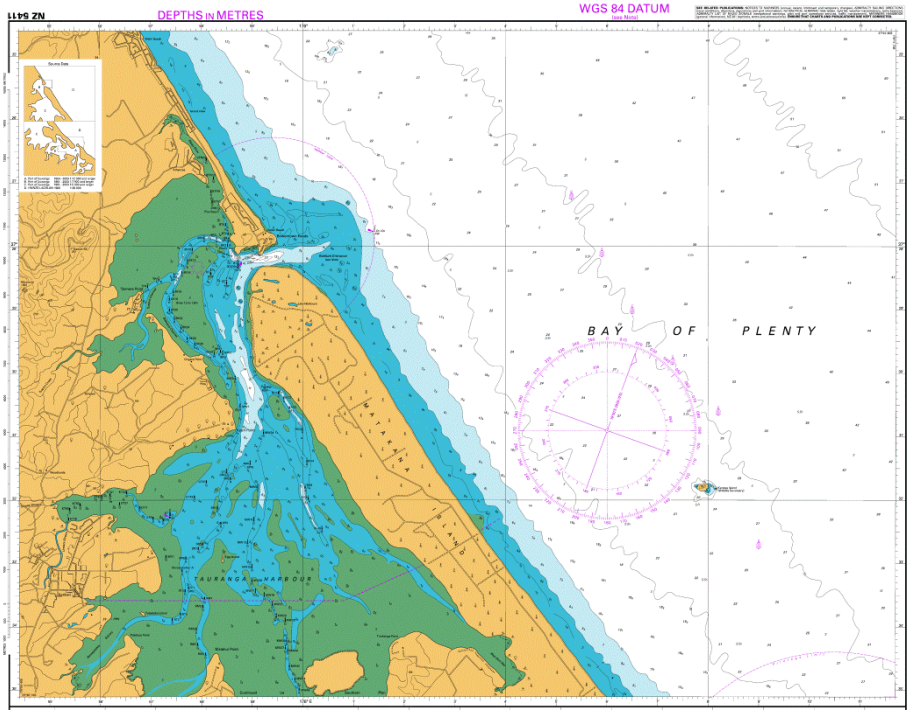

Figure 7.12: Location of Bowentown entrance and the tidal flats that reduce fetch for Omokoroa

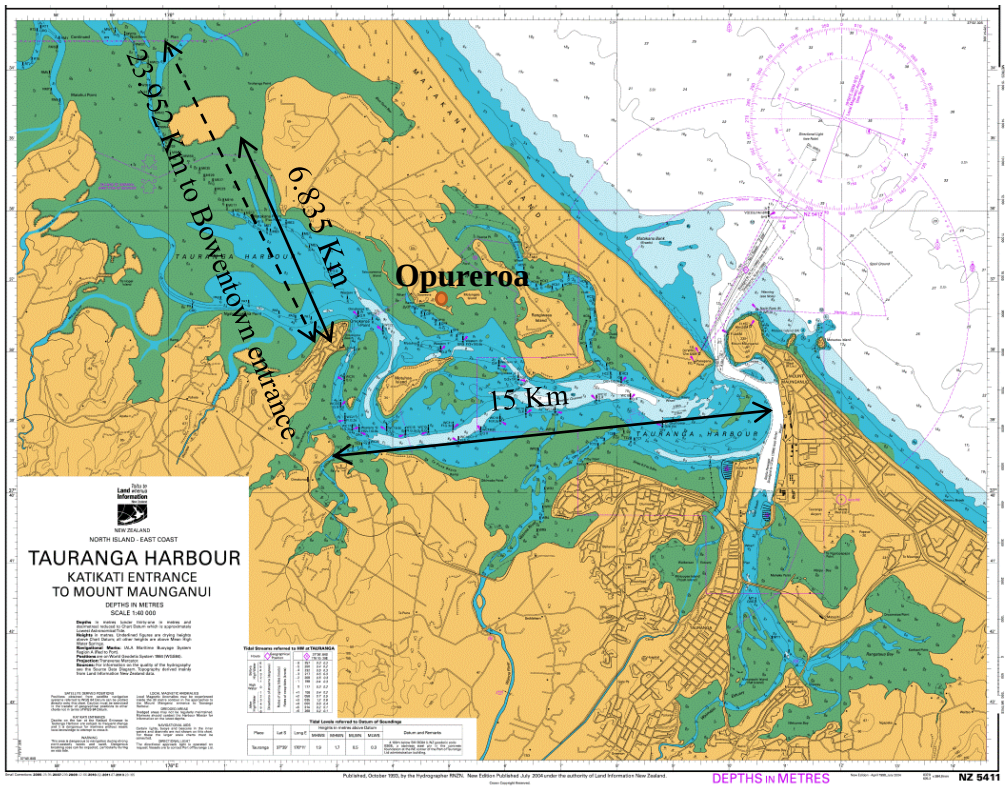

Figure 7.13: Extent of the Fetch for Plummers Point and Omokoroa

The DSAS analysis revealed that Opureroa Marae had the highest rate of erosion in Tauranga Harbour. Tidal flats surround the Opureroa shores causing waves to break well before they hit the shores. As a result, the wave action does not have a large effect on eroding the cliffs. This is also supported by Christophers (*in prep*, 2015) data for Matakana Island that there is less wind and wave impacting the area (Opureroa) compared to exposed areas such as Bramley Drive at Omokoroa. However, there is a high chance that the cliffs are eroding at Opureroa at a fast rate due to the effect of wetting and drying. This is because Opureroa faces the southwesterly direction and receives the southwesterly winds. This was evident when a site assessment was conducted of the site and the coastal cliffs near Opureroa Marae looked very weathered compared to Plummers Point cliff face and Bramley Drive cliff face (Figure 7.14 and Figure 7.15).

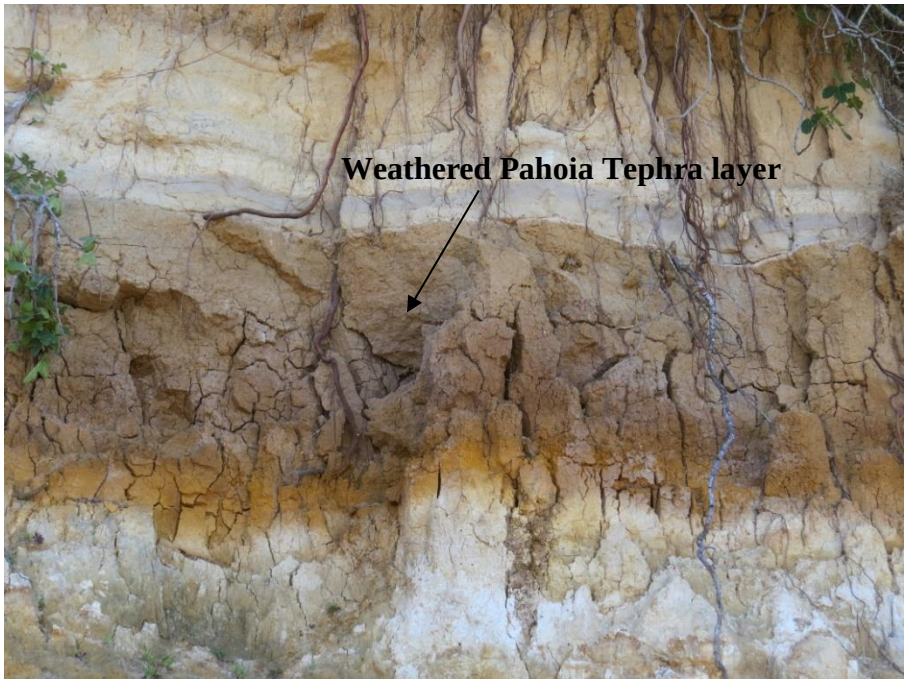

Figure 7.14: Strongly weathered Pahoia Tephra north of Matakana Jetty

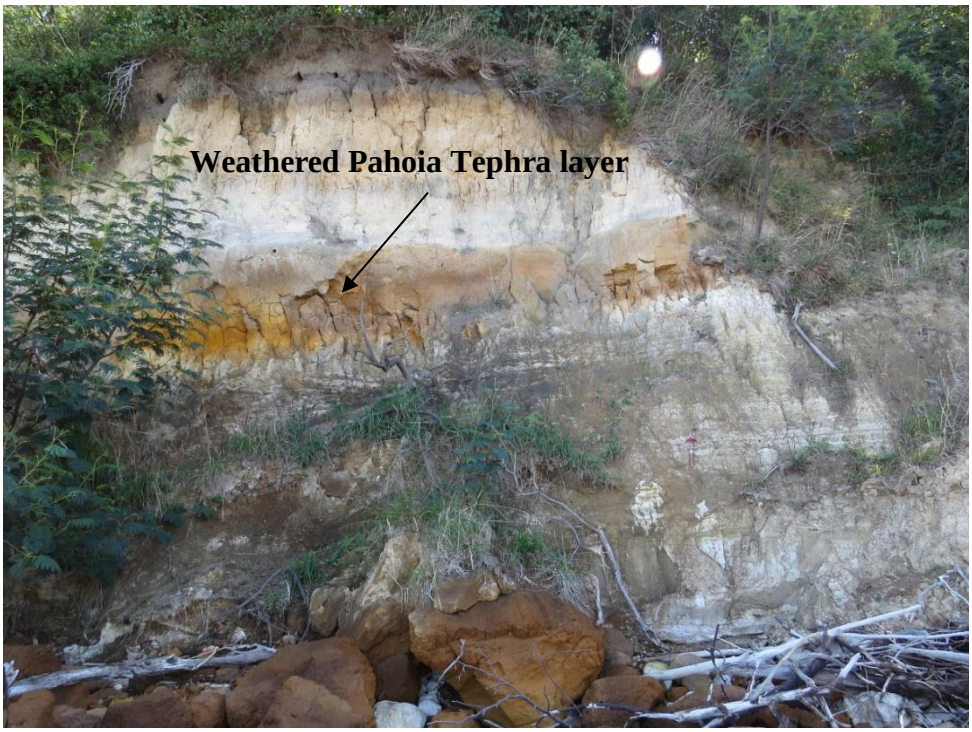

Figure 7.15: Weathered Pahoia tephra on coastal cliffs below Opureora Marae

The rates obtained from Omokoroa and Plummers Point are lower than the rates obtained from International studies (Figure 7.3). This is probably due to the short period that the laser scan surveys were conducted. Another reason for the low rate of cliff retreat is due to the cliffs in Tauranga not being subject to storm events such as that of these international studies.

7.3.4 **Lithological Units**

It is apparent that the principal contributing factor for cliff retreat is the underlying geological units and their resistance to conditions of erosion. This study has identified through the DSAS analysis that the Matua Subgroup is the dominant group prone to erosion with high rates of cliff retreat. Briggs *et al.* (1996) stated that this subgroup contains a wide variety of lithologies which change vertically and horizontally in the sequence. Wyatt (2009) stated that deep seated failures in Omokoroa occurred within older ashes which are the volcanic deposits older than the Rotoehu Ash i.e Hamilton Ash and Pahoia Tephra. The Matua Subgroup underlays the Pahoia Tephra but is also intercalated into other units above its position in the stratigraphic column as a result of it being a fluviatile layer Briggs *et al.* (1996).

There is the probability that soil sensitivity may be a contributing factor to soil failure and presumably lead to cliff recession. Cunningham (2012) has stated that pyroclastic sensitive soils may contain halloysite and allophane clay minerals. These minerals promote porous structures within soils to form allowing moisture content to build up to a high liquid limit increasing sensitivity. Cunningham (2012) analysed samples by Xray diffraction (XRD) from Omokoroa and confirmed that the sample was clayey silt. The unit was considered to be rhyolitic in composition and associated with the Te Puna Ignimbrite intercalataed with Matua Subgroup sediments.

Field observations have also indicated the presence of piping structures within the Plummers Point site. The pinhole test carried out for some of the sampled layers indicated that at the Back site and Midway site soil layer was dispersive. Since the piping structure occurred near the base of the cliff face this has suggested that such pipes may have initiated landslip failures. As a result, overhanging cliffs are

not able to withstand the unstable eroded lower cliff face. Therefore, from the discussions carried out it can be concluded that the lithology of the underlying units is the main control for the rate of cliff retreat. The weather conditions only have minor contributions to rate of retreat at the locations that laser scan was conducted.

7.4 **Management issues**

The rates obtained from this research are less than that of national and international rates. However, rates occur as episodic events with landslides promoting higher rates compared to normal conditions. Therefore, although the current rate of erosion is relatively slow, considering episodic events which may occur there is still the need for management steps to be undertaken. Ramsay *et al.* (2012) stated that cliffs that undergo change over time require a moving baseline setback to ensure there is a constant level of protection. This has been addressed by Tonkin & Taylor (2011) for the three different landslips at Ruamoana, a minimum setback from the cliff edge is imposed to ensure that the risk of loss of life is reduced. Keam (2011) suggested a setback for the existing fence of the Bramley Drive be made away from the headscarp and this be adjusted with future landslip events. Herbst *et al.* (2002) has suggested that in order to improve the stability of a slope, some geotechnical improvements need to be undertaken such as ensuring surface water is kept away from the cliff face by improving stormwater disposal and runoff. Keam (2008) also proposed the option of installing horizontal drains at the base of the main scarp to lessen the likelihood of the cliff regressing further. These pipes had been installed at the site when field assessments were conducted.

Keam (2008), Nautilus (2011), and Tonkin & Taylor (2011) all suggest the replanting of shrubs and deep rooted plants to support slope stability and remove excess water. This was also evident on the cliff slopes at Ruamoana, Bramley and South landslip as confirmed by field assessments conducted. Field observations show that previous landslips could not hold vegetation cover as failure occurred. Therefore, scrubs do not have the capacity to stabilise a cliff structure from deep seated failure and the root system cannot grow in depth to remove all excess water.

7.5 **Summary**

Overall, it seems that the pattern of erosion does not match rainfall data or marine action. Therefore, it can be confirmed that the contributing factor to the rate of erosion is the lithology of the units. The dominant unit that is prone to cliff erosion is the Matua Subgroup. This unit was identified in the field and it showed at Plummers Point that piping had formed at some of the lower units of the stratigraphy and these layers proved to be dispersive when a pinhole test was conducted. For Omokoroa, particularly Ruamoana, Bramley Drive and South landslip these sites showed a base unit of Te Puna Ignimbrite. The Te Puna Ignimbrite has been identified by Cunningham (2012) and Wyatt (2009) as a unit intercalated within the Matua Subgroup. Therefore, it can be suggested that the Matua Subgroup is prone to erosion however, being comprised of a variety of deposits, it is not clear as to which unit erodes rapidly.

Chapter 8
CONCLUSION

8.1 Summary of research findings

The rate of cliff recession within the Tauranga region was determined following the two methods used in this research. They included Digital Shoreline Analysis System (DSAS) for long term rate of retreat and laser scan surveys for determining short term rate of retreat. DSAS rate of retreat was calculated for the study area within Tauranga Harbour while the laser scan surveys were only conducted for a selected site (Main site) at Plummers Point and Bramley Drive at Omokoroa. Fieldwork was undertaken at these sites and at adjacent sites to determine the likely cause of failure. The primary aim of this thesis is to evaluate the types and rates of coastal erosion around the entire harbour. Three objectives were set to achieve that aim:

- to determine the long term rate of retreat;
- to determine the short term rate of retreat and
- to generate a map of the distribution of erosion rates.

This chapter summarises the research findings of these objectives and presents the outcomes and conclusions made.

8.2 Digital Shoreline Analysis System (DSAS)

DSAS has been used to calculate the long term rate of retreat. Three shorelines (1943, 1982 and 2011) were analysed to determine the rate of shoreline change. However, due to the poor resolution of the 1982 aerial photograph there was a lack of control points for georeferencing. As a result there was limited data for the 1982 shoreline.

DSAS software were also used for generating transect lines along constructed baselines in the map view. The two types of baselines constructed were buffer and straight. For each baseline a Linear Regression Rate (LRR) and End-Point Rate

(EPR) was calculated. The results computed directly by DSAS was limited since the software only computed LRR results for transects that intersected all three shorelines. This was the same issue for the DSAS generated EPR dataset. Although EPR only considers 1943 and 2011 shoreline data, the data generated by DSAS only produced results when all three shorelines intersections intersected a transect. As a result, this research followed the approach of calculating EPR results manually using intersection data from DSAS. This ensured that the 1982 shoreline data did not affect the overall results.

The buffer baseline is identified as the better type of baseline for generating rates since it is a more conservative approach. This method considers high erosional rates compared to the straight method. Therefore it can be suggested that the best method to calculate rate of retreat for cliffs is using the buffer EPR method.

The rates of retreat varied across the study area. This was identified after the rates were recorded for each location. The results obtained from the research ranged from -0.2 ± 0.16 to 0.07 ± 0.16. The maximum rate of erosion was found at Southwest Matakana and North Matakana. Some other high erosion rates were located at Western Pahoia and Western Omokoroa. Minimum rates were identified at Eastern Pahoia and Waitui Reserve.

Errors calculated for this method included standard errors and most importantly georeferencing errors. The georeferencing errors were significant and although the aerial photographs (1943 and 2011) were professionally orthorectified known measured points the at some places were off by metres. These errors arose as a result of georeferencing from NZAM and also manual georeferencing carried out for places that were significantly offset. The georeferencing error was then used to determine the offset distance and since it had significant values this estimate of error was used instead of the standard error.

The cliff retreat data was then plotted on a geology map and it was evident that the high recession rates are located on underlying geology comprised of Matua Subgroup, Pakaumanu Group, and Te Puna Ignimbrite. Desktop study as well as field work was undertaken to determine the probable cause triggering the rate of

retreat within these groups. The highest rate of retreat reached -0.2 ± 0.16 at southwest Matakana and north Matakana -0.2 ± 0.03.

The cliff retreat rates were compared to published international and Auckland rates. The maximum retreat rate in Auckland is -0.27 $m.y^{-1}$ and for international rates it ranged from -0.75 to -4.7 $m.y^{-1}$. This showed that the Tauranga cliff retreat rates from this research were less than the international and Auckland rates.

6.3 Field Assessment

Field work was conducted at Omokoroa Peninsula (Bramley Drive, Ruamoana landslip and South landslip) and at Plummers Point (Main site, Pa site, Midway site and Back site). The assessments indicated the type of failure found at the site and the possible factors triggering this failure.

During assessments at Bramley Drive it was evident that there were rills found on the surface of the cliff and this result corresponds to the changes observed by laser scans. For Ruamoana, this site was subject to planar failure and it was evident that debris was translating down the cliff face. However, at South landslip, the cliff was more vertical in angle suggesting that debris most likely eroded from the cliff face and just piled at the base as talus piles.

The field observations undertaken at the Plummers Point sites (Pa site, Midway site and Back site) suggested that piping found within these sites indicated that the material within the stratigraphy located at the base of the units was dispersive. After further analysis it was confirmed that the Back site and Midway site had units close to the base of the stratigraphy that were dispersive. These properties provide an indication that the dispersive character of such units in the Matua Subgroup probably initiates cliff failure.

6.4 Laser Scan survey

Laser scan survey was conducted for two selected sites (Plummers Point and Bramley Drive in Omokoroa). These sites had prominent cliff exposures that were surveyed periodically and were assessed by field work to prove if the surface

changes surveyed were accurate. The laser scan cloud data was used to generate DEMs which were later used to identify surface changes.

From the results obtained it was evident that the data was valid when high density data points were taken by the laser scan such as the data collected in September 2012 and July 2013 and the airborne LiDAR data of September 2011. Calculations were made to determine the rate of retreat in terms of volume/area. The value obtained from this calculation was then divided by the number of days between laser scan surveys to determine a rate retreat per day. The rate of retreat ranged from -0.01 to 0.02 $m.y^{-1}$. The maximum rate of erosion was identified in September 2011 and July 2013 as a result of landslide failure. These rates were consistent with the rates obtained from DSAS, however, these rates were slightly smaller. From May 2014 to October 2014 there were some technical issues with the laser scan setup which produced inaccurate results. Although some results were misleading, the surface changes were clearly noticeable when DEM images were compared for Bramley Drive. A limitation with this method is that the less scan survey points obtained from surveys the limited the dataset will have for comparing surface changes. Surface changes can also be noticeable during a prolonged period of monitoring. Surface volume rates have also been calculated per day however, the errors were significant.

8.3 **Recommendations and suggestions for future research**

This study focused on determining the rate of cliff retreat for long and short term periods within Tauranga Harbour. Although, rates were quantified there were still issues with regard to the method for collecting data. There is still room for improving the method for data collection. It is for this reason that the following recommendations are made:

- Conduct laser scans for a longer period exceeding 6 months and collect as much scan data points for each survey
- Select an area along the exposed cliff and mark it out then conduct scans in the same area each survey. This will ensure that scan points overlap each other to give precise data.
- Identify the units within the Matua Subgroup that are susceptible to piping

REFERENCES

Arthurs, J. M. (2010). *The nature and sensitivity of Rhyolitic Pyroclastic soils from New Zealand.* PhD Thesis thesis, University of Auckland, Auckland.

ASTM International. *Standard test methods for identification and classification of dispersive clay soils by the Pinhole Test, designation D4647/D4647M.*

ASTM International. *Standard test methods for determioning dispersive characteristics of clayey soils by the Crumb Test, designation D6572-13.*

Bear, A. L. (2009). *Erosion and Sedimentation Processes at Northern Waihi Beach.* Msc thesis, University of Waikato, Unpublished.

Bell, D., Richards , L., & Thomson, R. (2001). *Relic slip verification study, Tauranga District Council Environs.*

Bird, E. (2008). *Coastal Geomorphology, An Introduction.* (Second ed.). Chichester, England: John Wiley & Sons Ltd.

Bird, G. (1981). *The nature and causes of coastal landsliding on the Maungatapu Peninsula.* MSc thesis, University of Waikato, Hamilton.

Bray, M., & Hooke, J. M. (1997). Prediction of soft- cliff retreat with accelerating sea-level rise. *Journal of Coastal Research, 13*(2), 453-467.

Briggs, R. M., Houghton, B. F., McWilliams, M., & Wilson, C. J. N. (2005). 40Ar/39Ar ages of silicic volcanic rocks in the Tauranga‐Kaimai area, New Zealand: Dating the transition between volcanism in the Coromandel Arc and the Taupo Volcanic Zone. *New Zealand Journal of Geology and Geophysics, 48*(3), 459-469.

Briggs, R. M., Hall, G. J., Harmsworth, G. R., Hollis, A. G., Houghton, B.F., , Hughes, G. R., Morgan, M. D., & Whitbread-Edwards, A. R. (1996). *Geology of the Tauranga Area - Sheet U14 1:50 000.* Department of Earth Sciences, University of Waikato Occassional Report 22.

Brooks, S. M., & Spencer, T. (2010). Temporal and spatial variations in recession rates and sediment release from soft rock cliffs, Suffolk coast, UK. *Geomorphology, 124*, 26-41.

Brooks, S. M., & Spencer, T. (2013). Importance of decadal scale variability in shoreline response:examples from soft cliffs, East Anglian coast, UK. *Journal of coastal conservation, 18*(5), 581-593.

Budetta, P., Galietta, G., & Santo, A. (2000). A methodology for the study of the relation between coastal cliff erosion and the mechanical strength of soils and rock masses. *Engineering Geology, 56*(3–4), 243-256.

Carpenter, N., Stuiver, C., Nicholls, R. J., Powrie, W., & Walkden, M. (2012). Investigating the recession process of complex soft cliff coasts: an isle of wight case study. *Coastal Engineering*, 1-15.

Castedo, R., Murphy, W., Lawrence, J., & Paredes, C. (2012). A new process-response coastal recession model of soft rock cliffs. *Geomorphology, 177*, 128-143.

Castedo, R., de la Vega-Panizo, R., Fernández-Hernández, M., & Paredes, C. (2015). Measurement of historical cliff-top changes and estimation of future trends using GIS data between Bridlington and Hornsea – Holderness Coast (UK). *Geomorphology, 230*, 146-160.

Chand, P., & Acharya, P. (2010). Shoreline change and sea level rise along coast of Bhitarkanika wildlife sanctuary, Orissa: An analytical approach of remote sensing and statistical techniques. *International Journal of Geomatics and Geosciences, 1*(3).

Christophers, A. J. (*in press (2015)*). *The evolution and stability of Omokoroa cuspate foreland.* thesis, Waikato University, Unpublished.

Churchman, G. J., & Lowe, D. J. (2012). Alteration, formation, and occurrence of minerals in soils. In P. M. Huang, Y. Li & M. E. Sumner (Eds.), *Handbook of Soil Sciences* (2nd ed., pp. 20.1-20.7). Boca Raton, FL: CRC Press (Taylor & Francis).

Cruden, D. M., & Varnes, D. J. (1996). *Landslides Investigations and Mitigation*. Landslide types and processes.

Cunningham, M. J. (2012). *Sensitive rhyolitic pyroclastic deposits in the Tauranga region: Mineralogy, Geomechanics and Microstructures of peak and remoulded states.* thesis, University of Waikato.

Danišík, M., Shane, P., Schmitt, A. K., Hogg, A., Santos, G. M., Storm, S., Evans, N. J., Keith Fifield, L., & Lindsay, J. M. (2012). Re-anchoring the late Pleistocene tephrochronology of New Zealand based on concordant radiocarbon ages and combined 238U/230Th disequilibrium and (U–Th)/He zircon ages. *Earth and Planetary Science Letters, 349-350*, 240-250.

de Lange, W. P. (1988). *Wave climate and sediment transport within Tauranga Harbour in the vicinity of Pilot Bay.* PhD thesis, University of Waikato, Unpublished.

Del Río, L., & Gracia, F. J. (2009). Erosion risk assessment of active coastal cliffs in temperate environments. *Geomorphology, 112*(1-2), 82-95.

Del Río, L., Gracia, F. J., & Benavente, J. (2009). Mass movements and Cliff retreat along the SW Spanish Coast. *Journal of coastal Research*(56), 717-721.

Dornbusch, U., Robinson, D. A., Moses, C. A., & Williams, R. B. G. (2008). Temporal and spatial variations of chalk cliff retreat in East Sussex, 1873 to 2001. *Marine Geology, 249*(3–4), 271-282.

Folk, R. L. (1968). *Petrology of Sedimentary Rocks.* Austin, Texas: Hemphills.

Gibb, J. G. (1978). Rates of coastal erosion and accretion in New Zealand. *New Zealand Journal of Marine and Freshwater Research, 12*(4), 429-456.

Gibb, J. G. (1979). *Late quaternary shoreline movements in New Zealand.* PhD thesis, Victoria University, Wellington.

Gibb, J. G. (1999). *Assessment of areas sensitive to coastal hazards from Makorori point to pouawa river mouth, Gisborne region, Report prepared for Gisborne District Council.* Coastal Management Consultancy.

Grocott, G. (1989). *Initial site suitability Report on Lot 2, DPS 34478, Minden Road, Minden.* Worley.

Gulliver, C. P., & Houghton, B. F. (1980). *Omokoroa Point Land Stability Investigation.* Tonkin & Taylor. from http://books.google.co.nz/books?id=kdictgAACAAJ.

Hall, D. R. (2013). *Sensible Farming on Sensitive and Steep Land - A Catchment Management Approach in Tauranga Harbour*. New Zealand Grassland Association.

Hall, J. W., Meadowcroft, I. C., Lee, E. M., & van Gelder, P. H. J. M. (2002). Stochastic simulation of episodic soft coastal cliff recession. *Coastalk Engineering, 46*, 159-174.

Hapke, C., & Richmond, B. (2002). The impact of climatic and seismic events on the short-term evolution of seacliffs based on 3-D mapping: northern Monterey Bay, California. *Marine Geology, 187*(3–4), 259-278.

Hapke, C., & Plant, N. (2010). Predicting coastal cliff erosion using a Bayesian probabilistic model. *Marine Geology, 278*(1–4), 140-149.

Harmsworth, G. R. (1983). *Quaternary stratigraphy of the Tauranga Basin.* MSc thesis, University of Waikato.

Head, K. H., & Epps, R. J. (Eds.). (2011). *Manual of soil laboratory testing* (Vol. 2): Pentech Press.

Healy, T., & Kirk, R. M. (1982). *Coasts.* Landforms of New Zealand. Auckland: Longman Paul.

Healy, T., Scarfe, B., & Schimel, A. (2010). Eastern Tauranga Harbour historical erosion assessment: Aerial photograph GIS analysis (pp. 1-14). Coastal Marine Group & Department of Earth and Ocean Sciences, University of Waikato: Hamilton, New Zealand.

Herbst, P. H., Schuler, A. A., & Lawrie, A. (2002). *Erosion protection works: guidelines for Tauranga harbour.* Environment Bay of Plenty.

Hughes, M. W. (1998). *Report on landslips at Omokoroa.* Shrimpton & Lipinski Ltd.

Hungr, O., Leroueil, S., & Picarelli, L. (2013). *The Varnes classification of landslide types, an update*. Landslides. Accessed 10 September 2014 from.

Jacquet, D. (1987). *Bibliography on the physical and engineering properties of volcanic soils in New Zealand.* Lower Hutt, New Zealand.

Katz, O., & Mushkin, A. (2013). Characteristics of sea-cliff erosion induced by a strong winter storm in the eastern Mediterranean. *Quaternary Research, 80*(1), 20-32.

Keam, M. J. (2008). *Engineering geology and mass movement on the Omokoroa peninsula, Bay of Plenty, New Zealand.* thesis, University of Auckland, Auckland.

Keam, M. J. (2011). *Landslip Assessment - Ruamoana Place, Omokoroa.* Unpublished Report 851378.150, Tonkin and Taylor.

Kear, D., & Waterhouse, B. C. (1961). Quaternary surfaces and sediments at Waihi Beach. *New Zealand Journal of Geology and Geophysics, 4*(4), 434-445.

Kuhn, D., & Prüfer, S. (2014). Coastal cliff monitoring and analysis of mass wasting processes with the application of terrestrial laser scanning: A case study of Rügen, Germany. *Geomorphology, 213*(0), 153-165.

Lawrie, A. (2006). *Tauranga Harbour Integrated Management Strategy.* Whakatane, Environment Bay of Plenty. 40-44p.

Lee, E. M., Hall, J. W., & Meadowcroft, I. C. (2001). Coastal cliff recession: the use of probabilistic prediction methods. *Geomorphology, 40*, 239-269.

Lee, M., & Clark, A. (2002). *Investigation and management of soft rock cliffs.* London, U.K: Thomas Telford Publishing.

Leonard, G. S., Begg, J. G., & Wilson, C. J. N. (2010). *Geology of Rotorua,*. 1:250 000 geological map 5. Lower Hutt, New Zealand: Institute of Geological and Nuclear Sciences.

Lowe, D. J., Tippett, M., Kamp, P. J. J., Liddell, I. J., Briggs, R. M., & Horrocks, J. L. (2001). Ages on weathered Plio-Pleistocene tephra sequences, western North Island, New Zealand. *Les Dossiers de l'Archeo-Logis, 1*, 45-60.

McCraw, J. (2011). *The Wandering river.* Landforms and geological history of the Hamilton basin. Geoscience Society of New Zealand.

Moon, V. G., Cunningham, M. J., Wyatt, J. B., Lowe, D. J., Morz, T., & Jorat, M. E. (2013). *Landslides in sensitive soils, Tauranga, New Zealand*. Proceedings 19th NZGS Geotechnical Symposium. Queenstown.

Nautilus Contracting Ltd. (2011). *Omokoroa Escarpment Stabilisation - A Proposed Action Plan Integrating Hard and Soft Engineering.*

New Zealand Aerial Mapping (NZAM). (2014). Aerial Photographs of Tauranga Harbour (1943, 1982, 2011).

New Zealand Geotechnical Society (NZGS). (2005). *Guidelines for field classification and description of soil and rock for engineering purposes.*: New Zealand Geotechnical Society Inc.

New Zealand Geotechnical Society (NZGS). (2011). *Guideline for hand held shear vane test.* New Zealand Geotechnical Society Inc.

Oliver, R. C. (1997). *A geotechnical characterisation of volcanic soils in relation to coastal landsliding on the Maungatapu peninsula, Tauranga, New Zealand.* thesis, University of Canterbury, Christchurch, New Zealand.

Olsen, M., Johnstone, E., Driscoll, N., Ashford, S., Kuester, F. (2009). Terrestrial Laser Scanning of Extended Cliff sections in Dynamic Environments: Parameter Analysis. *Journal of Surveying Engineering, 135*(4), 161-169.

Oppikofer, T., Jaboyedoff, M., Blikra, L., Derron, M.-H., & Metzger, R. (2009). Charcterisation and monitoring of the Aknes rockslide using terrestrial laser scanning. *Natural Hazards and Earth System Sciences, 9*, 1003-1019.

OPUS International consultants (OPUS). (2000). *Omokoroa Point Groundwater Stormwater and Erosion Control.* Unpublished report. Report Number 2136.

Pierre, G. (2006). Processes and rate of retreat of the clay and sandstone sea cliffs of the northern Boulonnais (France). *Geomorphology, 73*(1–2), 64-77.

Ramsay, D. L., Gibberd, B., Dahm, J., & Bell, R. G. (2012). *Defining coastal hazard zones and setback lines. A guide to good practice.* National Institute of Water & Atmospheric Research Ltd, Hamilton, New Zealand.

Rosser, N. J., Petley, D. N., Lim, M., Dunning, S. A., & Allison, R. J. (2005). Terrestrial laser scanning for monitoring the process of hard rock coastal cliff erosion. *Quarterly Journal of Engineering Geology and Hydrogeology, 38*(4), 363-375.

Selby, M. J. (1993). *Hillslope materials and processes.* New York: Oxford University Press.

Sherard, J. L., Dunnigan, L.P., Decker, R.S., Steele, E.F. (1976). Pinhole test for identifying dispersive soils. *Journal of the geotechnical engineering division, 102*(1), 69-85.

Shrimpton & Lipinski Ltd. (1998). *Report on landslips at Omokoroa.* Unpublished report. Report Number 14010.

Sunamura, T. (1992). Geomorphology of Rocky Coasts. Chichester, England: John Wiley & Sons Ltd.

Thieler, E. R., & Danforth, W. W. (2010). Historical shoreline mapping (II): application of the Digital Shoreline Mapping and Analysis Systems (DSMS/DSAS) to shoreline change mapping in Puerto Rico. *Journal of Coastal Research, 10*(3), 600-620.

Thieler, E. R., Martin, D., & Ergul, A. (2003). *The Digital Shoreline Analysis System, version 2.0: Shoreline change measurement software extension for ArcView.*

Thieler, E. R., Himmelstoss, E. A., Zichichi, J. L., & Ergul, A. (2009). *Digital Shoreline Analysis System (DSAS) version 4.0 - An ArcGIS extension for calculating shoreline change: U.S. Geological Survey Open-File Report 2008-1278. *current version 4.3.*

Tonkin & Taylor. (1981). *Stability Assessment of Coastal Land in Tauranga County.* Unpublished Report. Report Number 4879.

Tonkin & Taylor. (2011). *Bramely Drive Landslip Hazard Assessment.* Unpublished Report. Report Number 851378.150.

Tonkin & Taylor Ltd. (2006). *Regional assessment of areas susceptible to coastal erosion* Unpublished report. Report Number 19891.100.

Tonkin & Taylor Ltd. (2014). *Bramley Drive Landslip Hazard Assessment.* . Unpublished report. Report Number 851735.518.v2.

Udden, J. A. (1914). Mechanical composition of clastic sediments. *Bulletin of the Geological Society of America, 25*, 655-744.

Umesh, T. S., Dinesh, S. V., & Sivapullaiah, P. V. (2011). Characterisation of Dispersive Soils. *Materials Sciences and Applications, 2*, 629-633.

Wang, G., Joyce, J., Phillips, D., Shrestha, R., & Carter, W. (2013). Delineating and defining the boundaries of an active landslide in the rainforest of Puerto Rico using a combination of airborne and terrestrial LIDAR data. *Landslides, 10*(4), 503-513.

Wendt, M. (2013). *Geotechnical Landslide Investigation on Omokoroa Peninsula, New Zealand in Geoscientific Project VAK:05-08-3-P-1.* Hamilton, The University of Waikato, Universitat Bremen.

Wentworth, C. K. (1922). A Scale of Grade and Class Terms for Clastic Sediments. *The Journal of Geology, 30*(5), 377-392.

Wesley, L. D. (2007). Slope behaviour in Otumoetai, Tauranga. *New Zealand Geomechanics News*, 63-70, 75.

Whitbread-Edwards, A., N. (1994). *The Volcanic Geology of the Western Tauranga Basin.* MSc thesis, University of Waikato, Hamilton, New Zealand.

Wyatt, J. (2009). *Sensitivity and clay mineralogy of weathered tephra-derived soil materials in the Tauranga region.* Msc thesis, Universty of Waikato, Hamilton.

Young, A. P., Guza, R. T., Reilly, W. C. O., Flick, R. E., & Gutierrez, R. (2009). Short-term retreat statistics of a slowly eroding coastal cliff. *Natural Hazards and Earth System Sciences, 11*(0), 205-2011.

Young, A. P., Olsen, M. J., Driscoll, N., Flick, R. E., Gutierrez, R., Guza, R. T., Johnstone, E., & Kuester, F. (2010). Comparison of Airborne and Terrestrial Lidar Estimates of Seacliff Erosion in Southern California. *American Society for Photogrammetry and Remote Sensing, 76*(4), 421-427.

Zhang, K., Chen, S. C., Whitman, D., Shyu, M. L., Yan, J., & Zhang, C. (2003). A progressive morphological filter for removing nonground measurements from airborne LIDAR data. *Geoscience and Remote Sensing, IEEE Transactions, 41*(4), 872-882.